SU-SEL-65-091

Radar Studies of the Cislunar Medium

by

Philip Yoh

December 1965

Scientific Report No. 12

Prepared under

National Aeronautics and Space Administration

Research Grant NsG-377

RADIOSCIENCE LABORATORY

STANFORD ELECTRONICS LABORATORIES

STANFORD UNIVERSITY • STANFORD, CALIFORNIA

SEL-65-091

RADAR STUDIES OF THE CISLUNAR MEDIUM

by

Philip Yoh

December 1965

Scientific Report No. 12

Prepared under
National Aeronautics and Space Administration
Grant No. NsG-377

Radioscience Laboratory
Stanford Electronics Laboratories
Stanford University Stanford, California

ABSTRACT

The aim of this research was to determine properties of the cislunar medium by means of lunar radar investigations. Simultaneous Doppler-frequency and Faraday-polarization measurements were made at Stanford, California, on harmonic radio frequencies near 25 and 50 Mc over a period of about five months during sunspot minimum, from December 1963 to April 1964.

The experimental results have led to discovery of both temporal and spatial variations of the electron content in the cislunar medium above the earth's ionosphere. The temporal variation of the electron content is attributed to the close coupling by means of exchange of ionization between the ionosphere and the lower magnetosphere. A net upward electron flux of about 3.7×10^{12} m^{-2} sec^{-1} is found in the morning; the corresponding number for the downward flow in the afternoon is 2.8×10^{12} m^{-2} sec^{-1}.

The spatial variation is believed to correspond to the plasma wake of the earth in the solar wind. The observations are consistent with a model in which:

1. The wake extends at least to the orbit of the moon, where its outer boundary intersects the lunar orbit at about 120 deg from the earth-sun line.
2. The electron density inside the wake averages about 2×10^{8} el/m^{3} greater than the solar-wind density.
3. The diameter of the plasma wake at the lunar orbit is about 100 earth radii.

CONTENTS

		Page
I.	INTRODUCTION	1
II.	BASIC THEORIES AND APPROXIMATIONS	3
	A. Doppler Excess Frequency	3
	B. Faraday Polarization	6
	C. Discussion of Approximations	9
	1. High-Frequency Approximation	9
	2. Refraction Approximation	12
	3. Magnetoionic Path Splitting	12
	4. Effect of Ionization at the Moon	13
	5. Second-Order Effect	13
III.	EXPERIMENTAL PROCEDURE AND DATA ANALYSIS	15
IV.	IONOSPHERIC-ELECTRON-DENSITY PROFILE	24
	A. Geomagnetic Field	24
	B. Chapman Model	24
	C. Diffusive-Equilibrium Model	29
	1. Theory	30
	2. Profile Fitting	32
	3. Number of Faraday Rotations and the Ratio R	34
	D. Error of Estimating Electron-Density Content from Faraday-Rotation Measurements	39
V.	RESULTS OF ANALYZED DATA	42
	A. Results of Combined Doppler and Faraday Measurements	42
	B. Results of Faraday-Polarization Measurements	47
	1. Diurnal Electron Content	47
	2. Slab Thickness τ and Ratio $B = I_a/I_b$	49
VI.	IONIZATION FLOW BETWEEN IONOSPHERE AND MAGNETOSPHERE	56
	A. Daytime Results	56
	B. Identifying the Possible Region of Large Change of Ionization	58
	C. Model Calculations	60
	D. Comparison with Other Results	69

Page

VII. PLASMA WAKE OF THE EARTH 71

VIII. CONCLUSIONS AND RECOMMENDATIONS 80

APPENDIX

A. DATA PROCESSING 81

REFERENCES 86

TABLES

1 Calculation of Number of Faraday Rotations 28

2 Ratio of Number of Faraday Rotations above 2000 km to that Below 29

3 Comparison of Measured and Calculated Ionospheric Electron Content 48

4 τ and I_a/I_b for the Period from Sunspot Maximum to Sunspot Minimum 53

ILLUSTRATIONS

Figure		Page
1	Earth's dipole field up to one earth radius (by courtesy of Helliwell [Ref. 19])	11
2	Block diagram of system used for moon-echo experiments	16
3	Block diagram of data-processing equipment for moon-echo measurements	17
4	Equipment for data conversion	18
5	Typical output of IBM-7090 computer	20
6	Typical result of Faraday-polarization measurement	22
7	Typical result of Doppler-excess-frequency measurement	23
8	Values of $H \cos \theta$ as a function of azimuthal angle	25
9	Normalized electron-density profile for Chapman model with constant scale height	26
10	Normalized electron-density profile for Chapman model with scale-height gradient of 0.15 km/km	27
11	Normalized measured topside electron-density profile at midlatitude for different local times	33
12	Comparison of measured topside electron-density profile and theoretical profile for 0600 LMT	35
13	Comparison of measured topside electron-density profile and theoretical profile for 1200 LMT	36
14	Comparison of measured topside electron-density profile and theoretical profile for 1800 LMT	37
15	Comparison of measured topside electron-density profile with theoretical profile for 2200 LMT	38
16	Comparison of measured transition levels of O^+ and He^+, from Ariel [Ref. 33], with theoretical results	39
17	Error of calculating electron content from Faraday method for Chapman models	40
18	Error of calculating electron content from Faraday method for diffusive-equilibrium model	41
19	Results of combined Doppler and Faraday measurements	44
20	Averaged results of diurnal changes of electron content	45
21	Difference of averaged results of lunar measurements	46

Figure		Page
22	Averaged results showing diurnal variation of vertical electron content in the ionosphere, measured by Faraday polarization	47
23	Diurnal variation of bottomside electron-density profile	51/52
24	Diurnal variation of slab thickness of the ionospheric electron content	54
25	Diurnal variation of the ratio of the topside electron content to that of the bottomside	55
26	Averaged daytime results of relative electron content measured by Faraday polarization and Doppler excess frequency	56
27	Difference of averaged daytime results of lunar measurements	57
28	Regions in the cislunar medium showing example of radar path	59
29	Averaged electron content in the different regions in the cislunar medium in the solar direction	60
30	Transition levels between He^+ and O^+ for different compositions at the base level (500 km)	64
31	Transition levels between H^+ and He^+ for different compositions at base level (500 km)	65
32	Normalized electron-density profile above base level for different temperatures	67
33	Averaged maximum electron density, N_{max}, measured at Stanford during the lunar-radar-echo experiment	68
34	Spatial position of the "knee" for relative quiet days (Carpenter and Jewell [Ref. 43])	72
35	Diurnal and directional changes in average difference between columnar electron content determined from Doppler and Faraday measurements	73
36	Simplified model of earth's magnetospheric wake, used to explain nighttime radar results	75
37	Comparison of measured and computed boundaries	78
38	Electron density measured by retarding-potential analyzer on board IMP-I	79
39	Examples of the received signal	82

SYMBOLS

c	velocity of light in vacuum
d	distance from transmitter to moon
d_s	distance to shock on earth-sun line
f	operating frequency
f_b	beat frequency
$f_o F2$	critical frequency
f_p	plasma frequency
f_{DE}	Doppler excess frequency
f_H	electron gyrofrequency
g	acceleration of gravity
g_o	acceleration of gravity at earth's surface
h	height, measured from ground
h_{max}	height of maximum electron density above earth
h_o	base level for diffusive-equilibrium region
h_j	scale height
i	$\sqrt{-1}$
k	Boltzmann constant
m_e	electron mass
m_i	ion mass
m_j, m_k	j^{th} and k^{th} ionic constituents
n	integer
p	total number of 10-msec intervals in W zero crossings
q	electron charge

t	time after t_i
t_i	starting time of experiment
z	$(h-h_{max})/h_j$
A'	reduced altitude $= \dfrac{h - h_o}{(1+h/R_\oplus)(1+h_o/R_\oplus)}$
B	I_a/I_b
E	electric field
G	geometrical parameter = $\tan x\,(\tan x - \tan \theta)$
H	magnetic field intensity
I_a, I_b	electron content in ionosphere above and below maximum density
$\Delta I_D(t)$	change of electron content measured by the Doppler-frequency method
$\Delta I_f(t)$	change of electron content measured by the Faraday method
I_t	total ionospheric electron content
K	constant $= 9.45 \times 10^{-3}$
L	height of transition level
M	mach number
M_+	mean ionic mass
N_e	electron density
N_i	ion density
N_{io}	i^{th} ion density at base level
N_o	electron density at base level
N_{max}	maximum electron density in ionosphere
N_M	electron density at moon
P	phase path
R	ratio of Faraday polarization rotations above 2000 km to that below

$\overline{R}$	mean Zurich sunspot number
$R_{\oplus}$	earth radius
T	temperature
T_e	electron temperature
T_i	ion temperature
W	number of zero crossings
X	f_p^2/f^2
$\overline{X}$	mean X
Y_L	$(f_H/f) \cos \theta$
Y_T	$(f_H/f) \sin \theta$
Z	$\nu/2\pi f$
θ	angle between wave normal and direction of earth's magnetic field
λ	wavelength in medium
λ_c	free-space wavelength
μ	refractive index of medium
ν	frequency of collision of electrons with heavy particles
τ	slab thickness = I_t/N_{max}
ϕ	angle (origin at earth) measured from earth-sun line
χ	zenith angle
Ω	total number of rotations of polarization

ACKNOWLEDGMENT

The author is indebted to his advisor, Professor V. R. Eshleman, for his constant encouragement and valuable guidance during the course of this research, to Professor L. A. Manning for his constructive criticism and helpful suggestions, and to Professor R. L. White for his careful reading of the manuscript.

The author would like also to extend his sincere appreciation to Professor B. B. Lusignan for his interest and encouragement of this work.

Thanks are also due to Mr. H. T. Howard and his colleagues at the field site, who spent numerous days and nights in setting up the experiment and collecting the data, to Mr. B. Humphrey for his help in writing the program for the IBM-1620 computer, and to Miss B. Frank of the Stanford Research Institute who reduced the vertical-sounder data. Without the assistance and cooperation of these individuals and many unnamed members of this laboratory, this research could not have been completed.

Financial support for this work has been provided by the National Aeronautics and Space Administration under Grant No. NsG-377.

I. INTRODUCTION

In recent years, an increasing number of experiments has been designed to measure the physical characteristics of the earth's environment in space. One of the most important characteristics is the concentration of ionized particles. For many years, the sole means for investigating the ionized regions within a few hundred kilometers above the earth's surface was vertical-incidence radio sounding.

Since man first made radio contact with the moon, a new technique has been developed for studying the total electron content up to about 1000 km, based on measuring polarization changes (Faraday effect on moon echoes caused by the magnetized plasma near the earth) [Ref. 1]. The successful launching of Sputnik I opened a new avenue for studying the upper atmosphere, based on measurements of the radio waves transmitted from satellites. The principal characteristics of interest are the Faraday polarization [Ref. 2] and dispersive Doppler frequency [Ref. 3], which give information on electron content up to the height of the satellite. Other methods of investigating the electron density in the upper atmosphere include use of incoherent scatter [Refs. 4, 5], rf-impedance probes [Ref. 6], and topside sounders [Ref. 7].

For the medium beyond the ionosphere, whistler (natural vlf signals) investigations [Ref. 8] cover the region from about 6000 to tens of thousands of kilometers in distance. Plasma probes carried on spacecraft have been used to measure the particle density in deep space--for example, Mariner II's solar plasma measurements [Ref. 9].

Several methods for studying the cislunar medium were suggested by Eshleman et al [Ref. 10] based on phase-path (Doppler excess frequency, also called dispersive Doppler frequency), group-path, and Faraday-polarization measurements of moon echoes at harmonic radio frequencies. A number of these have been demonstrated by Howard et al [Refs. 11, 12], and continuing measurements using improved equipment and techniques promise to improve materially our information on the density and dynamics of the ionized regions between the earth and the moon.

In the present experiment, simultaneous Doppler and Faraday lunar-radar-echo measurements were obtained continuously for a few hours daily over a period of five months. The results of the measurements, when combined, enable us to describe the characteristics of the ionized region from the top of the earth's ionosphere to the moon. The Faraday polarization is a function of the electron density and the magnetic-field strength, both of which are greater near the earth. Thus the Faraday-polarization technique describes the ionospheric electron content as a function of time over the periods measured. The Doppler technique, on the other hand, measures the time rate of change of electron content along the entire radar path. By integrating the Doppler measurements over a period of time, the net change of electron content along the entire radar path is obtained. Therefore, by subtracting the Faraday from the Doppler, we can determine the change of electron content between the top of the ionosphere and the moon--the area of interest for the present investigation.

The results of the five-months' measurement of the combined Doppler and Faraday lunar-radar-echoes will be presented along with the interpretation of the results. The principal new contributions of this study are the following:

1. A new technique of analyzing the data was developed--the five-months of data were reduced entirely by an analog-to-digital converter and digital computers on a real-time basis.
2. The study of the regions in which the Faraday rotation occurred indicates that most of the Faraday rotation takes place within the first 2000 km above the surface of the earth.
3. The systematic analysis of long-time combined Doppler and Faraday measurements has led to a discovery of large variations of the electron content above the ionosphere--both temporal and spatial.
4. The variations of the electron content above the ionosphere are two-fold: (1) the temporal variation is caused by the diurnal exchange of electrons between the ionosphere and the magnetosphere, and (2) the spatial variation is caused by the plasma wake of the earth in the solar wind.

This experiment demonstrates further the usefulness of the radar techniques as well as suggests new phenomena to be studied.

II. BASIC THEORIES AND APPROXIMATIONS

A. DOPPLER EXCESS FREQUENCY

The phase path P of a transmitted radio wave reflected back from the moon is given as

$$P = \int_{\text{earth}}^{\text{moon}} \frac{1}{\lambda} ds + \int_{\text{moon}}^{\text{earth}} \frac{1}{\lambda} ds , \qquad (2.1)$$

where λ is the wavelength in the medium.* The first integral refers to the path between the transmitter and the moon and the second integral is the phase path between the moon and the receiver. Since the signal is transmitted from and received at the same point on the earth, the two integrals are thus identical, except for changes in the 2½-sec flight time. Therefore, Eq. (2.1) can be written as

$$P = 2 \int_0^d \frac{1}{\lambda} ds . \qquad (2.2)$$

Note that the lower limit of the integral has been set to zero and d is the distance from the transmitter to the moon.

For an ionized medium, Eq. (2.2) can be expressed as

$$P = \frac{2}{\lambda_c} \int_0^d \mu ds , \qquad (2.3)$$

where λ_c is the free-space wavelength and μ is the refractive index of the medium. The refractive index μ of an ionized medium without magnetic field and collisions is given as

*All symbols are defined in the notation, pp. viii-x.

$$\mu = \left(1 - \frac{f_o^2}{f^2}\right)^{1/2} , \qquad (2.4)$$

where f_o is the plasma frequency (related to the electron density N_e by the expression $f_o^2 = 80.6\ N_e$ mks) and f is the operating frequency.

In the present experiment, in which the operating frequency is much higher than the plasma frequency, the right-hand side of Eq. (2.4) can be approximated by the first two terms of the binomial expansion. Thus,

$$\mu \cong 1 - \frac{f_o^2}{2f^2} \qquad \text{or} \qquad \mu \cong 1 - \frac{80.6\ N_e}{2f^2} . \qquad (2.5)$$

Substituting Eq. (2.5) into Eq. (2.3) gives, for the phase path,

$$P = \frac{2}{\lambda_c} \int_0^d \left(1 - \frac{80.6\ N_e}{2f^2}\right) ds . \qquad (2.6)$$

The time derivative of Eq. (2.6) is

$$\frac{dP}{dt} = \frac{2}{\lambda_c} \left(1 - \frac{80.6}{2f^2} N_M\right) \frac{dd}{dt} - \frac{1}{\lambda_c} \frac{80.6}{f^2} \int_0^d \frac{\partial N_e}{\partial t} ds , \qquad (2.7)$$

where N_M is the electron density at the moon and dd/dt is the relative radial velocity of the moon with respect to the ground station. The amount of change of frequency Δf is given as

$$\Delta f = - \frac{dP}{dt} = - \frac{2}{\lambda_c} \left(1 - \frac{80.6}{2f^2} N_M\right) \frac{dd}{dt} + \frac{1}{\lambda_c} \frac{80.6}{f^2} \int_0^d \frac{\partial N_e}{\partial t} ds . \qquad (2.8)$$

However, there is little or no ionization at the lunar orbit [Ref. 13] (this will be discussed in more detail in Section C.4). Equation (2.8) reduces to

$$\Delta f \cong - \frac{2}{\lambda_c} \frac{dd}{dt} + \frac{1}{\lambda_c} \frac{80.6}{f^2} \int_0^d \frac{\partial N_e}{\partial t} \, ds \ . \tag{2.9}$$

The first term of Eq. (2.9) is the usual Doppler frequency; the second term is called "Doppler excess frequency" f_{DE}, which is of interest, where

$$f_{DE} = \frac{1}{\lambda_c} \frac{80.6}{f^2} \int_0^d \frac{\partial N_e}{\partial t} \, ds \tag{2.10a}$$

and

$$\int_0^d \frac{\partial N_e}{\partial t} \, ds = \frac{\lambda_c f^2}{80.6} f_{DE} \ . \tag{2.10b}$$

This particular term (2.10b) would yield information on the rate of change of ionization along the path of radio waves. Equation (2.9) can be rewritten in a more familiar form, as

$$\Delta f = - \frac{2f}{c} \frac{dd}{dt} + \frac{80.6}{fc} \int_0^d \frac{\partial N_e}{\partial t} \, ds \ , \tag{2.11}$$

where c is the velocity of light in vacuum.

If one can calculate the rate of change of range, then the Doppler excess frequency is simply the difference between the measured change of frequency and the predicted one. Howard et al [Ref. 11] have used this method to measure the Doppler excess frequency, thus yielding information on the time rate of change of electron density along the radar path. When two harmonically related frequencies are transmitted, the Doppler excess frequency is readily measured.

The frequency shift for the operating frequencies of f and nf are, from Eq. (2.11),

$$\Delta f = - \frac{2f}{c} \frac{dd}{dt} + \frac{80.6}{fc} \int_0^d \frac{\partial N_e}{\partial t} ds \qquad (2.12)$$

and

$$\Delta f_n = - \frac{2nf}{c} \frac{dd}{dt} + \frac{80.6}{nfc} \int_0^d \frac{\partial N_e}{\partial t} ds \ . \qquad (2.13)$$

Combine Eqs. (2.12) and (2.13) as follows--

$$n\Delta f - \Delta f_n = f_b$$

$$= \frac{80.6}{fc} \left(n - \frac{1}{n} \right) \int_0^d \frac{\partial N_e}{\partial t} ds \ , \qquad (2.14)$$

where f_b is the beat frequency and n is an integer. The rate of change of ionization along the entire radio path can readily be calculated from Eq. (2.14).

The rate of change of electron density is given by

$$\int_0^d \frac{\partial N_e}{\partial t} ds = \frac{fc}{80.6} \left(\frac{n}{n^2 - 1} \right) f_b \ . \qquad (2.15)$$

The time integral of f_b should be proportional to the net change of electron content along the entire radio path. Therefore, the Doppler-excess-frequency measurements yield the relative electron content.

B. FARADAY POLARIZATION

It is well known that a radio wave with linear polarization traversing a magnetoionic medium splits into two counter-rotating waves (ordinary and extraordinary) with different phase velocities. The

vector sum of these two waves results in a rotation of the plane of polarization, known as the Faraday effect. The total rotation Ω of the plane of polarization of a radio wave propagating through the medium twice between the moon and the observer is given by [Ref. 1]

$$\Omega = \frac{2K}{f^2} \int_0^d H \cos \theta \, N_e \, ds \text{ rotations}, \tag{2.16}$$

where: K is a constant = 9.45×10^{-3} (mks),

H is the magnetic-field intensity,

N_e is the electron density, and

θ is the angle between the wave normal and the direction of the earth's magnetic field H.

The above expression is valid if the quasilongitudinal approximation for the index of refraction [Ref. 14] is observed.

For the present experiment, the total rotation of polarization of a radio wave passing through the earth's ionosphere would greatly exceed one rotation at the operating frequencies. Thus, there would be an uncertainty in the number of rotations. Evans [Ref. 15] showed that this uncertainty could be resolved by means of the two-frequency technique. The total rotation is given by

$$\Omega = \frac{\Delta\Omega(f + \Delta f)^2}{2f\Delta f + \Delta f^2} \tag{2.17}$$

where $\Delta\Omega$ is the difference between polarization angles at two frequencies, and Δf is the frequency difference, which is much smaller than the operating frequency. Therefore, Eq. (2.17) simplifies to

$$\Omega \cong \frac{f\Delta\Omega}{2\Delta f} , \tag{2.18}$$

which is the actual form used to determine the total number of rotations.

Both the electron density N_e and the earth's magnetic-field intensity H decrease with increasing distance. Therefore, most of the contribution to the rotation of polarization is from the ionosphere

[Refs. 1, 15-18]. The upper limit of Eq. (2.16) can be changed to a certain height h (height will be considered in detail in Chapter IV). Thus Eq. (2.16) becomes

$$\Omega \cong \frac{2K}{f^2} \int_0^h \cos\theta \, N_e \, ds \ . \tag{2.19}$$

Since within the height h, H cos θ varies much more slowly than the electron density (electron density varies about two orders of magnitude between the peak of electron density and 1000 km above the surface of the earth, while the value of H cos θ varies by only a small factor), it is reasonable to take the term H cos θ outside the integral. Thus, Eq. (2.19) becomes

$$\Omega \cong \frac{2K}{f^2} \overline{H \cos\theta} \int_0^h N_e \, ds \ , \tag{2.20}$$

where

$$\overline{H \cos\theta} = \frac{\int_0^h H \cos\theta \, N_e \, ds}{\int_0^h N_e \, ds} \ .$$

Finally, the electron content can be deduced from Eq. (2.20), as

$$\int_0^h N_e \, ds = \frac{f^2}{2K} \frac{\Omega}{\overline{H \cos\theta}} \ . \tag{2.21}$$

The upper limit of the integral is about a height of 2000 km.

C. DISCUSSION OF APPROXIMATIONS

1. High-Frequency Approximation

The complete expression for the refractive index [Ref. 14] in an ionized medium with a static magnetic field is given in the standard notation by

$$n^2 = 1 - X\left\{1 - iZ - \frac{Y_T^2/2}{1-X-iZ} \pm \left[\frac{Y_T^4/4}{(1-X-iZ)^2} + Y_L^2\right]^{1/2}\right\}^{-1} . \qquad (2.22)$$

During the entire period of the moon-echo experiment, the most unfavorable conditions in the ionosphere were the following values of X, Y, and Z at F2-layer heights with a frequency of 25 Mc:

$$X = (f_o F2/f)^2 < 0.08 \qquad (2.23)$$

$$Y = f_H/f \qquad < 0.04 \qquad (2.24)$$

$$Z = \nu/2\pi f \qquad < 10^{-5} \qquad (2.25)$$

where $f_o F2$ is the critical frequency,
f_H is the gyrofrequency, and
ν is the frequency of collision of electrons with heavy particles.

It is permissible to use a quasilongitudinal approximation only if

$$Y_L^2 \gg \frac{Y_T^4/4}{(1-X-iZ)^2} , \qquad (2.26)$$

which implies

$$\cos\theta \gg \frac{1}{2} Y \sin^2\theta \qquad (2.27)$$

or

$$\theta < 88 \text{ deg.} \qquad (2.28)$$

The geomagnetic latitude at Stanford is about 44 °N and the position of the moon is always to the south of the station. During the entire period of the experiment, the elevation of the moon was between 75 and 30 deg. Figure 1 shows the dipole-magnetic-field lines up to one earth's radius above the surface of the earth. The shaded area indicates the lunar radar-signal path. It is clear that, within one earth's radius, the angle θ is nowhere near 88 deg. Hence the quasi-longitudinal approximation is satisfied. On the basis of these approximations, one can rewrite Eq. (2.22) to a very good approximation:

$$\mu = 1 - \frac{1}{2} X(1 \pm Y_L)^{-1} \quad . \tag{2.29}$$

Since Y_L is much less than one, we can expand the term $(1 \pm Y_L)^{-1}$ and retain the first two terms of the expression

$$\mu = 1 - \frac{1}{2} X(1 \mp Y_L) \tag{2.30}$$

and

$$\mu_o = 1 - \frac{1}{2} X(1 + Y_L) \tag{2.31}$$

$$\mu_X = 1 - \frac{1}{2} X(1 - Y_L) \quad , \tag{2.32}$$

where the subscripts o and x refer to an ordinary wave and an extraordinary wave respectively. The Doppler-excess-frequency measurement gives an indication of the mean time rate of change of the phase path of the two waves. Therefore,

$$\frac{dP}{dt} = \frac{(dP_o/dt) + (dP_x/dt)}{2} = \frac{2}{\lambda_c} \frac{d}{dt} \int_0^d \left(\frac{\mu_o + \mu_x}{2} \right) ds \quad . \tag{2.33}$$

But

$$\frac{\mu_o + \mu_x}{2} = 1 - \frac{X}{2} \tag{2.34}$$

$$= 1 - \frac{80.6N}{2f^2} \tag{2.35}$$

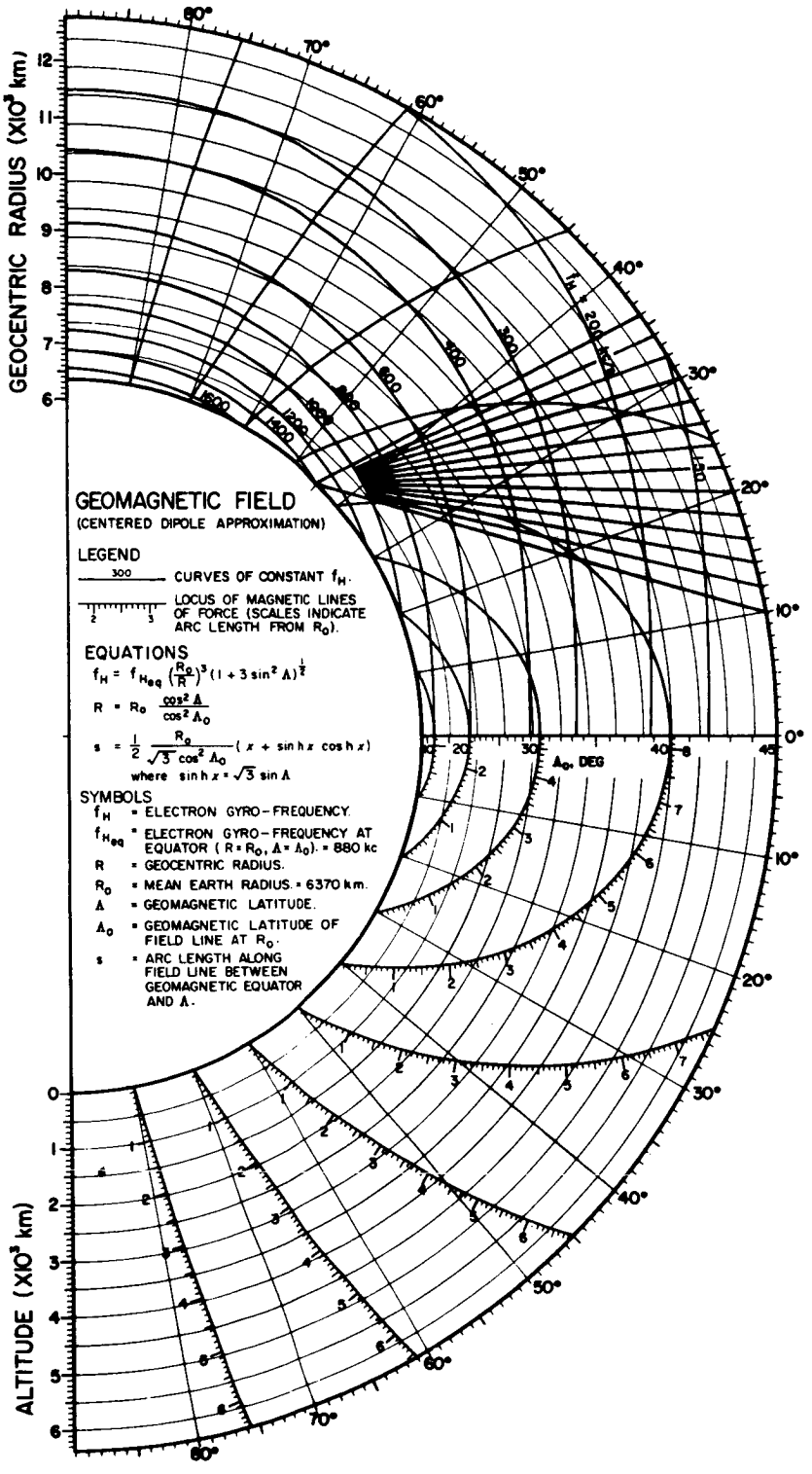

FIG. 1. EARTH'S DIPOLE FIELD UP TO ONE EARTH RADIUS
(By courtesy of Helliwell [Ref. 19]).

is the same as the refractive index in Eq. (2.6). Thus the Doppler excess frequency is indeed a measure of the time rate of change of electron content along the entire radar path.

2. Refraction Approximation

In deriving Eq. (2.14), it is implicitly assumed that the ray paths at 25 and 50 Mc are the same. However, the refractive index μ is frequency dependent; thus the signal paths may traverse different paths for different frequencies. The deviation of the paths of signals at 25 and 50 Mc in the ionosphere is about 10 km for the following conditions:

Elevation angle, 25 deg
Critical frequency, 8 Mc
Height of maximum electron density in the F layer, 300 km.

The maximum deviation of the ray path from the line of sight at the frequencies used is less than 1 percent within the elevation angle range of 70 to 30 deg [Refs. 3, 20]. Hence, the electron-content difference between the line of sight and the ray path is less than about 2 percent for the case of a 25-deg elevation angle.

3. Magnetoionic Path Splitting

Because the ordinary and extraordinary waves have slightly different ray paths, the expression for the Faraday rotation Ω should contain an extra term describing the path-splitting effect.

The path-splitting correction calculated by Garriott [Ref. 2] can be applied to the present case. The contribution of the path-splitting effect to the rotation angle is about 6 percent of that of the dispersion effect for the following conditions:

Elevation angle, 25 deg
Critical frequency, 8 Mc.

Therefore, the correction is neglected in the calculation of the electron content from the Faraday-rotation measurements.

4. Effect of Ionization at the Moon

In deriving Eq. (2.14) for Doppler excess frequency, it is assumed that there is no ionization at the lunar orbit. Opik [Ref. 13] suggested that the ionization may be as large as 200 electrons/cc at the surface of the moon. Therefore, it is reasonable to assume that the maximum ionized density at the lunar orbit would be on the same order of magnitude. Hence, we can calculate the effect of the second term of Eq. (2.7). The value of $80.6N_M/2f^2$ at 25 Mc is about 10^{-5}. The maximum value of the Doppler frequency, the first term of Eq. (2.7), at about two hours from the local transit time is less than 50 cps. Therefore, the net effect of the frequency shift due to the ionization at the lunar orbit is simply the product of the Doppler frequency f_D and $80.6N_M/2f^2$, i.e., $10^{-5}f_D$. When the Doppler frequency is 50 cps, the contribution to the shift of frequency is only 0.005 cps. The sensitivity of the experiment is about one tenth of a cycle. Therefore, it is reasonable to neglect the effect of the ionized region at the moon.

5. Second-Order Effect

The second-order effect arises because the distribution of ionization enters into ray theory. Thus the expression for the Faraday rotation Ω and phase path P should contain the term for the ionization distribution. Ross [Ref. 21] has given the expressions for the Faraday polarization rotation Ω and phase-path deviation ΔP for the case in which the source is at a great distance:

$$\Omega = \Omega_o\left[1 + \frac{1}{2}\beta\bar{X}(G+1)\right] \tag{2.36}$$

and

$$\Delta P = \Delta P_o\left[1 + \frac{1}{4}\beta\bar{X}\sec^2\theta\right], \tag{2.37}$$

where Ω_o is the first-order Faraday-polarization rotation,

ΔP_o is the first-order phase-path deviation,

$$\beta = 80.6d\left[\int_0^d N_e^2 ds \Big/ \left(\int_0^d N_e ds\right)^2\right] ,$$

$$X = (80.6/f^2)\left(\int_0^d N_e ds/d\right) ,$$

G is a geometrical parameter that could be expressed as $G = \tan \chi (\tan \chi - \tan \theta)$ where χ is the zenith angle and θ is the angle between the direction of the magnetic field and the direction of propagation.

It would be interesting to learn the magnitude of the second-order effect, which is represented by the second term in Eqs. (2.36) and (2.37). For the known distribution of the electron density along the radar path the quantities $[\beta\bar{X}(G+1)]/2$ and $(\beta\bar{X}\sec^2\theta)/4$ can be calculated. This magnitude can be estimated.

The values of $[\beta\bar{X}(G+1)]/2$ and $(\beta\bar{X}\sec^2\theta)/4$ are calculated for the following electron-density distributions:

1. Chapman electron-density distribution in the ionosphere,
2. $1/R^3$ electron-density distribution in the magnetosphere,
3. Constant electron density for the rest of the radar path,

$\theta = 60$ deg, and $\chi = 30$ deg

yielding the calculated quantities shown below.

f = 25 Mc	$[\beta\bar{X}(G+1)]/2 = 0.004$
	$(\beta\bar{X}\sec^2\theta)/4 = 0.008$
f = 50 Mc	$[\beta\bar{X}(G+1)]/2 = 0.001$
	$(\beta\bar{X}\sec^2\theta)/4 = 0.002$

The above values are less than 1 percent of those of the first-order effect. Hence it is reasonable to neglect the second-order effect in the present experiment.

III. EXPERIMENTAL PROCEDURE AND DATA ANALYSIS

Daily measurements of Doppler excess frequency, Faraday polarization, and echo amplitude were made from December 1963 to April 1964. The experiment was conducted over a period of two to three hours each day during the local lunar transit time. The time limitation was due to the limited coverage of one of the antennas (the 48-element log periodic antenna) [Ref. 22]. It takes about 27 days for the moon to rotate around the earth once. Over a period of about five months, the radar path scanned the entire cislunar region five times.

The equipment and experimental procedures have been described in some detail by Howard et al [Refs. 11, 12, 22, 23]. The equipment parameters are listed below, and a block diagram of the system is shown in Fig. 2.

Parameters	50 Mc	25 Mc
Transmitted Power	50 kw	300 kw
Transmitted Frequencies	49.802 Mc	24.901 Mc
Transmitted Pulse Lengh	2.5 sec	2.5 sec
Transmitting Antennas (linearly polarized)	150-ft dish	48-element log-periodic array
Receiving Antennas		
Doppler-Frequency and Amplitude Measurements	150-ft dish	48-element log-periodic array
Faraday-Rotation Measurements	60-ft dish with crossed-dipole feed	2 crossed-dipole yagis
Receiver Bandwidths		
Doppler-Frequency Measurements	2 kc	1 kc
Amplitude Measurements	0.1 kc	0.1 kc
Faraday-Rotation Measurements	0.1 kc filter detector	0.1 kc filter detector

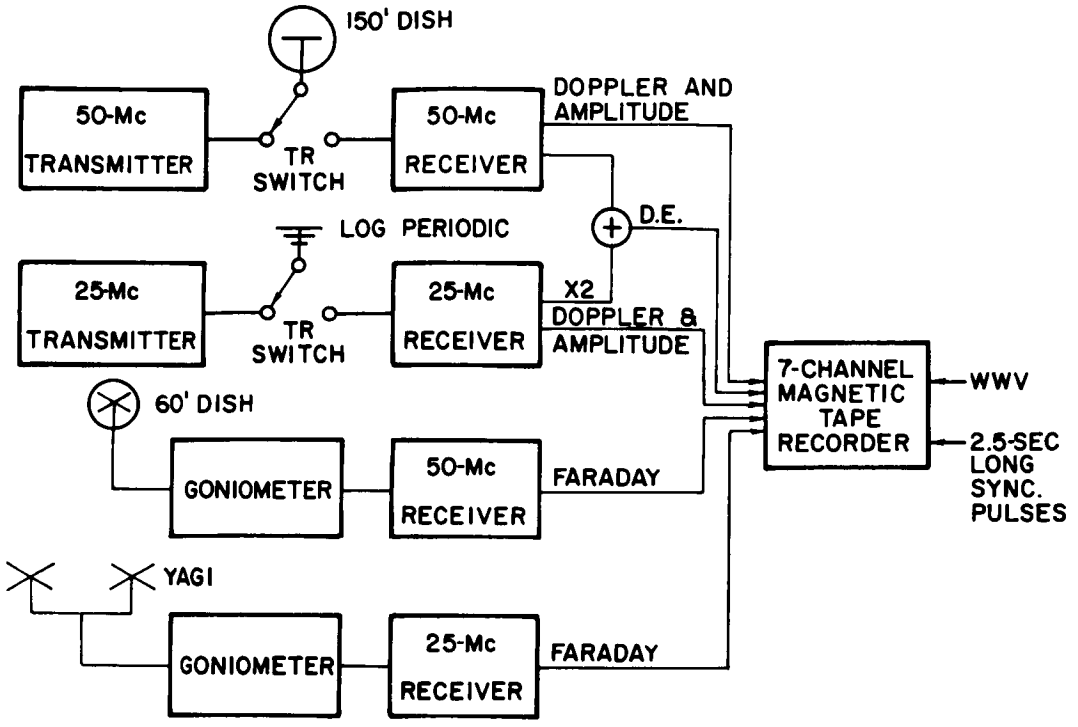

31650

FIG. 2. BLOCK DIAGRAM OF SYSTEM USED FOR MOON-ECHO EXPERIMENTS.

The same transmitting antennas were used for the three types of measurements recorded--a 150-ft dish for 50 Mc and a 48-element log-periodic array for 25 Mc. Receiving antennas, however, were varied, as shown in the listing above. The complete cycle of operation for all was 5 sec--a 2.5-sec transmission pulse followed by an equal period of reception. All the information was recorded on a seven-channel magnetic-tape recorder.

The transmitting antennas were also used as receiving antennas for the Doppler-excess-frequency measurements and the amplitude measurements, as shown in the listing. (The information on the amplitudes was not used in this study but was stored for other studies--e.g., irregularities of the medium.)

For the Faraday-polarization measurements at 50 Mc, the 60-ft dish receiving antenna was located within 1 km of the transmitting antenna,

and the crossed-dipole feed lines were terminated in a rotating-capacitor goniometer, whose output was connected to a receiver. The 25-Mc Faraday-polarization measurements were not used in the present study because the signals were much weaker than the 50-Mc signals and gave no additional information on the electron content of the ionosphere.

Data processing consisted of two steps as shown in Fig. 3--(1) converting the analog form of signals into digital form, and (2) using an IBM-7090 digital computer to reduce the data.

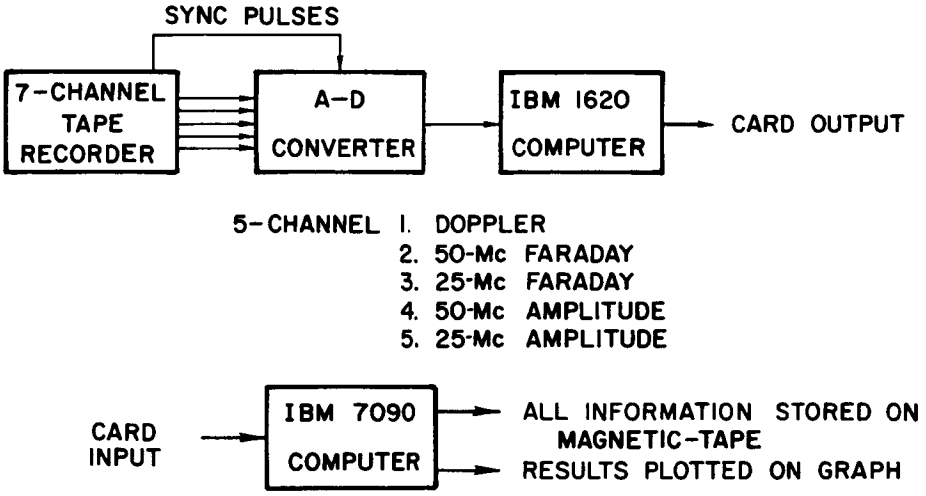

31649

FIG. 3. BLOCK DIAGRAM OF DATA-PROCESSING EQUIPMENT FOR MOON-ECHO MEASUREMENTS.

The first step involved the process of converting the analog forms of signals into digital forms by means of the analog-to-digital converter, the IBM-1620 computer, and recording equipment, as shown in Fig. 4. The Sanborn tape recorder is shown on the panel second from the left. To the right of the recorder is the panel for the multiverter, the multiplexer, and the timer. The output of the converter is connected to the digital computer in the same room (not shown). The computer was used to command the start of sampling and to store the samples

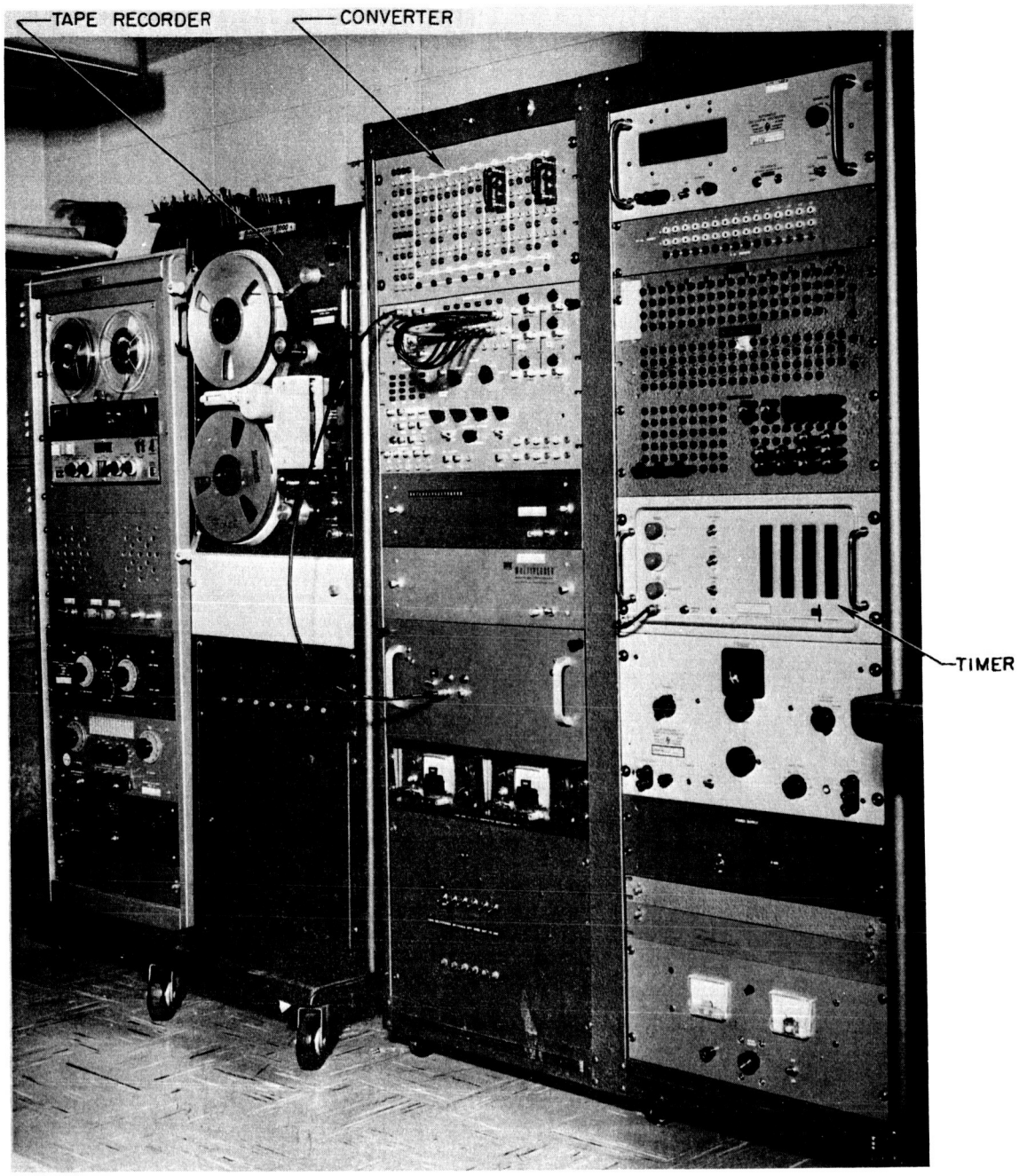

FIG. 4. EQUIPMENT FOR DATA CONVERSION.

in the computer memory during the 2.5-sec receiving period. The computer edited the earlier-received data during the following 2.5-sec transmitting period and punched the data on cards. (The detailed process of converting the lunar-radar echoes to digital form is described in Appendix A.)

The cards were then fed into the IBM-7090 for the second processing step, the main functions of which were to:

1. Select good data.
2. Search for the minimum position of the Faraday polarization signal. Since the goniometer rotates the receiver-antenna polarization synchronously with the 5-sec transmit-receive period, the position of the minimum signal strength is a direct measure of the Faraday-polarization angle of the received signal.
3. Calculate the true Doppler excess frequency for each operation cycle. The point-by-point Doppler excess frequency was smoothed by taking a running mean of the data over successive 1-min intervals. This procedure eliminated the large spread introduced by the libration of the moon. The resulting running-mean values of Doppler excess frequency were proportional to the time rate of change of electron content along the path between the earth and the moon. This time rate of change was then integrated to give the net change of electron content.

The output of the computer consisted of Faraday polarization angles at 25 Mc and 50 Mc, the Doppler excess frequency, the running mean of Doppler excess frequency, and the integrated mean Doppler excess frequency. Figure 5 shows typical results of one day's measurements. It is clear that the results of Faraday polarization at 50 Mc were much better than those at 25 Mc. The electron content in the ionosphere (measured by the Doppler) as well as the number of rotations of the Faraday polarization were decreasing at this particular time, as can be seen in the figure.

The bottom two plots are the results of the Doppler-excess-frequency measurements. The discontinuities in the mean Doppler excess frequency were caused by the following factors:

1. Because of the limited size of the memory of the IBM-7090 computer, the processing was carried out in only 20-min intervals.

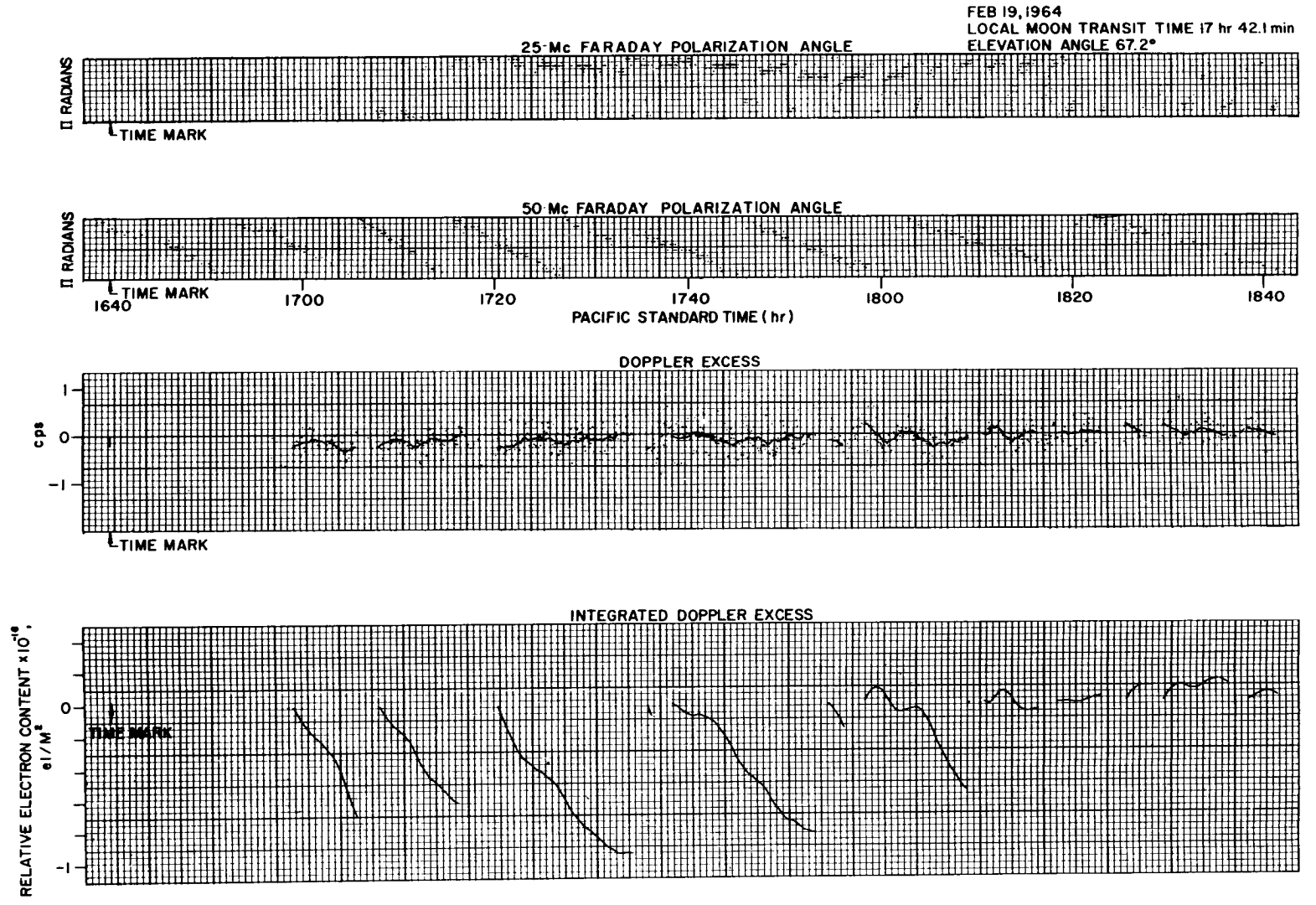

FIG. 5. TYPICAL OUTPUT OF IBM-7090 COMPUTER. The top two graphs show the positions of the Faraday polarization angles for 25 and 50 Mc, plotted in opposite directions because of the equipment setup. The third graph shows the individual Doppler excess frequency (dots) and the running mean of the Doppler excess frequency (lines). The bottom graph presents the integrated values of the mean Doppler excess frequency.

2. If fewer than three Doppler-excess-frequency values existed in a 1-min interval, the resulting running-mean value was discarded and discontinuities occurred.

The integrated values of mean Doppler excess were plotted on the ordinate of the last graph with units of 10^{16} el/m^2. The reasons for the discontinuities in the line are the same as above. All the curves were plotted against local standard time (Pacific Standard Time = UT-8 hr).

Figures 6 and 7 show typical results obtained with the second step on the IBM-7090 computer. To obtain these continuous plots, a new computer program was written in such a fashion that only one type of measurement was read into the computer memory, from a magnetic tape that was used to store data after the first process, thus eliminating the 20-min time limitation. For the insufficient points of Doppler excess frequency, extrapolation to the nearest points both before and after was used to obtain a necessary minimum number of points for the averaging. The same method was applied to the Faraday-polarization data.

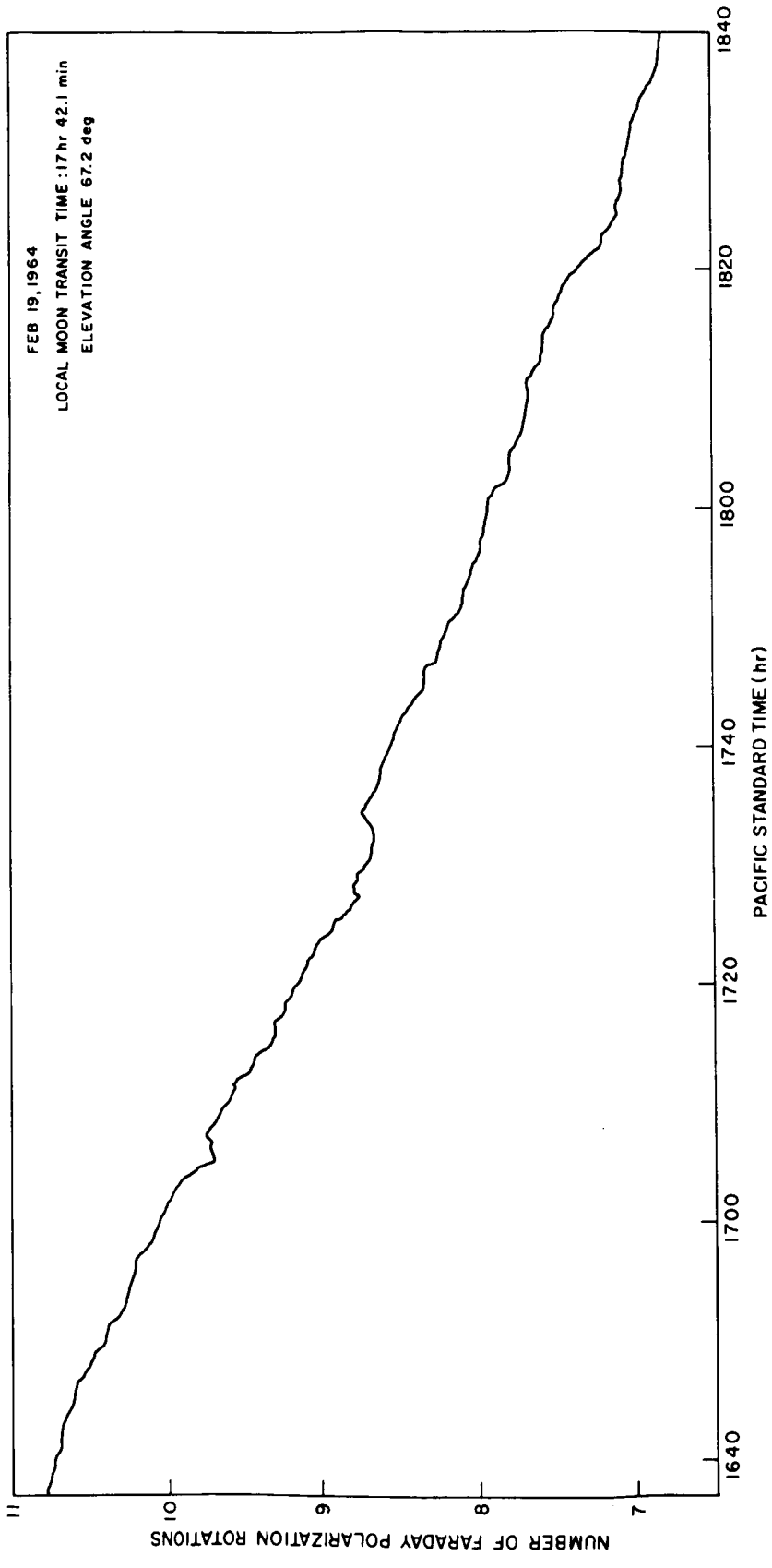

FIG. 6. TYPICAL RESULT OF FARADAY-POLARIZATION MEASUREMENT.

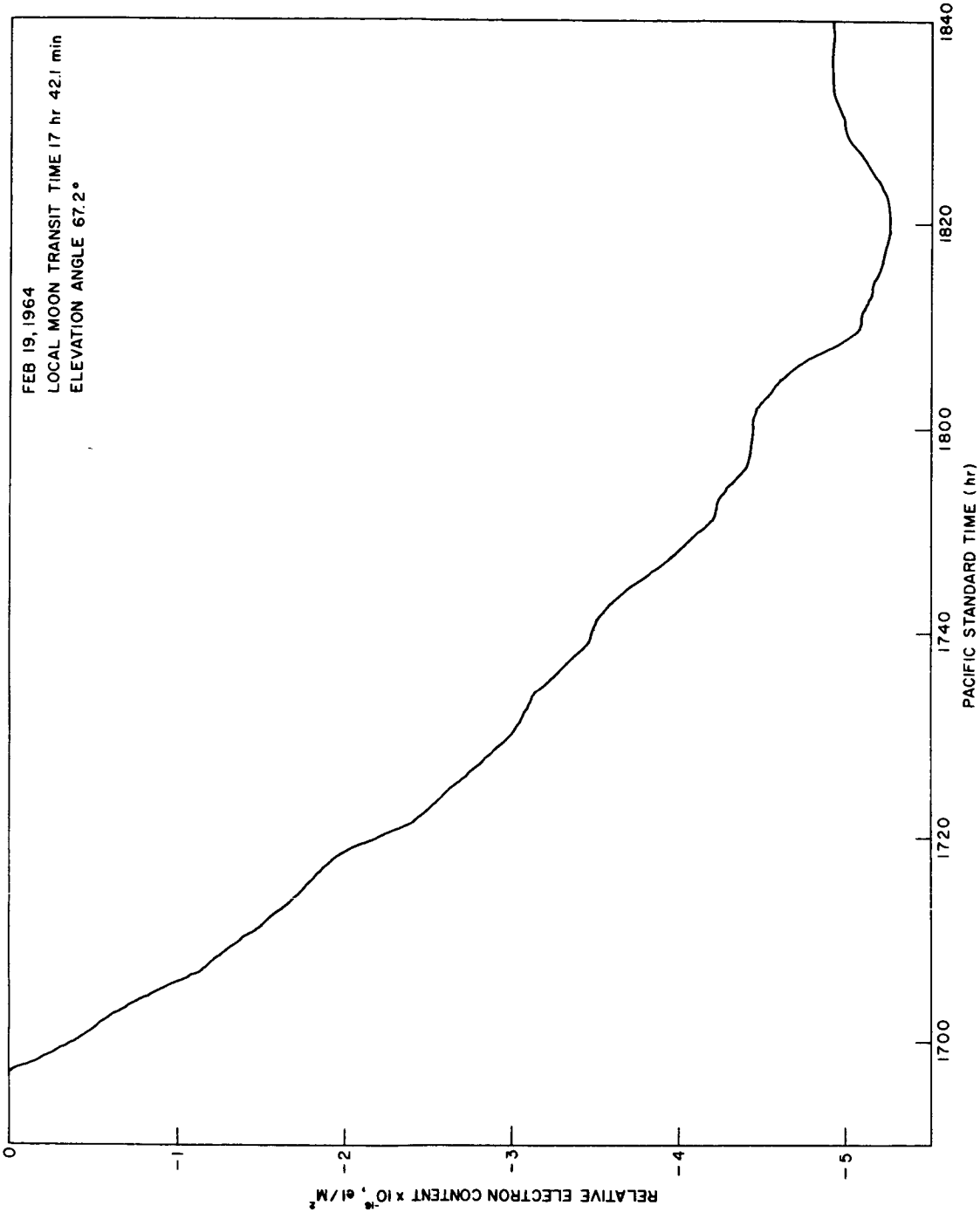

FIG. 7. TYPICAL RESULT OF DOPPLER-EXCESS-FREQUENCY MEASUREMENT.

IV. IONOSPHERIC-ELECTRON-DENSITY PROFILE

A. GEOMAGNETIC FIELD

In the course of investigating the propagation of radio waves through the ionosphere, it became necessary to calculate the magnitude and direction of the geomagnetic fields as accurately as possible. In the present calculation, a sixth-order spherical harmonic model was adopted. It can be shown [Ref. 24] that the accuracies of the magnitude and direction of the geomagnetic field are 1 percent and 0.5 deg, respectively. A computer program originally written by Yeh and Gonzalez [Ref. 25] was subsequently translated into computer language for the equipment at Stanford Computer Center by da Rosa. The gaussian coefficients used are those computed by Jenson [Ref. 26]. Figure 8 shows the values of $H \cos \theta$ at 400 and 500 km as a function of azimuth. Each curve represents a moon sweep past the antenna beam for a given elevation angle at the meridian plane. It can be seen that for one sweep the value of $H \cos \theta$ varies slowly with respect to the position of the moon.

B. CHAPMAN MODEL

In this section two types of the Chapman model will be taken into consideration. They are the usual, simple Chapman model (constant scale height) and the modified Chapman model (scale height increasing linearly with height). The ratio of the number of Faraday rotations above 2000 km to those below this height can be calculated. The variation of height of the maximum electron density is taken into account.

The expression for the well-known simple Chapman model for electron-density distribution in the ionosphere is given as

$$N_e = N_{max} \exp\left[\frac{1}{2}(1-z-e^{-z})\right]. \qquad (4.1)$$

(The symbols used in this equation are given in the Notation.)

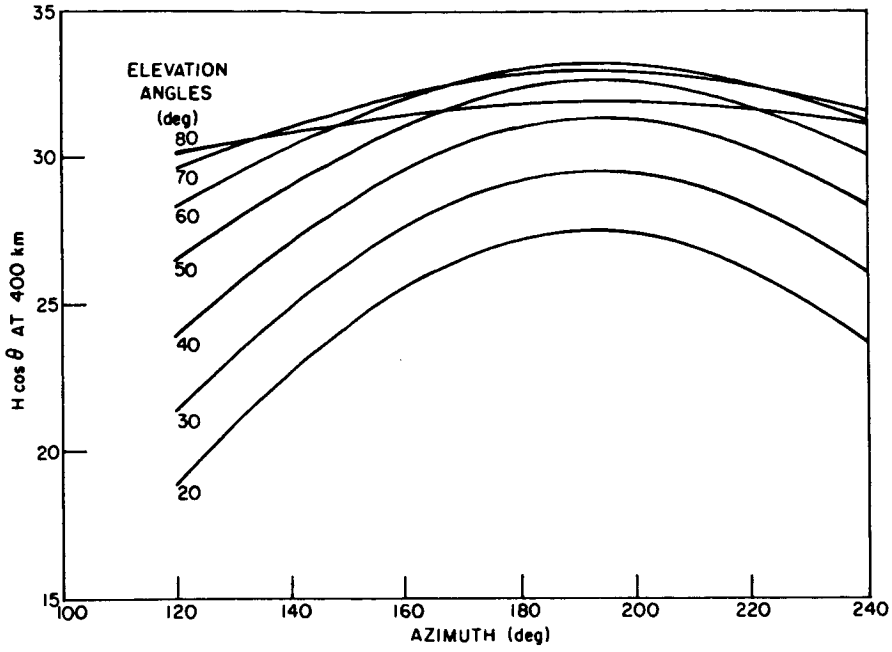

a. At 400 km

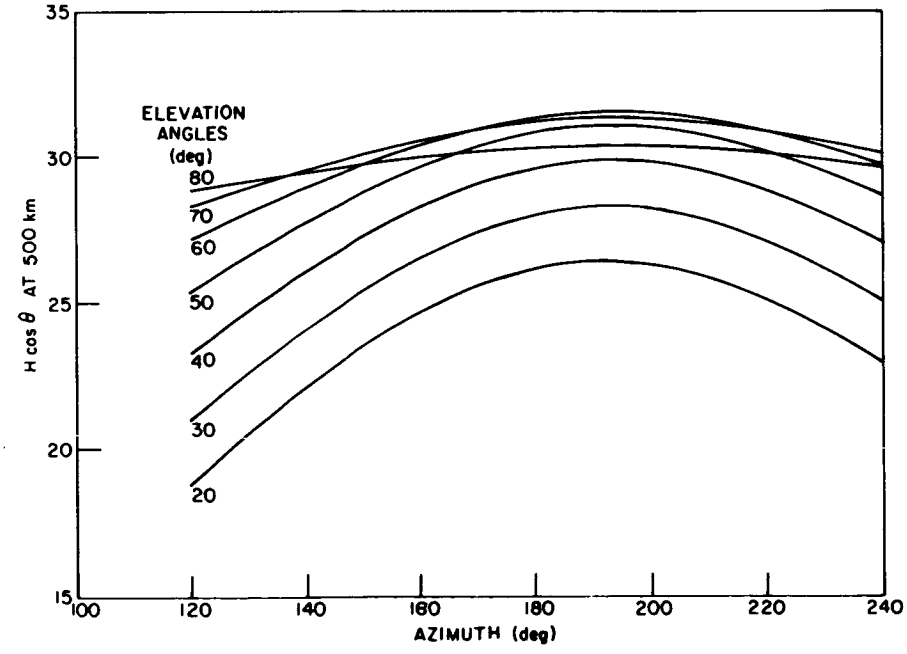

b. At 500 km

35261

FIG. 8. VALUES OF H cos θ AS A FUNCTION OF AZIMUTHAL ANGLE.

Wright [Ref. 27] has found a Chapman model (scale height of 100 km) to be in good agreement with observed profiles. Figure 9 shows the simple Chapman profile for scale heights of 80 and 120 km and h_{max} of 200 and 400 km. Later, Nisbet [Ref. 28] and Berning [Ref. 29] suggested that the scale height of electron density above the maximum electron density increases linearly with height. The rate of increasing scale

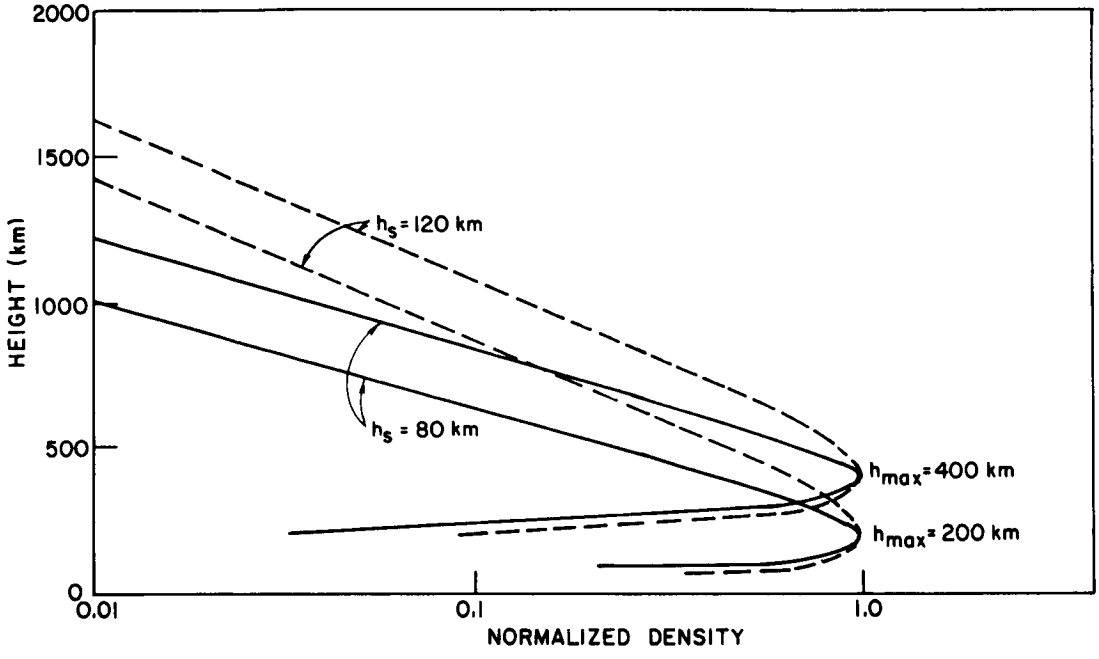

35262

FIG. 9. NORMALIZED ELECTRON-DENSITY PROFILE FOR CHAPMAN MODEL WITH CONSTANT SCALE HEIGHT.

height is about 0.15 km/km. Figure 10 shows electron-density profiles for two scale-height values at the height of maximum electron density. The lower value of scale height, 40 km, is close to that measured by Berning [Ref. 29].

The number of Faraday rotations can thus be calculated if $H \cos \theta$ and N are known. The model of H has been discussed in Section A, and Eq. (4.1) gives the expression for the electron-density distribution for the Chapman model. The calculations for the number of Faraday rotations in this model are divided into two parts--the first part

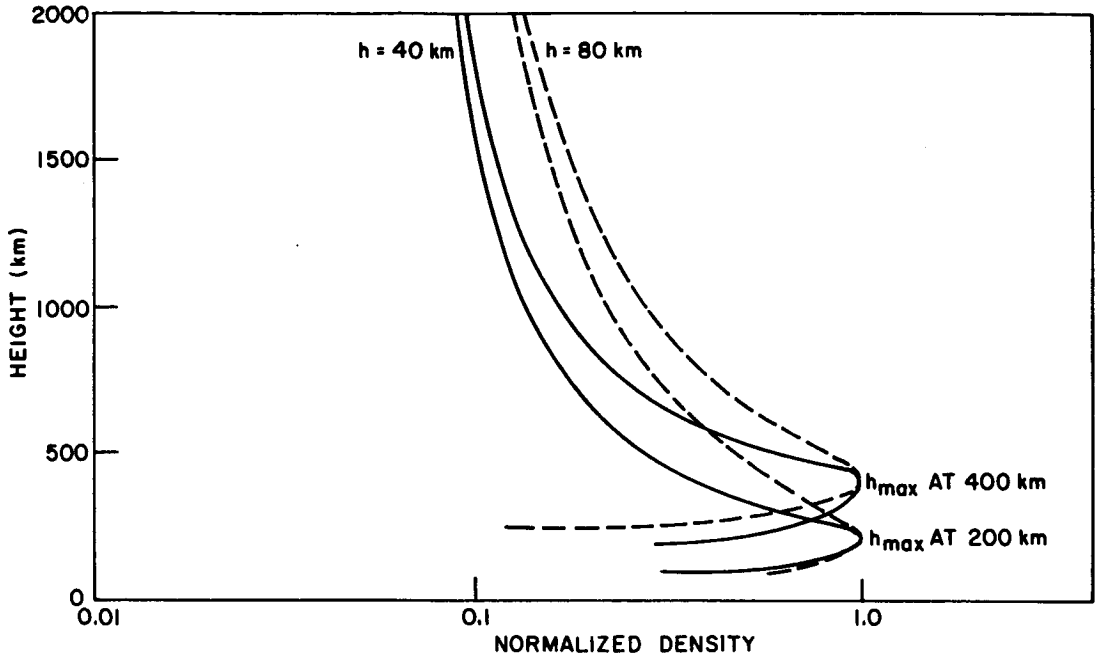

FIG. 10. NORMALIZED ELECTRON-DENSITY PROFILE FOR CHAPMAN MODEL WITH SCALE-HEIGHT GRADIENT OF 0.15 KM/KM.

involves calculating the rotations up to the height of 2000 km; the second calculating beyond 2000 km by means of the expression

$$(H \cos\theta \, N_e h_s)\Big|_{2000 \text{ km}} ,$$

where the value of the magnetic field, the electron density, and the scale height at 2000 km are known. Since the expression is a Chapman function, at great height it is nearly an exponential function and is easy to integrate. It can be shown that, for an exponential type of electron distribution, the following inequality is true:

$$(H \cos\theta \, N_e h_s)\Big|_{2000 \text{ km}} > \int_{2000 \text{ km}}^{\infty} H \cos\theta \, N_e ds . \qquad (4.2)$$

Because the value of H decreases with the increase of altitude, the number of Faraday rotations calculated is the upper limit. Table 1 shows the results of calculations for different scale heights and heights of maximum electron density. It is assumed that the value of maximum electron density is 10^6 electrons/cc.

TABLE 1. CALCULATION OF NUMBER OF FARADAY ROTATIONS

Parameter	h_{max} (km)	h_s (km)	No. of Faraday Rotations	
			Ω (for h < 2000 km)	Ω (for h > 2000 km)
Constant scale height	200	80	21	0.042
		120	26	0.044
	400	80	19	0.038
		120	24	0.040
Scale-height gradient 0.15 km/km	200	40	22.6	0.43
		80	42.7	0.64
	400	40	20.6	0.41
		80	39.4	0.63

The next step is to calculate the ratio of the Faraday polarization above 2000 km to that below, by means of

$$R = \frac{(H \cos \theta \, Nh_s)\Big|_{2000 \text{ km}}}{\int_0^{2000} H \cos \theta \, Ndh} .$$

Table 2 gives the result of such a calculation for different scale heights and heights of maximum electron density.

TABLE 2. RATIO OF NUMBER OF FARADAY ROTATIONS ABOVE 2000 KM TO THAT BELOW

Parameter	h_{max} (km)	h_s (km)	Ratio R
Constant scale height	200	80	0.002
		120	0.0017
	400	80	0.0019
		120	0.0017
Scale-height gradient 0.15 km/km	200	40	0.019
		80	0.015
	400	40	0.020
		80	0.016

C. DIFFUSIVE-EQUILIBRIUM MODEL

Recent measurements of the electron density in the topside ionosphere [Refs. 7, 30-32] show that the distribution of electron density departs from Chapman's model. The results of analyses of these measurements indicate that at least the topside-ionosphere electron-density profile is much closer to the diffusive-equilibrium model. The measurements by the Ariel [Ref. 33] and Alouette [Ref. 7] satellites show that there are three main ionic constituents--O^+, He^+, and H^+. The level at which two ionic constituents have the same density varies with the time of day and latitude.

The electron temperature has been found to be much higher than the neutral-particle temperature in the upper atmosphere [Ref. 34]. The ion temperature approaches the electron temperature at high altitudes whereas, at low altitudes, it is close to the neutral-particle temperature. All temperatures vary with the time of day as well.

1. Theory

In the upper ionosphere, where the production and loss rates are small, the major processes of removing or restoring ionization is largely due to vertical-transport movement. For low collision rates [Ref. 35], the momentum-transport equation for the electrons is given as

$$kT_e N_e \frac{\partial N_e}{\partial h} = -gm_e N_e - qEN_e \tag{4.3}$$

and that for the ions of one species is

$$kT_i \frac{\partial N_i}{\partial h} = -gm_i N_i + qEN_i \ . \tag{4.4a}$$

The expression for more than one type of ion is simply summing over Eq. (4.4) for various ionic species to give

$$kT_i \sum_i \frac{\partial N_i}{\partial h} = -g \sum_i m_i N_i + qE \sum_i N_i \ , \tag{4.4b}$$

assuming that all species of ions have the same temperature. Assume that charge neutrality exists in the region; then

$$N_e = \sum_i N_i \tag{4.5}$$

and

$$\frac{\partial N_e}{\partial h} = \sum_i \frac{\partial N_i}{\partial h} \ . \tag{4.6}$$

From Eqs. (4.3) and (4.4a) and the relations given above, one finds a first-order differential equation for the electron density

$$\frac{1}{N_e} \frac{\partial N_e}{\partial h} = - \frac{gM_+}{(T_e+T_i)k} \tag{4.7}$$

where M_+ is mean ionic mass, which could also be expressed as

$$M_+ = \frac{\sum_i N_i m_i}{\sum_i N_i} \quad .$$

Equation (4.7) is easily integrated, giving

$$N_e(h) = N_e(h_o) \exp\left[- \int_{h_o}^{h} \frac{gM_+}{k(T_e+T_i)} \right] dh \quad , \tag{4.8}$$

where h_o is the base level for the diffusive-equilibrium region. From Eqs. (4.3), (4.4a), and (4.7), the single species ion distribution is given as

$$N_i(h) = N_i(h_o) \exp\left[\int_{h_o}^{h} \frac{gM_+}{k(T_e+T_i)} \frac{T_e}{T_i} dh - \int_{h_o}^{h} \frac{m_i g}{kT_i} dh \right] \quad . \tag{4.9}$$

Thus the mean mass M_+ can be obtained from Eq. (4.9) as

$$M_+ = \frac{\sum_i m_i N_i(h_o) \exp\left[- \int_{h_o}^{h} (m_i g/kT_i) dh \right]}{\sum_i N_i(h_o) \exp\left[- \int_{h_o}^{h} (m_i g/kT_i) dh \right]} \quad . \tag{4.10}$$

Note that the mean mass is a function of the ion temperature only. The transition level is defined at a certain height where two ionic species have the same density, i.e.,

$$N_1(h) = N_2(h) \quad . \tag{4.11}$$

Substituting Eq. (4.9) into (4.11) yields

$$N_1(h_o) \exp\left[- \int_{h_o}^{h} \frac{m_1 g}{kT_i} dh \right] = N_2(h_o) \exp\left[- \int_{h_o}^{h} \frac{m_2 g}{kT_i} dh \right] \tag{4.12}$$

$$\frac{N_1(h_o)}{N_2(h_o)} = \exp\left[-\int_{h_o}^{h} \frac{(m_2-m_1)g}{kT_i}\,dh\right] \tag{4.13}$$

or

$$\ell n\,\frac{N_1(h_o)}{N_2(h_o)} = -\int_{h_o}^{h} \frac{(m_2-m_1)g}{kT_i}\,dh\ . \tag{4.14}$$

Equation (4.14) states that, when the ratio of the ionic composition at the base level is known, the height of the transition level can be determined; or, when the height of the transition level is given, then the ratio of the ionic composition at the base level can be found, provided that the ion temperature is known for all heights.

2. Profile Fitting

In this part, the electron-density profile obtained from Alouette topside-sounder measurements [Ref. 31] at the midlatitude is to be fitted to the model by the diffusive-equilibrium model for the different times of day. The values of ion and electron temperatures are adopted from incoherent-backscatter measurements [Ref. 34]. It is assumed that the temperature above 700 km is constant; this assumption seems to be quite reasonable, since Evan's incoherent measurement [Ref. 35] and rocket measurement [Ref. 36] show that the electron temperature is approaching a constant value at high altitudes--above approximately 500 km. The electron-density profile is fitted by varying the relative ionic concentration at the base level, which is chosen as 400 km because the range of the electron-density profile from the topside-sounder measurements is between 400 to 1000 km. Finally, from the calculated profile, the heights of the transition levels can be calculated for different times of day. These transition levels will be compared with the measured transition levels at midlatitudes [Ref. 33].

Figure 11 shows the normalized measured electron-density profiles. It is clear that the shape of the upper ionosphere changes greatly throughout the day. Hence there is no standard electron-density profile to fit the distribution at all times.

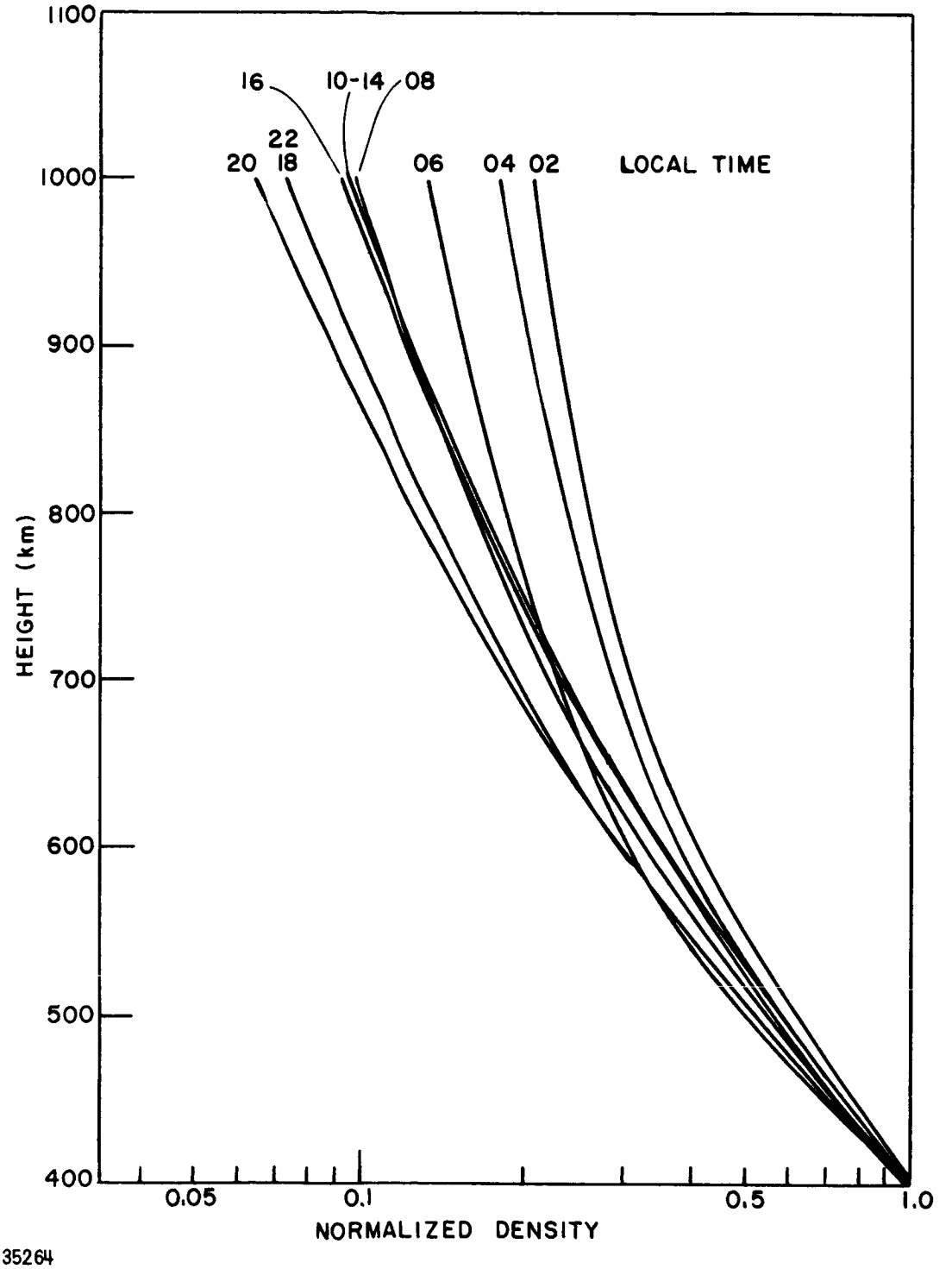

FIG. 11. NORMALIZED MEASURED TOPSIDE ELECTRON-DENSITY PROFILE AT MIDLATITUDE FOR DIFFERENT LOCAL TIMES.

Figures 12 to 15 show the calculated and the measured electron-density profiles at sunrise, noon, sunset, and near-midnight. The bottom-side electron-density distribution is fitted to the ionogram-sounder measurements at Stanford. Electron density at all heights is normalized to 400 km.

Figure 16 shows that the heights of the transition levels of O^+ and He^+ from the calculated profile are in good agreement with the transition levels measured by Ariel satellite [Ref. 33]. These measurements were taken at different years and during various seasons, but all measurements were taken near sunspot minima (i.e., between 1962 and 1964).

3. Number of Faraday Rotations and the Ratio R

From Section A and the previous two parts, the number of Faraday rotations can be calculated. The following tabulation shows the results of the calculation for different times of the day--sunrise, noon, sunset, and midnight.

Height of Ω (km)	No. of Faraday Rotations at Local Time (hr)			
	0600	1200	1800	2200
< 2000	5.1	18	10.4	4.0
> 2000	0.45	1.0	0.6	0.25

The ratio R can be calculated from the above table. The results of the calculations are shown below.

Local Time	Ratio R	Local Time	Ratio R
0600	0.09	1800	0.05
1200	0.05	2200	0.06

The number of Faraday rotations above 2000 km is less than 10 percent of the total number of rotations.

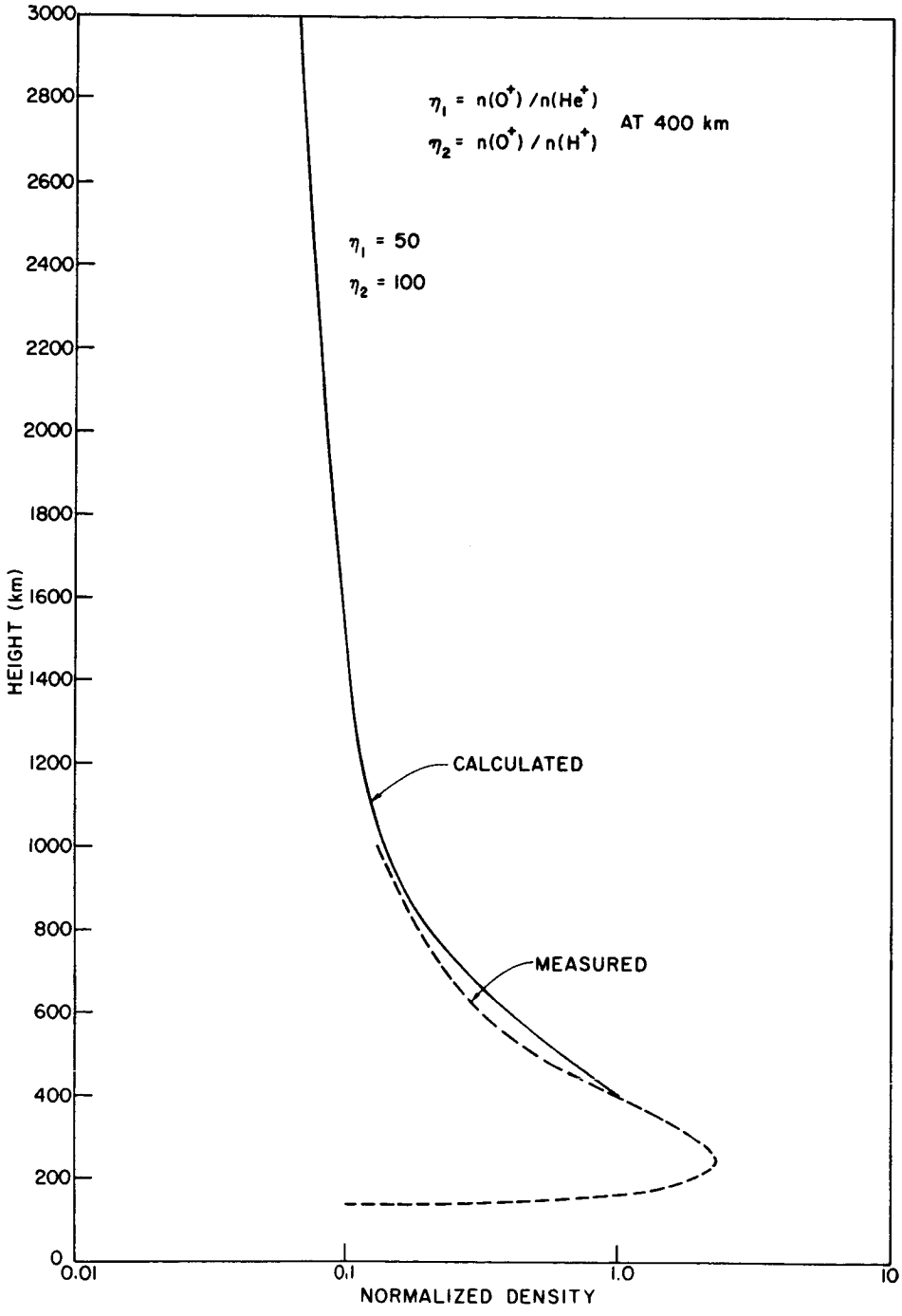

35265

FIG. 12. COMPARISON OF MEASURED TOPSIDE ELECTRON-DENSITY PROFILE AND THEORETICAL PROFILE FOR 0600 LMT.

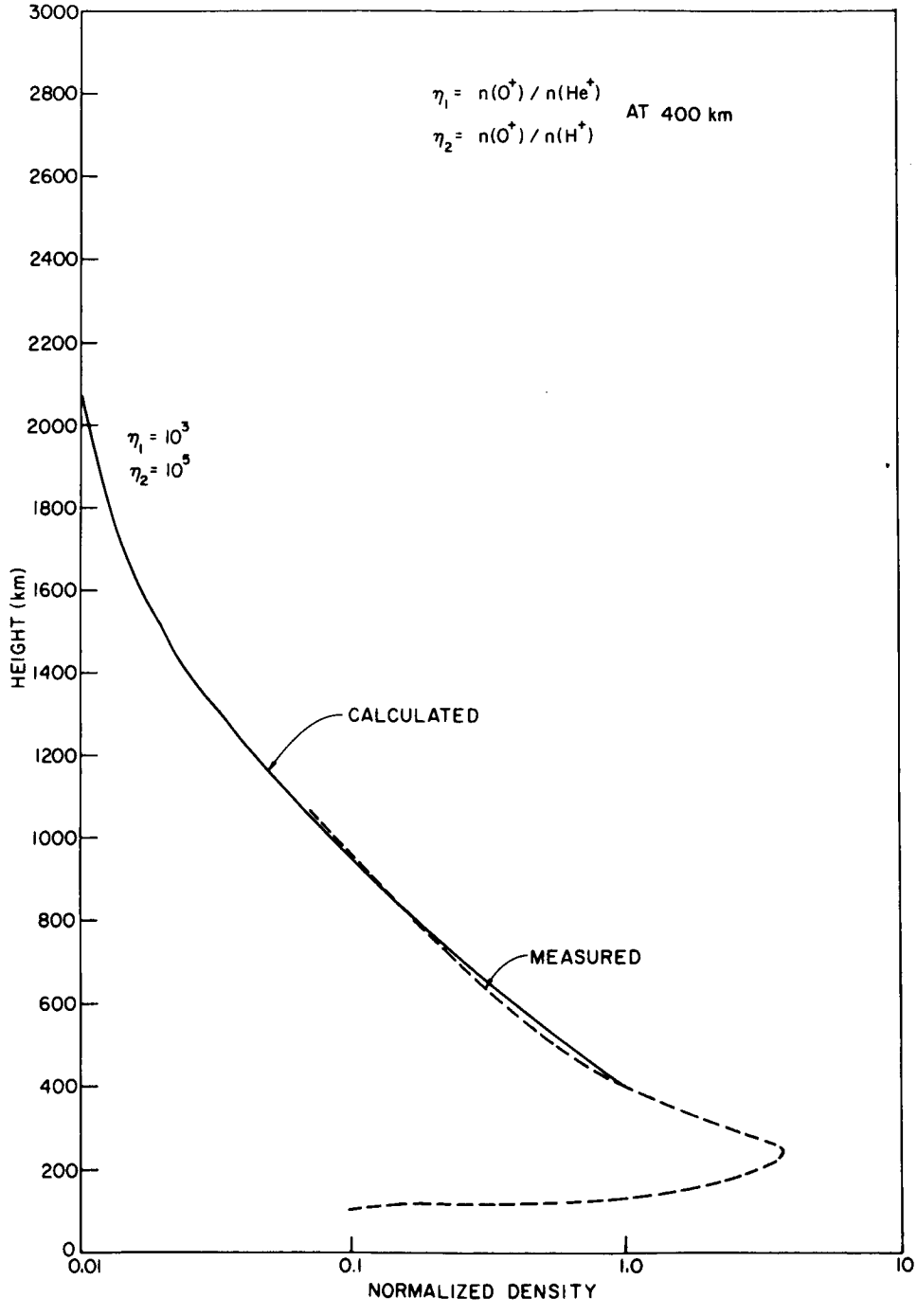

35266

FIG. 13. COMPARISON OF MEASURED TOPSIDE ELECTRON-DENSITY PROFILE AND THEORETICAL PROFILE FOR 1200 LMT.

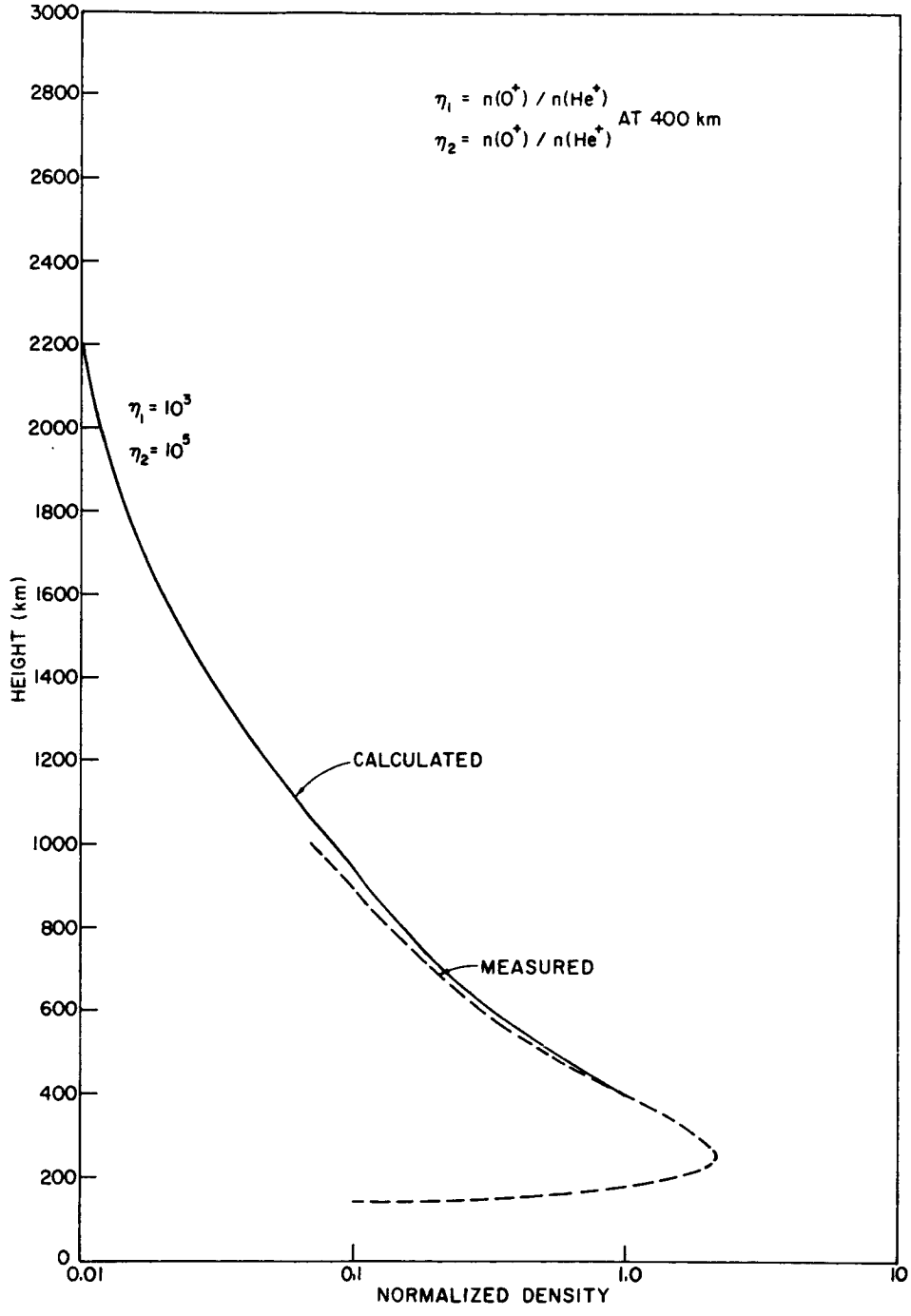

35267

FIG. 14. COMPARISON OF MEASURED TOPSIDE ELECTRON-DENSITY PROFILE AND THEORETICAL PROFILE FOR 1800 LMT.

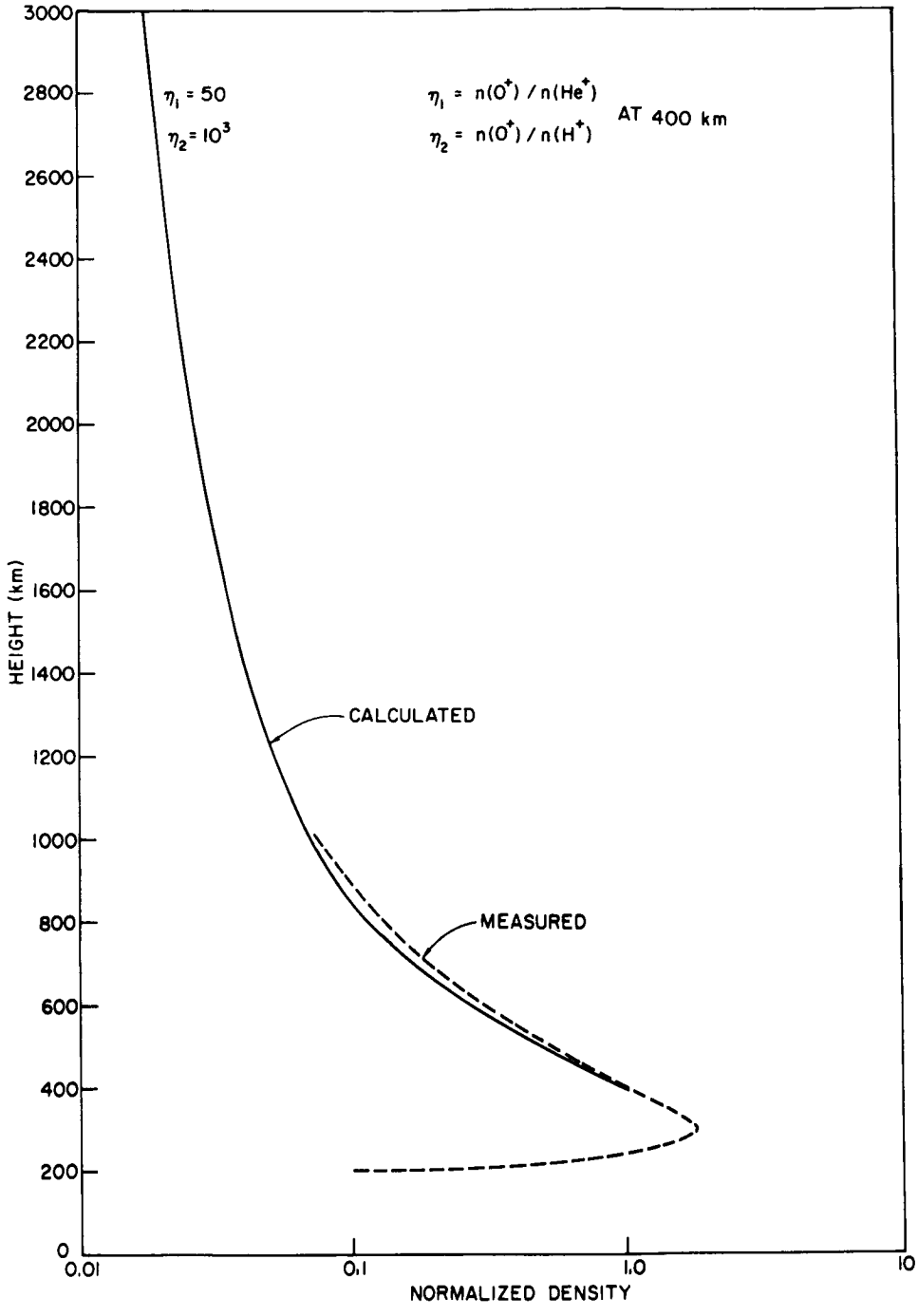

35268

FIG. 15. COMPARISON OF MEASURED TOPSIDE ELECTRON-DENSITY PROFILE WITH THEORETICAL PROFILE FOR 2200 LMT.

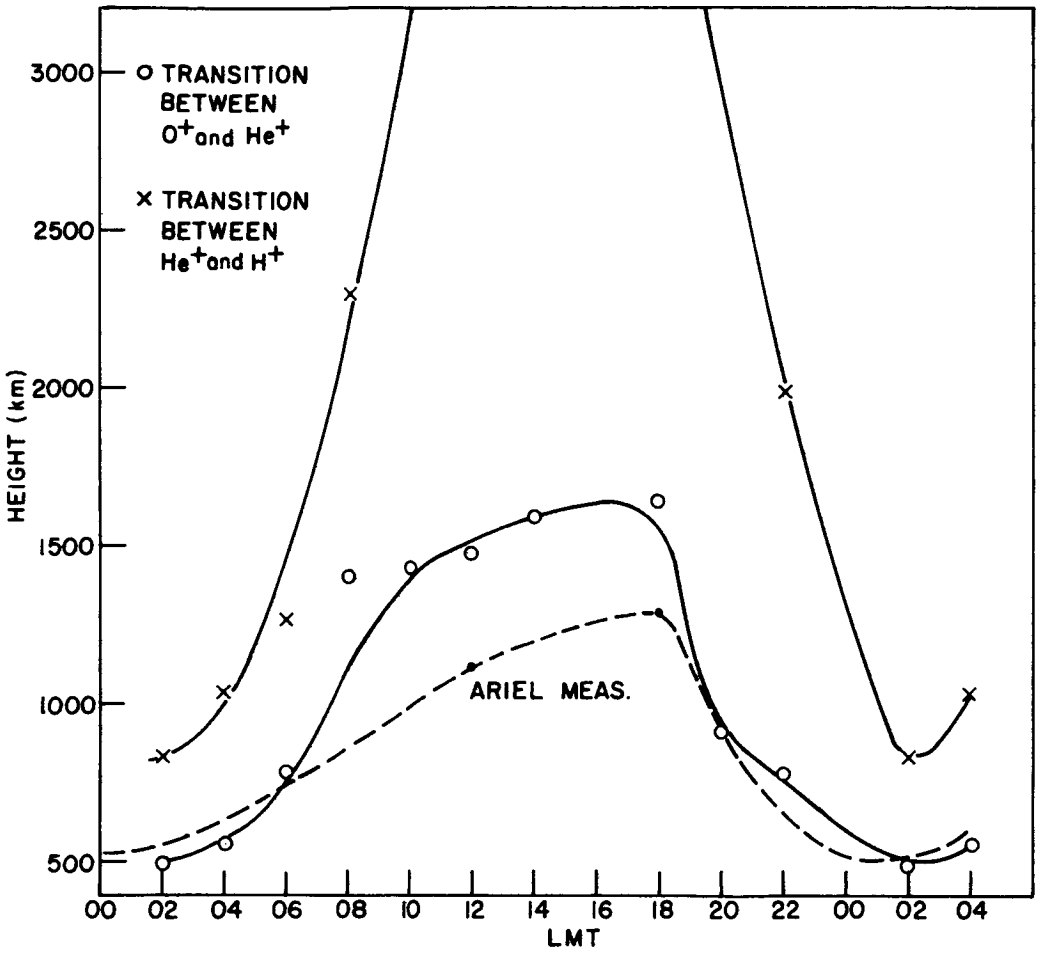

35269

FIG. 16. COMPARISON OF MEASURED TRANSITION LEVELS OF O^+ AND He^+, FROM ARIEL [REF. 33], WITH THEORETICAL RESULTS.

D. ERROR OF ESTIMATING ELECTRON-DENSITY CONTENT FROM FARADAY-ROTATION MEASUREMENTS

In the last two sections, it was shown that over 90 percent of Faraday rotations occurred in the range within 2000 km above the surface of the earth. The steps of estimating the error of electron content from the Faraday-polarization measurements are as follows:

1. The electron content and the number of Faraday rotations are calculated up to the height of 2000 km.
2. From the number of Faraday rotations, the electron content at 400 km for daytime and 500 km for nighttime is calculated by using the value of $\overline{H \cos \theta}$.

The results of the above calculations are shown in Figs. 17 and 18 for Chapman and diffusive-equilibrium models respectively. The positive error indicates that the electron content calculated from Eq. (2.21) is higher than that of the given profile; the negative error indicates the reverse. It is shown in these two figures that the error in estimating the electron content up to 2000 km is less than 10 percent.

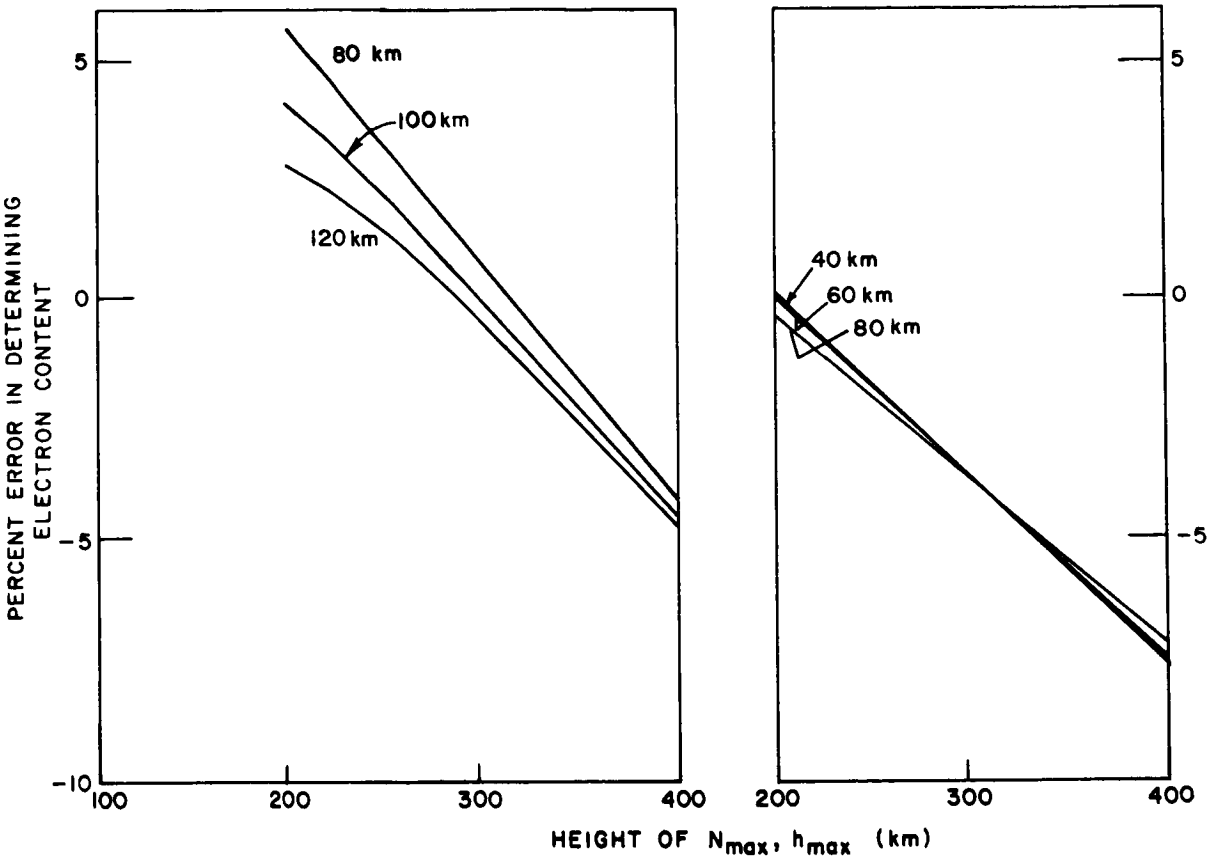

35270

a. Constant scale height

b. 0.15-km/km scale-height gradient

FIG. 17. ERROR OF CALCULATING ELECTRON CONTENT FROM FARADAY METHOD FOR CHAPMAN MODELS.

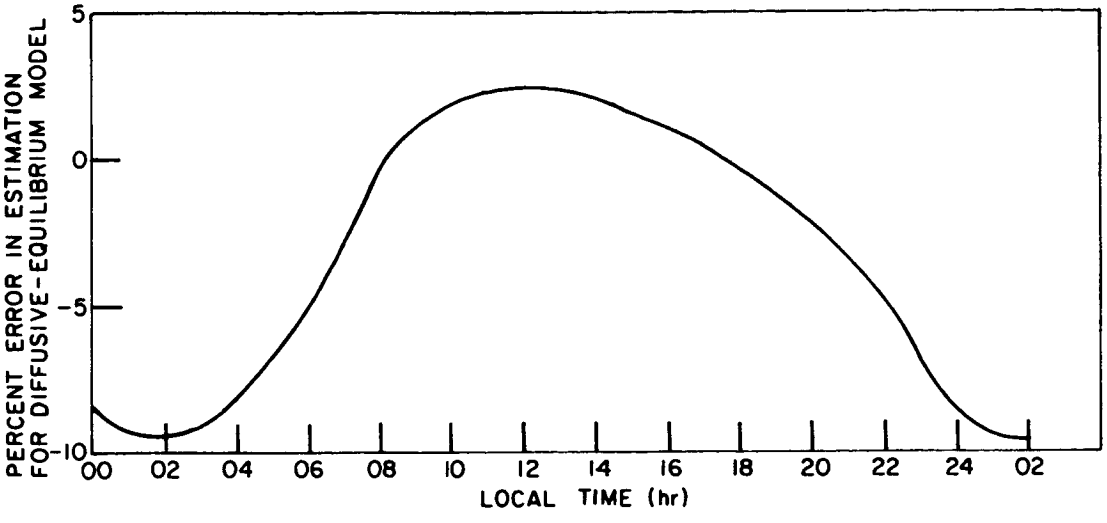

35271

FIG. 18. ERROR OF CALCULATING ELECTRON CONTENT FROM FARADAY METHOD FOR DIFFUSIVE-EQUILIBRIUM MODEL.

V. RESULTS OF ANALYZED DATA

A. RESULTS OF COMBINED DOPPLER AND FARADAY MEASUREMENTS

It was shown in Chapter IV that the Faraday-polarization measurement is a good way to measure the electron content in the ionosphere. Since the experiment was conducted over a period of two to three hours daily, the Faraday-polarization measurement should indicate the electron content as well as the change of electron content in the ionosphere. The expression for Faraday rotation related to the electron content is given, from Eq. (2.21), as

$$\int_o^h N_e ds = \frac{f^2}{2K} \frac{\Omega}{\overline{H \cos \theta}} . \tag{5.1}$$

The change of columnar electron content measured by the Faraday polarization is defined as

$$\Delta I_F(t) = \frac{f^2}{2K} \left(\frac{\Omega(t_i)}{\overline{H \cos \theta}(t_i)} - \frac{\Omega(t)}{\overline{H \cos \theta}(t)} \right), \tag{5.2}$$

where t_i refers to the starting time of the experiment and t is any time after t_i.

Equation (2.15) shows that the time rate of change of electron content along the entire lunar radar path is proportional to the Doppler excess frequency. Over a period of two to three hours of observation, both the earth and moon move in space, and one should observe changes of electron content both in time and space. Therefore the time integral of the Doppler excess frequency is a direct measure of any changes of electron content along the radar path. The change of electron content ΔI_D measured by this method is

$$\Delta I_D(t) = \frac{fc}{80.6} \left(\frac{n}{n^2-1} \right) \int_{t_i}^{t} f_b \, dt . \tag{5.3}$$

Since ΔI_D is a measure of the change of electron content along the entire path and ΔI_F is a measure of the change of part of the path,

the difference between these two quantities will be a measure of the change of electron content occurring beyond the ionosphere. Figure 19 shows some of the individual daily measurements. The vertical bars denote the uncertainty of the measured quantities, which is due to the uncertainty of the shape of the electron-density profile in the ionosphere (see Section IV.D). One remarkable feature of Fig. 19 is that, in the morning, the region beyond the ionosphere shows quite a large increase of ionization and in the afternoon the results show a large decrease of ionization beyond the ionosphere.

Since the daily measurements cover only a few hours a day, the average rates of change of electron content were calculated from all the measurements in order to see the diurnal and spatial variations. The relative electron content results from the integration of the average rate of change of electron content.

Figure 20 shows the relative electron contents for two different measurements. The solid curve represents the results measured from the Doppler excess frequency and the dashed curve represents those from Faraday polarization. The Faraday-polarization measurement shows a normal variation of electron content in the ionosphere (i.e., the electron content increases rapidly after the sunrise and reaches the maximum value near noon, starts to decay in the afternoon until after sunset, and remains fairly constant throughout the night).

The Doppler-excess-frequency measurement shows the normal variation of electron content in the ionosphere in the daytime as it should be. In addition, the Doppler excess frequency shows two main interesting features that are not detected by Faraday polarization--they are the predawn decay and postsunset increase of ionization. These interesting features are sure to have occurred in the region beyond the ionosphere. Figure 21 shows the difference between the two curves shown in Fig. 20--i.e., $I_D - I_F$. Here the variation of the electron content beyond the ionosphere exhibits a semidiurnal pattern. It is believed that the daytime peak is due to diurnal exchange of ionization between the upper ionosphere and lower magnetosphere and that the nighttime peak is due to a high electron density inside the earth's magnetospheric tail. These two subjects are discussed in some detail in Chapters VI and VII.

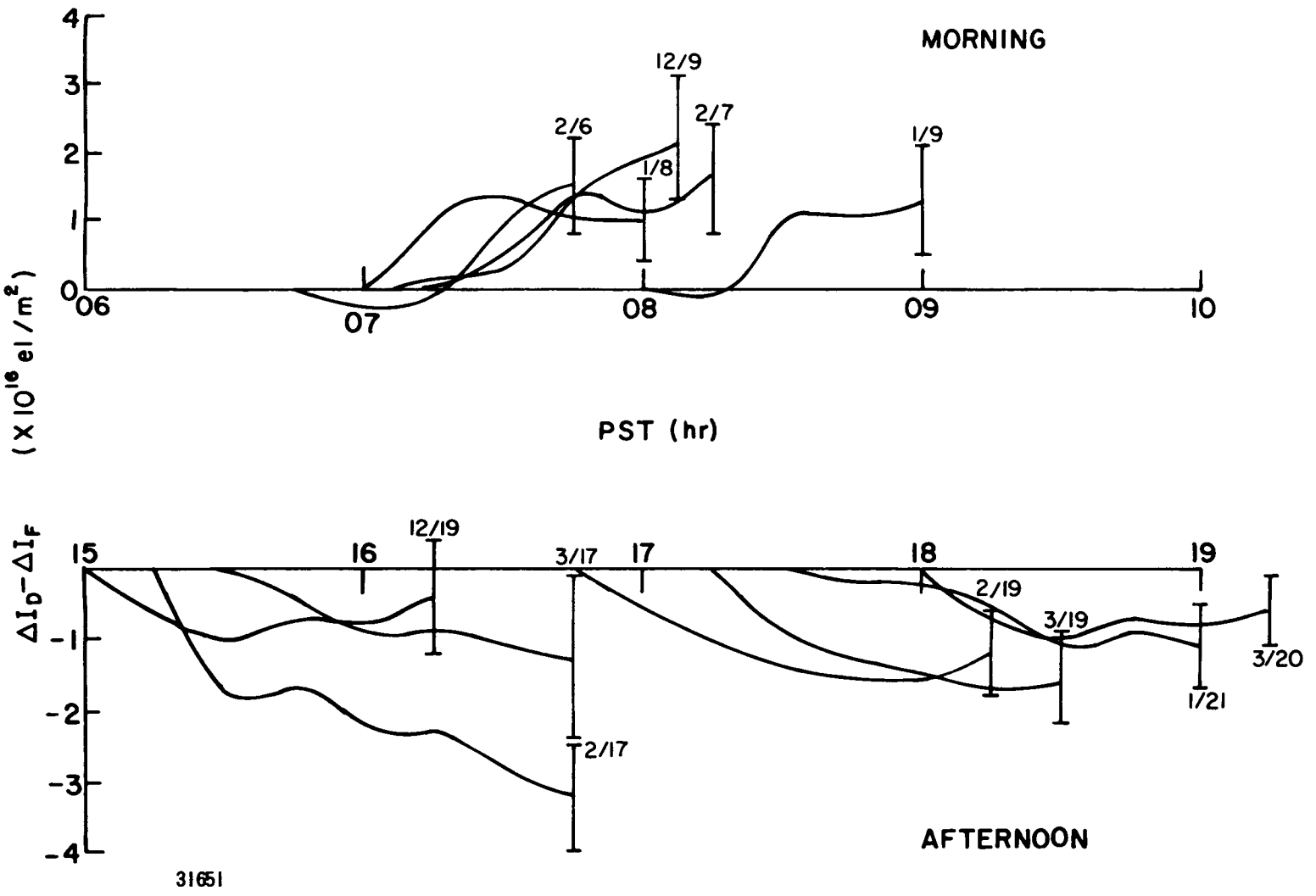

FIG. 19. RESULTS OF COMBINED DOPPLER AND FARADAY MEASUREMENTS.

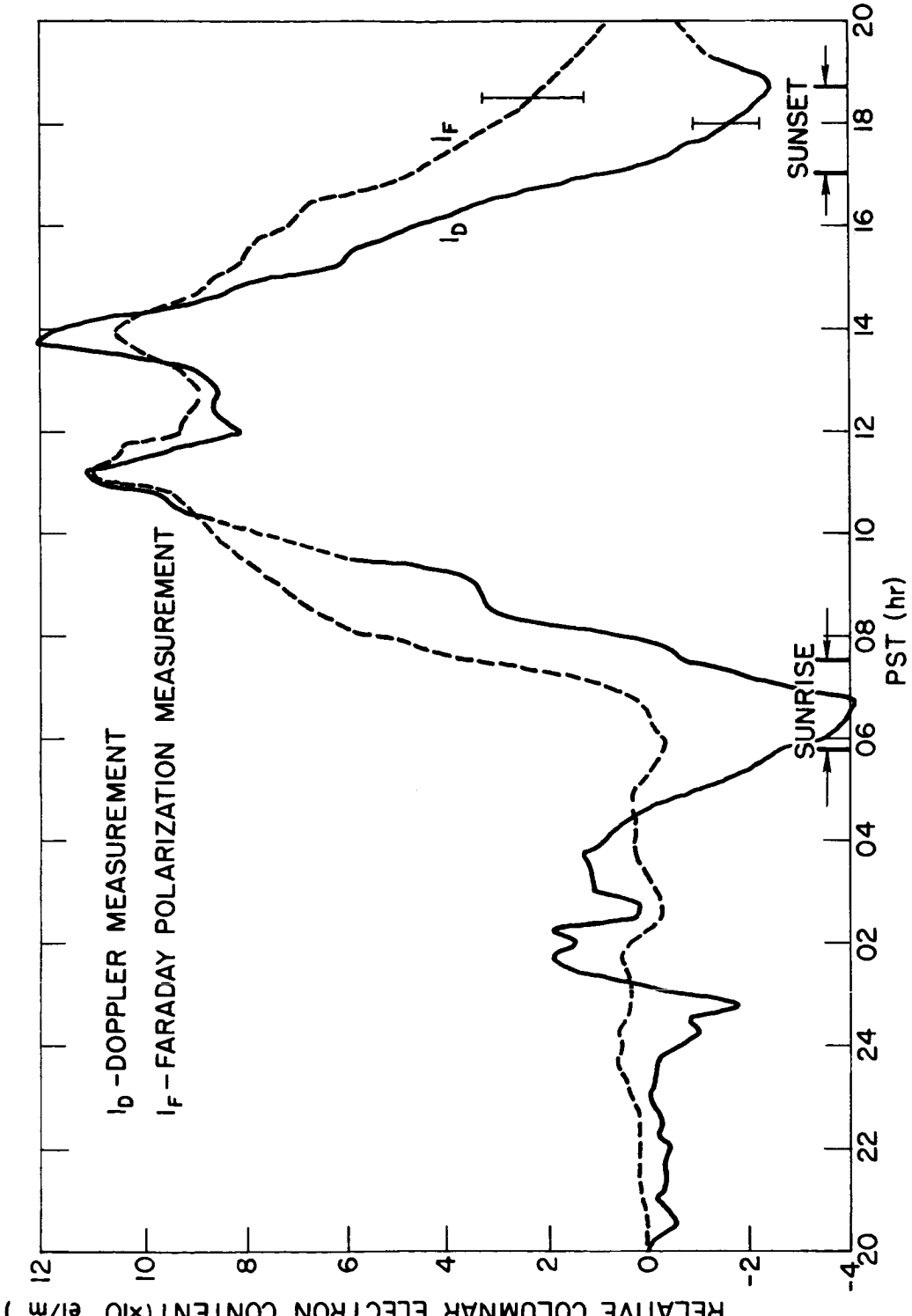

33248

FIG. 20. AVERAGED RESULTS OF DIURNAL CHANGES OF ELECTRON CONTENT.

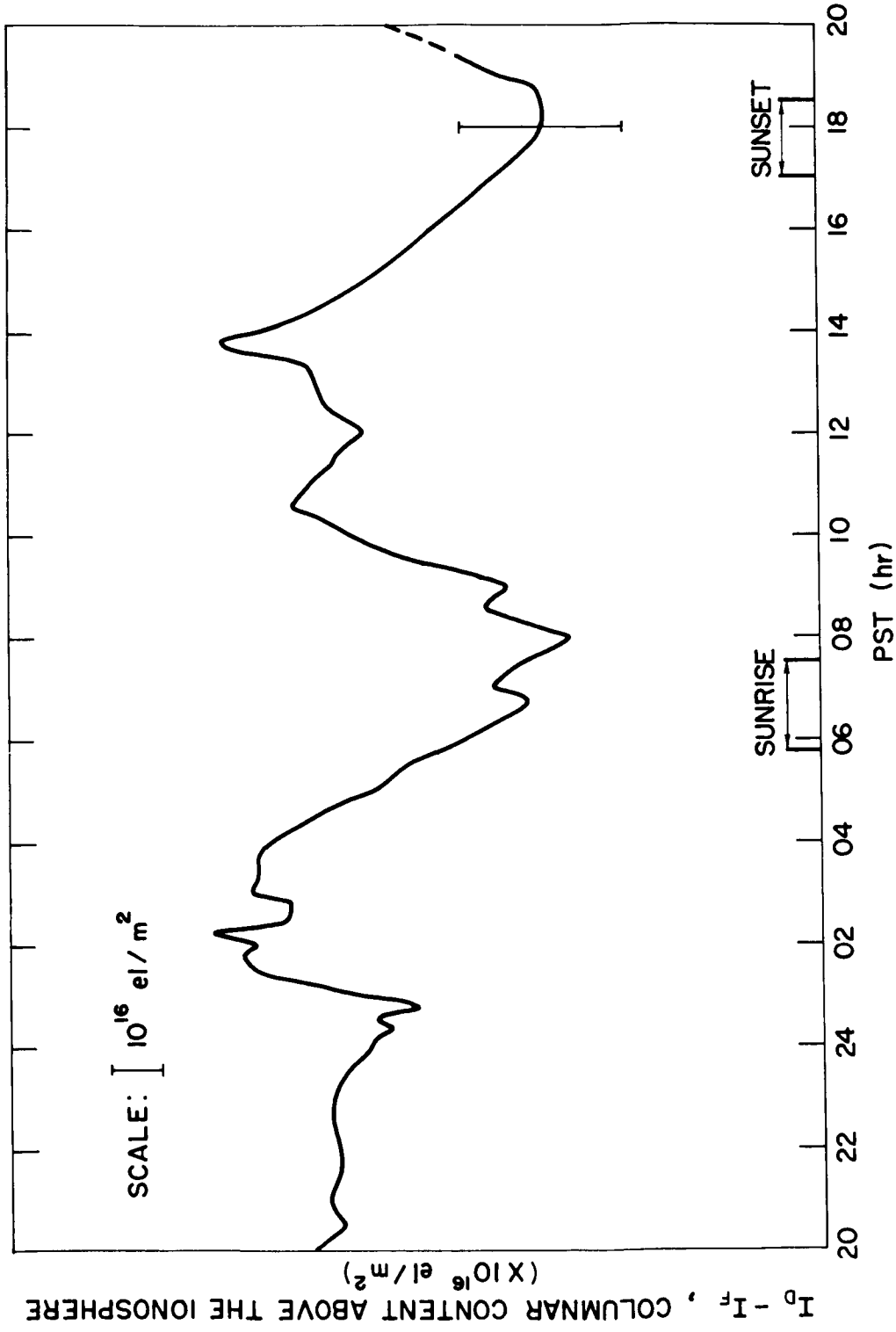

33166

FIG. 21. DIFFERENCE OF AVERAGED RESULTS OF LUNAR MEASUREMENTS.

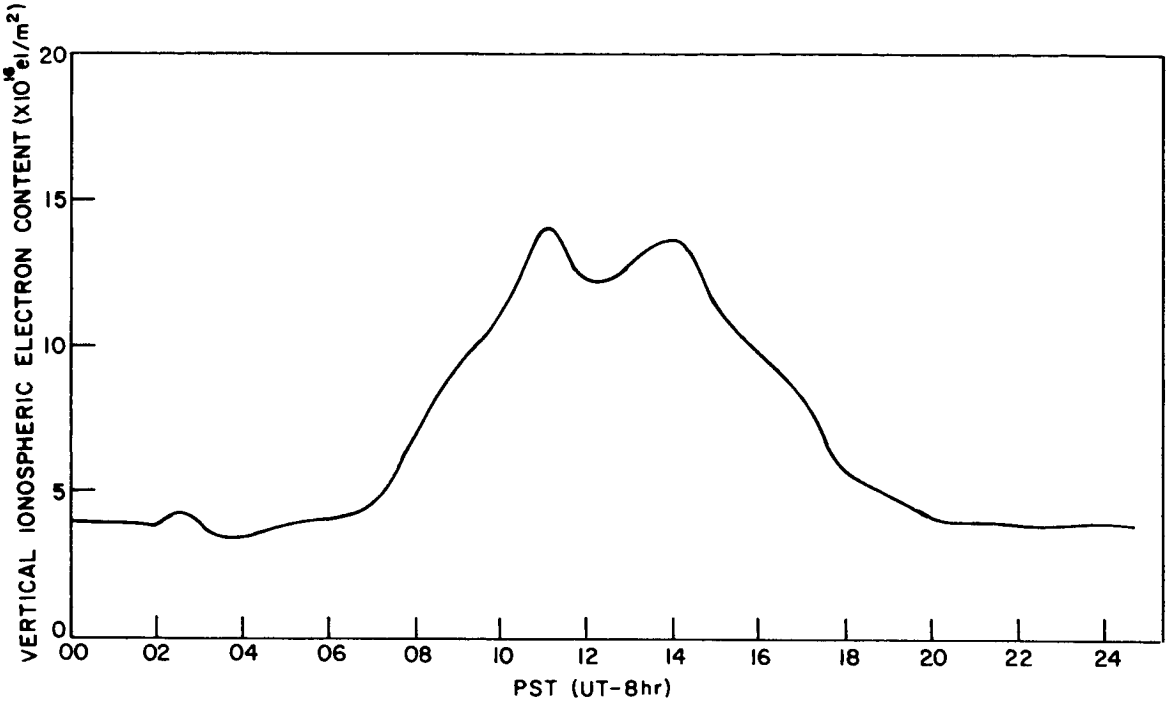

35272

FIG. 22. AVERAGED RESULTS SHOWING DIURNAL VARIATION OF VERTICAL ELECTRON CONTENT IN THE IONOSPHERE, MEASURED BY FARADAY POLARIZATION.

B. RESULTS OF FARADAY-POLARIZATION MEASUREMENTS

1. Diurnal Electron Content

The Faraday measurements consisted of both the change of Faraday polarization angle and the total number of Faraday rotations at the beginning and/or the end of each experiment. Thus the total number of Faraday rotations is known at all times. Equation (2.21) permits deduction of the total electron content in the ionosphere from the number of Faraday rotations. Over a period of five months, one should be able to deduce the average diurnal variation of electron content. The measurements have covered 24 hours of local time.

Figure 22 shows the results of five months' measurements. The results of average electron-content variation over the 24-hour period agree well with the results of the Faraday-polarization measurements from the radio signal transmitted from a geostationary satellite [Ref. 37].

Together, they show a rapid increase of electron content after sunrise and reach the maximum value of about 13×10^{16} el/m^2 about noon; the ionospheric electron content starts to decay in the early afternoon until after sunset; the nighttime electron content remains fairly constant at about 4×10^{16} el/m^2.

Bhonsle et al [Ref. 38] have deduced a linear relationship between the midday ionospheric electron content and the mean Zurich sunspot number $\bar{R}$ for the midlatitude region. The expression is given as

$$I_t = a\left[1 + \frac{b}{a}(\bar{R}-40)\right] \times 10^{17} \text{ el/m}^2 , \qquad (5.4)$$

in which I_t is the total ionospheric electron content and a and b are constants for a given season.

Table 3 shows the results of three different experiments conducted during different years at the same latitude and season.

TABLE 3. COMPARISON OF MEASURED AND CALCULATED IONOSPHERIC ELECTRON CONTENT

Location	Latitude	Date	$\bar{R}$	Method of Measurement	Calculated N_t ($\times 10^{16}$)	Measured N_t ($\times 10^{16}$)
Stanford	37.5 °N	Feb-Mar 1959	176	Faraday Polarization (Sputnik III) [Ref. 2]	88	85
Washington D.C.	40 °N	Mar 1962	44	Dispersive Doppler (Transit IV-A) [Ref. 38]	22	20
Stanford	37.5 °N	Jan-Mar 1964	24	Lunar Faraday Polarization	12	13

It appears from the above table that the lunar Faraday-polarization measurement is indeed a good indicator for the ionospheric electron content. It also appears that the change of the shape of the electron-density profile does not change the value of $\overline{H \cos \theta}$ to any large extent--say less than 10 percent.

2. Slab Thickness τ and Ratio $B = I_a/I_b$

The results of calculations on the slab thickness τ and the ratio of the ionospheric electron content above the maximum electron density to the electron content below the maximum electron density will be compared with other workers' results for the same season in different years. The slab thickness τ is defined as

$$\tau \equiv I_t/N_{max}, \tag{5.5}$$

where I_t is the total ionospheric electron content and N_{max} is the maximum electron density in the ionosphere. The ratio B is defined as

$$B \equiv I_a/I_b , \tag{5.6}$$

where I_a is the ionospheric electron content above the maximum density and I_b is the ionospheric electron content below the maximum density.

In addition to the total ionospheric electron content, measured by the lunar Faraday-polarization method, the maximum electron density and the ionospheric electron content below the maximum electron content should be known to calculate the quantities τ and I_a/I_b. These quantities were measured by using the bottomside ionogram operating at Stanford every 15 minutes throughout the entire period of the lunar-radar-echo experiment. True-height analysis of the ionogram was carried out for the period when the lunar-radar-echo measurements were taken. The results of the analysis were the height of maximum density, the maximum electron density N_{max}, the electron content below N_{max}, and the number of Faraday rotations below N_{max}. Figure 23 shows the results of the above quantities. All the plots are against the local standard time (PST).

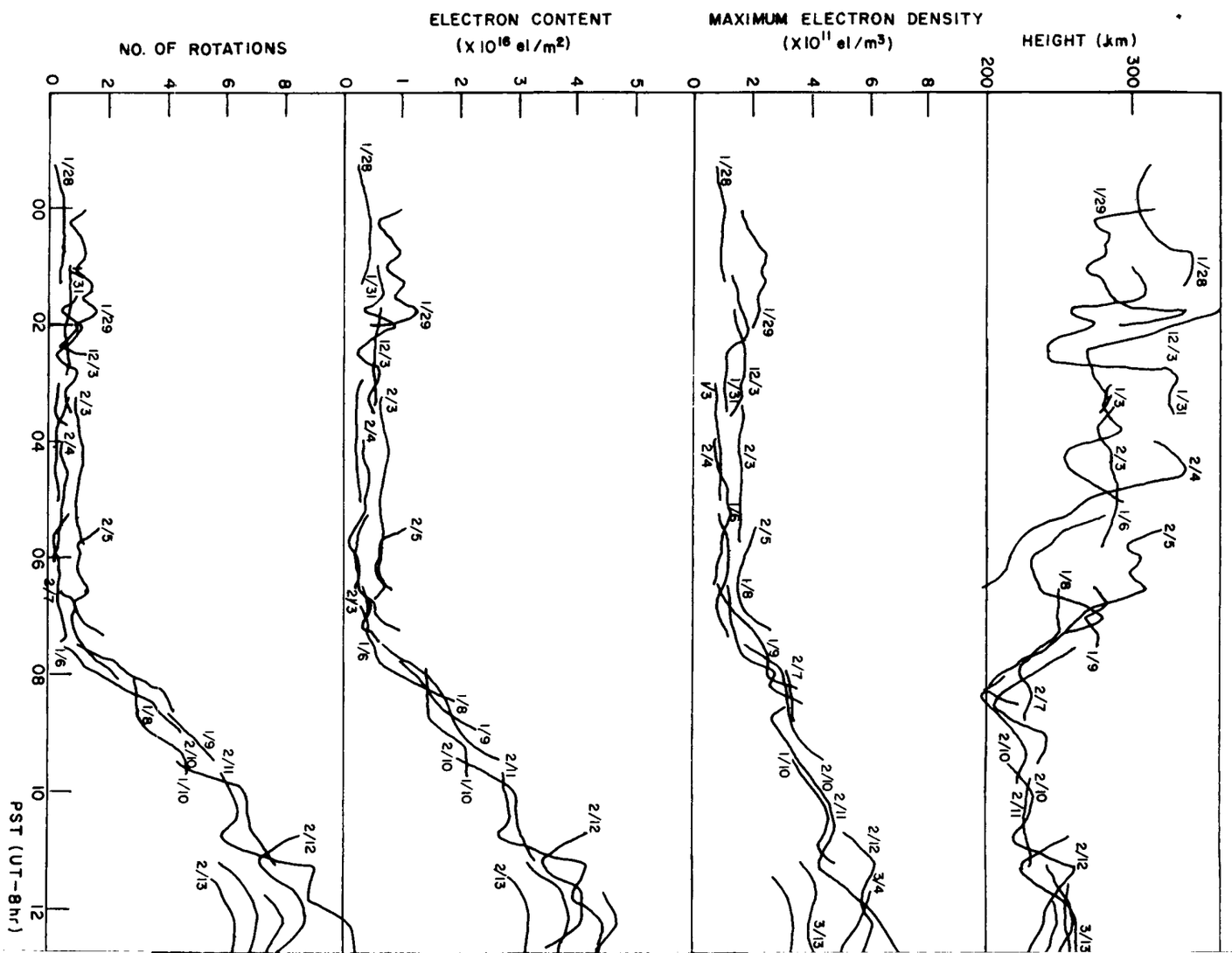
HEIGHT (km)
MAXIMUM ELECTRON DENSITY
(X10^11 el/m^3)
ELECTRON CONTENT
(X 10^16 el/m^2)
NO. OF ROTATIONS
PST (UT-8hr)

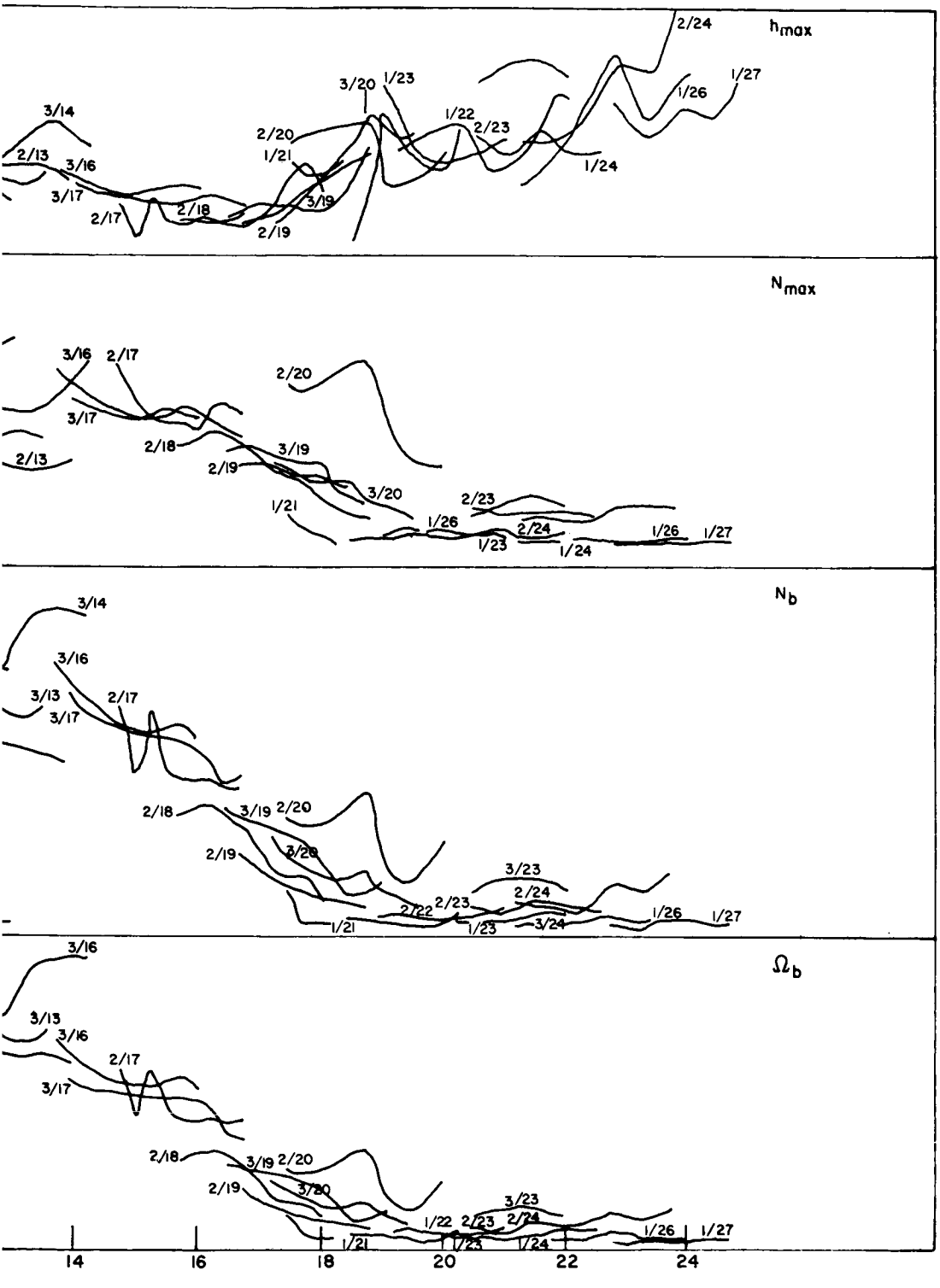

FIG. 23. DIURNAL VARIATION OF BOTTOMSIDE ELECTRON-DENSITY PROFILE. The top graph shows the variation of the height of maximum electron density; the second indicates the variation of the maximum electron density; and the last two show the variation of the bottomside electron content and the number of Faraday rotations, respectively.

Table 4 presents a comparison of τ and I_a/I_b measured by the various workers. Figures 24 and 25 show the diurnal variation of these quantities.

TABLE 4. τ AND I_a/I_b FOR THE PERIOD FROM SUNSPOT MAXIMUM TO SUNSPOT MINIMUM

Location	Latitude	Date	τ (km)		I_a/I_b		Methods
			Day	Night	Day	Night	
Stanford	37.5 °N	Jan-Mar 1959	370	336	3:1	5:1	Faraday Measurement (Sputnik III)[Ref. 2]
Jodrell Bank	52 °N	Jan-Feb 1960	206-290	250-750	3:1	2.5:1-10:1	Lunar Faraday Measurement [Ref. 16]
Trinidad	10.7 °N	Jan-May 1960	200-400	220-800	1.5:1	3:1-11:1	Lunar Faraday Measurement [Ref. 39]
Auckland, N.Z.	37 °S	Winter 1961	200-330	166-413			Refractive Measurement (Explorer) [Ref. 40]
University Park, Pa.	40.8 °N	Dec 1961-Feb 1962	150-250	100-200	1:1-2:1	2:1-4:1	Doppler Measurement (Transit 4A) [Ref. 41]
Washington D.C.	40 °N	Feb-Sep 1962	340	240-360			Doppler Measurement (Transit 4A) [Ref. 38]
Stanford	37.5 °N	Dec 1963-Apr 1964	120-370	190-550	3:1	3:1-16:1	Lunar Faraday Measurement

The above table shows that both τ and I_a/I_b are within the values of other workers' measurements. Hence, it is possible to say that the lunar-radar Faraday-polarization measurement does indeed give a good measure of the ionospheric electron content. (If one extrapolates from the above statement, the result of Section A is truly a variation of electron content above the ionosphere.)

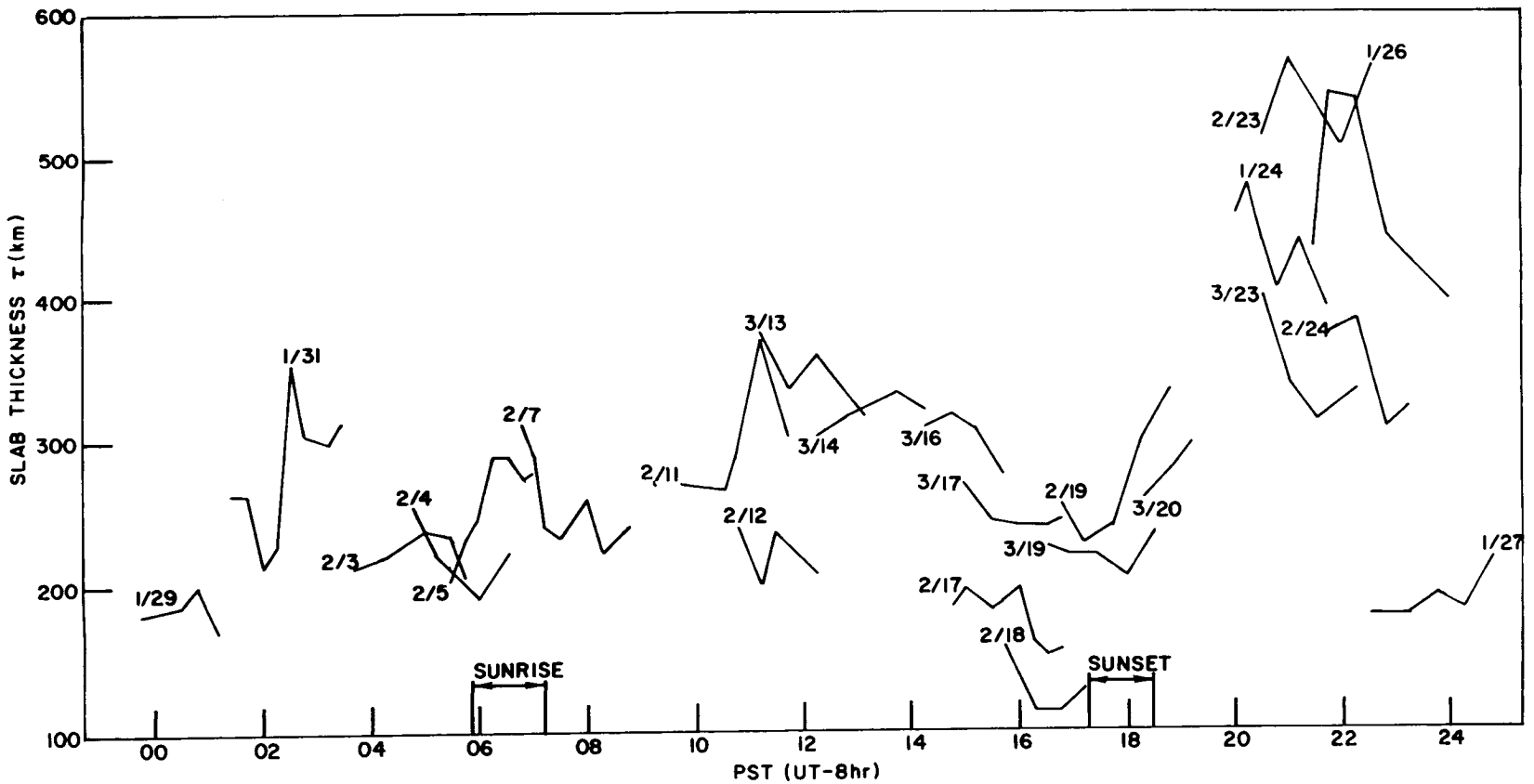

FIG. 24. DIURNAL VARIATION OF SLAB THICKNESS OF THE IONOSPHERIC ELECTRON CONTENT.

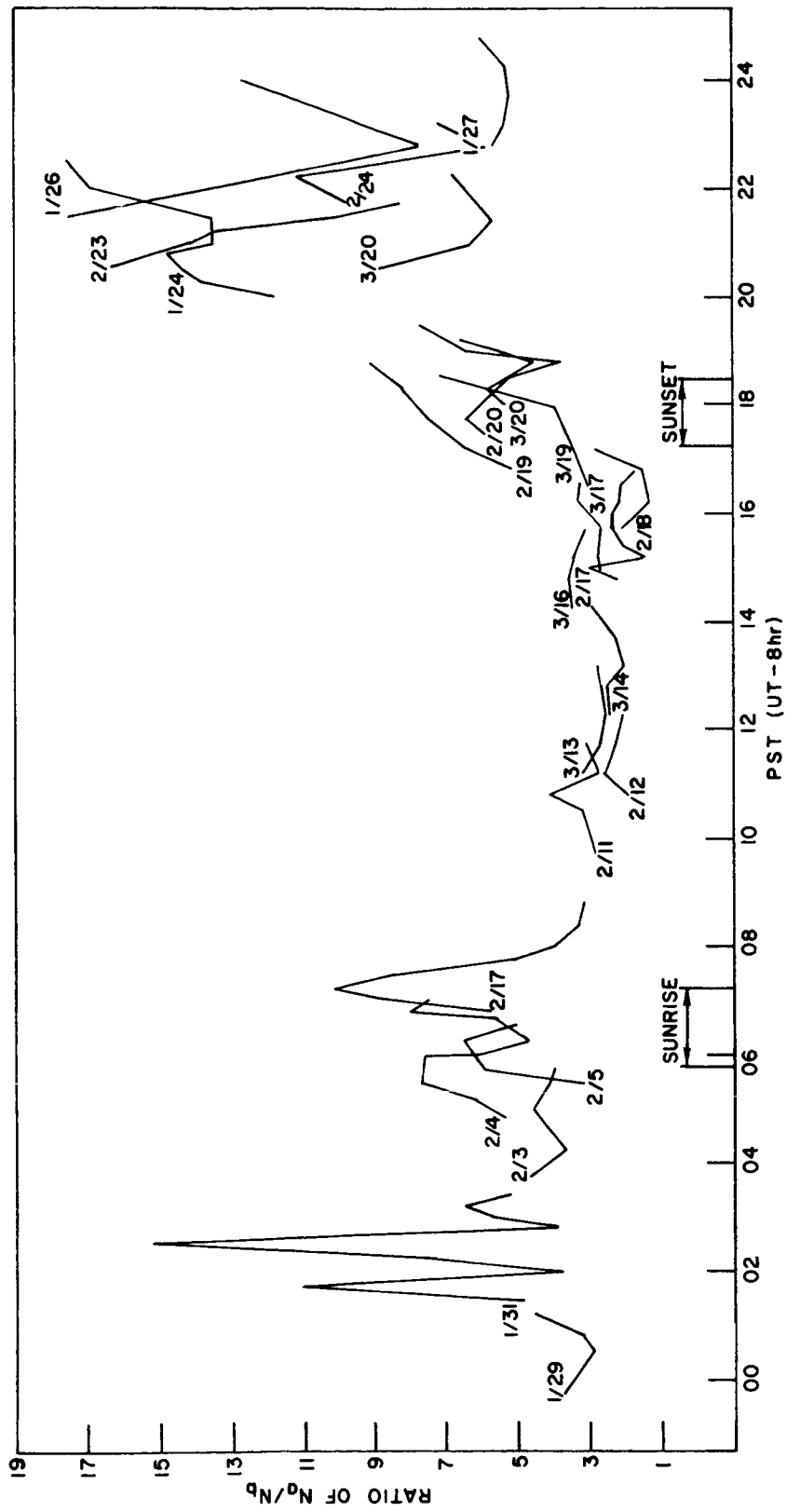

FIG. 25. DIURNAL VARIATION OF THE RATIO OF THE TOPSIDE ELECTRON CONTENT TO THAT OF THE BOTTOMSIDE.

VI. IONIZATION FLOW BETWEEN IONOSPHERE AND MAGNETOSPHERE

A. DAYTIME RESULTS

In this section, the daytime results of the previous chapters are presented again so that the effect of the difference in these two measurements on the daytime results will be more pronounced. Figure 26

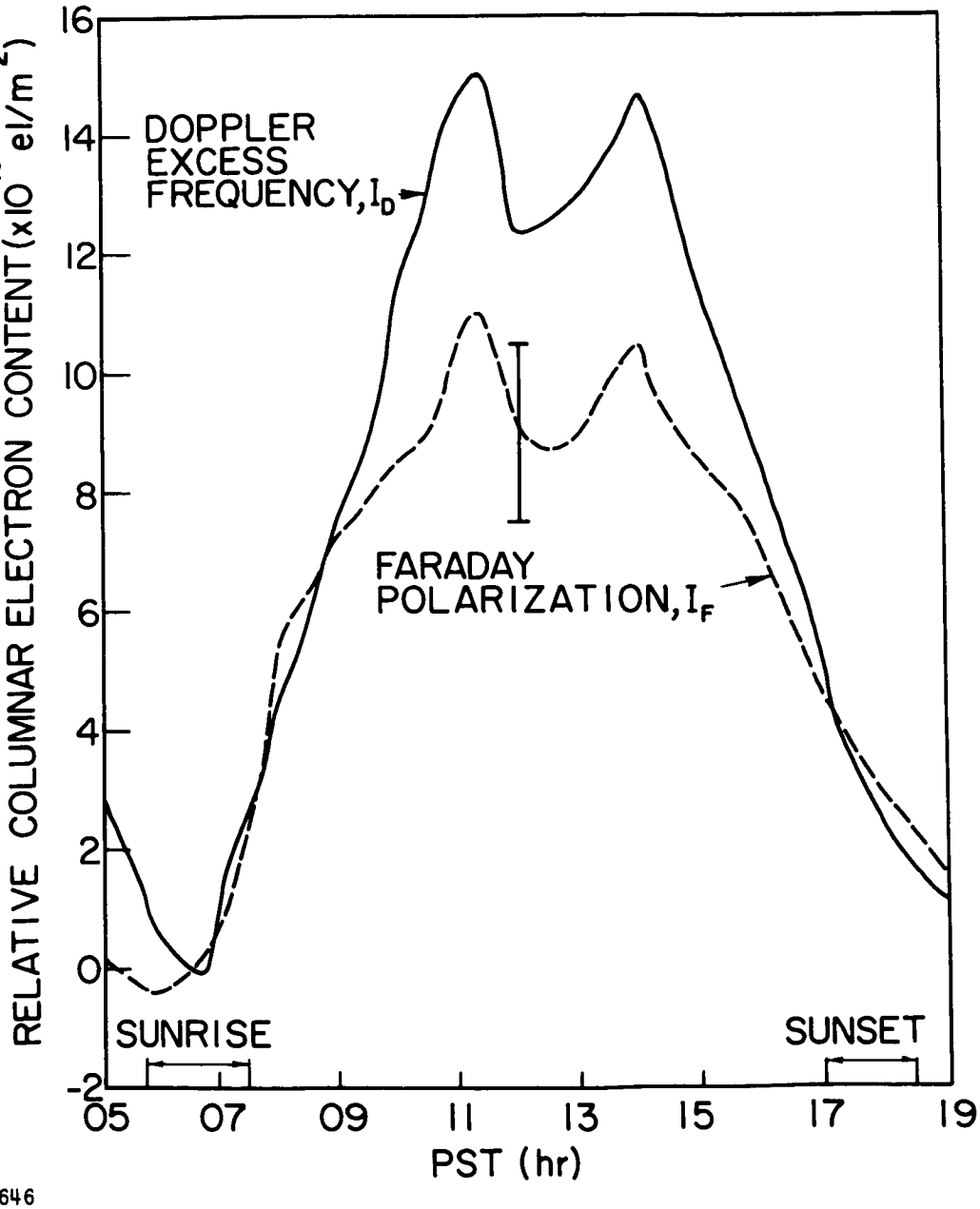

33646

FIG. 26. AVERAGED DAYTIME RESULTS OF RELATIVE ELECTRON CONTENT MEASURED BY FARADAY POLARIZATION AND DOPPLER EXCESS FREQUENCY.

shows the average relative electron contents measured by Faraday-polarization and Doppler-excess-frequency methods. The vertical bar denotes the uncertainty of measurements. It is clear that the Doppler-excess-frequency method detects a much larger change of ionization content. Figure 27 is the difference between the two curves in Fig. 26, $I_D - I_F$. The net difference of the change in ionization content between the two methods is about 4×10^{16} el/m^2. The decrease of ionization content detected by Doppler excess frequency during predawn hours is discussed in the next chapter. It is seen in Fig. 27 that the rate of increase of ionization content in the morning is slightly higher than the rate of decrease in the afternoon. In the morning the period of increasing ionization is about 3 hours (0800-1100 hr) and in the afternoon

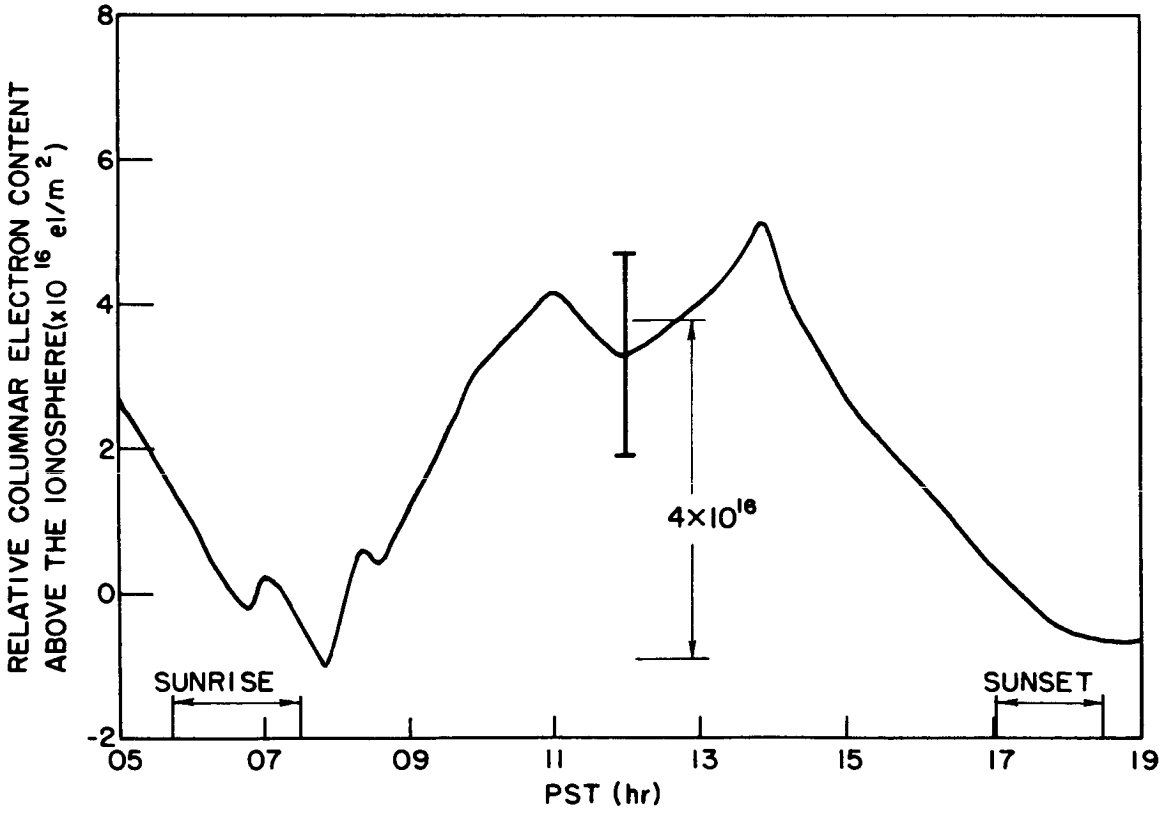

33645

FIG. 27. DIFFERENCE OF AVERAGED DAYTIME RESULTS OF LUNAR MEASUREMENTS.

the period of decaying ionization is about 4 hours (1400 - 1800 hr). Hence the average rate of change of columnar electron content can be calculated

	Average Rate of Change of Columnar Electron Content
Morning hours	3.7×10^{12} el/m^2/sec
Afternoon hours	2.8×10^{12} el/m^2/sec

Finally, the shape of change of ionization above the ionosphere is similar to the ionospheric change (i.e., a rapid increase of ionization after sunrise reaches its maximum value about noon; it starts to decay in the early afternoon and continues until after sunset).

B. IDENTIFYING THE POSSIBLE REGION OF LARGE CHANGE OF IONIZATION

There are several different regions in the cislunar medium--the ionosphere, inner and outer magnetospheres, transition region, and solar-wind region. These regions are characterized by their different magnetic fields, high- and low-energy densities, as well as density distributions and plasma-flow parameters. Figure 28 represents the plane of the lunar orbit, looking from the north celestial pole, and showing the different regions. Note that the dashed line of the magnetopause is the extrapolation from the IMP-I magnetometer measurements [Ref. 42]. The shock front in the antisolar hemisphere is derived from the present experiment (see Chapter VII). The transition region is defined between the boundaries of the shock front and the magnetopause. The outer magnetosphere is the region between the magnetopause and the "knee." The position of the knee around the earth was recently reported on by Carpenter and Jewell [Ref. 43]. The inner magnetosphere is the region between the boundaries of the knee and the top of the ionosphere.

Here one sees that the radar path lengths in different regions depend on the position of the moon. However, since the measurements are taken near the transit time, the moon is always in the solar direction for the daytime measurements. The radar path lengths in different regions during daylight hours do not change by any significant amount,

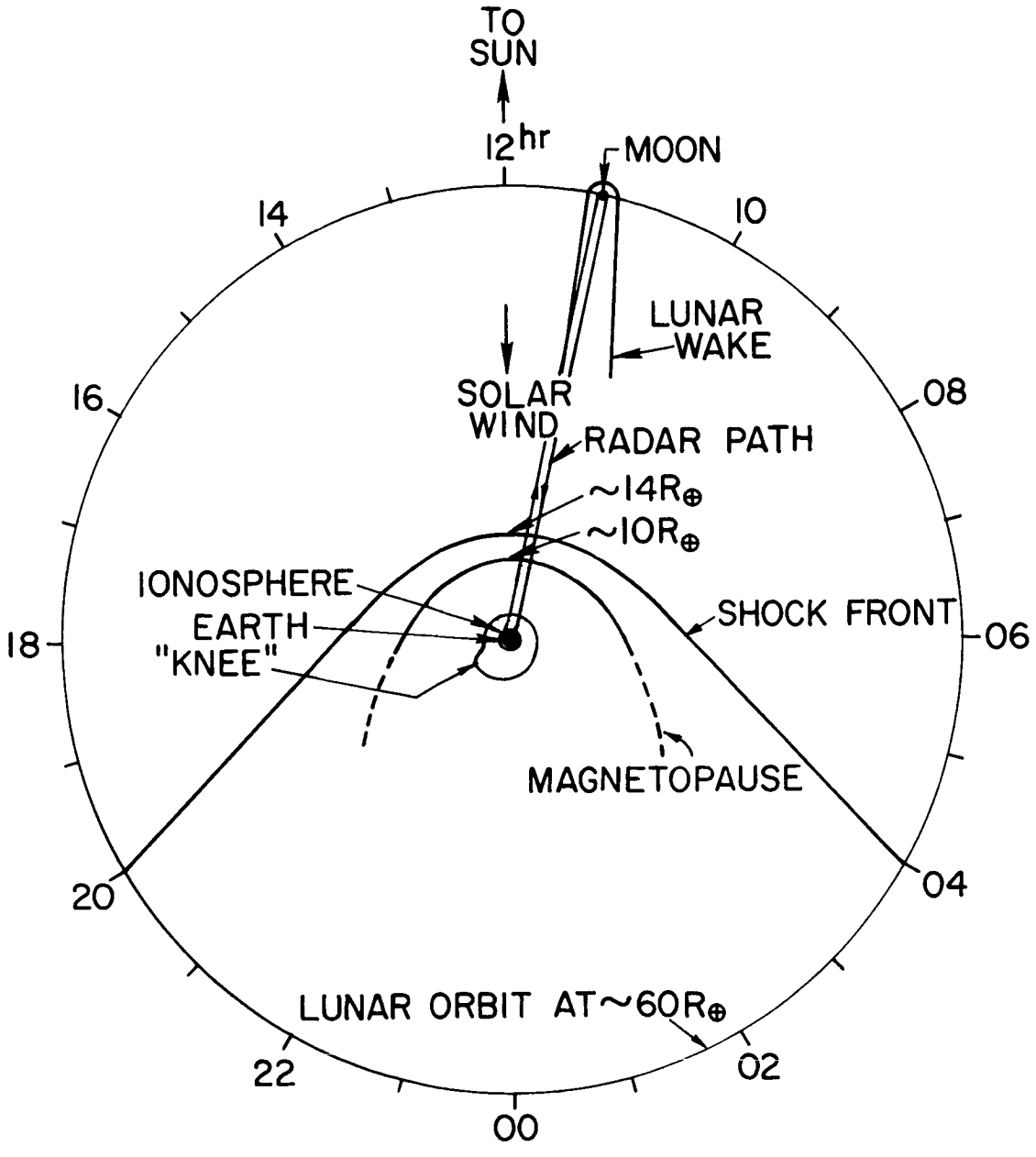

33236

FIG. 28. REGIONS IN THE CISLUNAR MEDIUM SHOWING EXAMPLE OF RADAR PATH.

whereas, when the moon is in the antisolar direction (nighttime hours), the radar path length changes significantly between the solar-wind region and inside the shock front.

Figure 29 shows the order of magnitude of a column of electron density in different regions on the daytime side. Since the observed

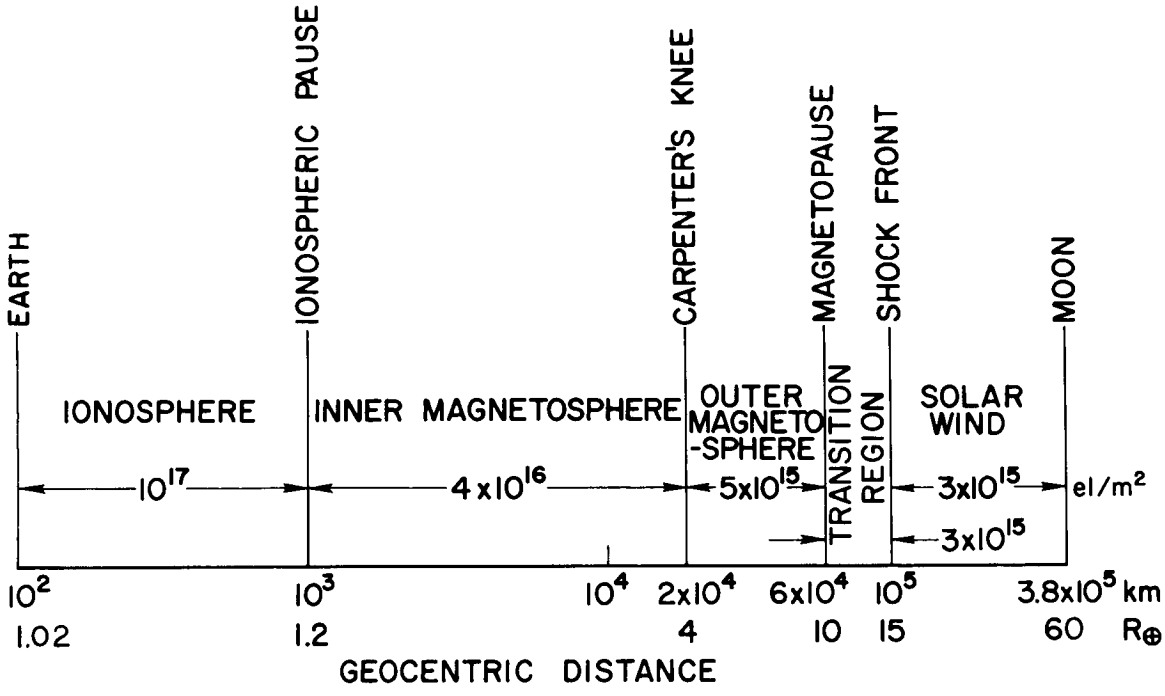

34975

FIG. 29. AVERAGED ELECTRON CONTENT IN THE DIFFERENT REGIONS IN THE CISLUNAR MEDIUM IN THE SOLAR DIRECTION.

change of ionization content is beyond the ionosphere, the only region that can possibly support the value 4×10^{16} el/m^2 is the inner magnetosphere. The total sum of electron content from the other three regions--outer magnetosphere, transition region, and solar-wind region--cannot account for the observed value of change of ionization content. Therefore, it is concluded that the only possible region that exhibits the diurnal variation is the inner magnetosphere. In the following paragraphs, a simple model will be constructed to explain the results shown in Fig. 27.

C. MODEL CALCULATIONS

Assumptions of this model are as follows:

1. The region is in diffusive equilibrium.
2. The region is isothermal: temperature is independent of height.

3. Ion temperature T_i equals electron temperature T_e.
4. The base of the diffusive equilibrium region is taken at 500 km.
5. The region has three ionic constituents: O^+, He^+, and H^+.

In Chapter IV, the diffusive-equilibrium model was considered in some detail. We shall consider the model briefly--in particular, an expression for the height of transition level.

It could be shown that the electron-density distribution can be expressed as [Ref. 44]

$$N_e = N_o \left\{ \frac{\exp[-A'/h_1] + \eta_{12} \exp[-A'/h_2] + \eta_{13} \exp[-A'/h_3]}{1 + \eta_{12} + \eta_{13}} \right\}^{1/2} , \qquad (6.1)$$

where N_o is the electron density at the base level,

h_j is the scale height, expressed by

$$h_j = k(T_e+T_i)/m_j g ,$$

the subscripts 1, 2, and 3 refer to O^+, He^+, and H^+ respectively,

A' is "reduced" altitude, defined as

$$A' \equiv (h-h_o)/[(1+h/R_\oplus)(1+h_o/R_\oplus)] \qquad (6.2)$$

where h is true height measured from the ground,

h_o is the height of base level,

$R_\oplus$ is earth's radius, 6370 km, and

η_{ij} is the ratio of ion densities at base level and is defined as

$$\eta_{ij} = N_j/N_i \Big|_{500 \text{ km}} .$$

Equation (6.1) states that the electron-density profile depends on the temperatures and ion compositions at the base level. If one of the parameters should change, the shape of the electron-density distribution will be changed.

Before considering further the electron-density distributions, we should consider a simple expression for determining the height of transition levels of different ionic species. The expression for a single ion species is given in Eq. (4.9), as

$$N_i = N_{io} \exp\left[-\int_{h_o}^{h} \frac{m_i g}{kT_i}\, dh + \int_{h_o}^{h} \frac{gM_+}{k(T_e+T_i)}\, dh\right] \tag{6.3}$$

where N_{io} is the density of the i^{th} ion species at base level. At the transition level,

$$N_i = N_j \,. \tag{6.4}$$

Substituting Eq. (6.3) into Eq. (6.4) yields

$$N_{io} \exp\left[-\int_{h_o}^{h} \frac{m_i g}{kT_i}\, dh + \int_{h_o}^{h} \frac{M_+ g}{k(T_e+T_i)}\, dh\right]$$

$$= N_{jo} \exp\left[-\int_{h_o}^{h} \frac{m_j h}{kT_j}\, dh + \int_{h_o}^{h} \frac{M_+ g}{k(T_e+T_j)}\, dh\right] \,. \tag{6.5}$$

We further assume that all ionic constituents have the same temperature; therefore,

$$T_i = T_j = T \tag{6.6}$$

and Eq. (6.5) reduces to

$$\frac{N_{io}}{N_{jo}} = \exp\left[-\int_{h_o}^{h} \frac{m_j g}{kT} - \frac{m_i g}{kT}\, dh\right]. \tag{6.7}$$

Let the upper limit of the integral be the height of the transition level L of the i^{th} and j^{th} ionic constituents and Eq. (6.7) becomes

$$\ell n \frac{N_{io}}{N_{jo}} = \int_{h_o}^{L} \frac{(m_i - m_j)g}{kT} dh \ . \tag{6.8}$$

Let

$$a = \ell n \frac{N_{io}}{N_{jo}} \tag{6.9}$$

and

$$b = \frac{m_i - m_j}{kT} \ . \tag{6.10}$$

Since the term $(m_i - m_j)/kT$ is constant, the integral requires a simple integration,

$$\frac{a}{b} = \int_{h_o}^{L} g dh \tag{6.11}$$

and

$$g = g_o \left(\frac{R_\oplus}{h+R_\oplus} \right)^2 \ , \tag{6.12}$$

where g_o is the acceleration of gravity at the earth's surface. After integration and some algebraic manipulation, the expression for L is given as

$$L = \frac{bh_o + a[1+(h_o/R_\oplus)]}{b - (a/R_\oplus)[1+(h_o/R_\oplus)]} \ . \tag{6.13}$$

The transition level is a function of both ion temperature and the composition of ionic constituents at the base level. The transition level of the two species does not depend on the third component. However, the ionic distribution of any particular species depends not only on the third species but also on the electron temperature. A family of curves is plotted in Figs. 30 and 31 to show the transition levels of He^+ and O^+, and H^+ and He^+, as functions of ion temperature.

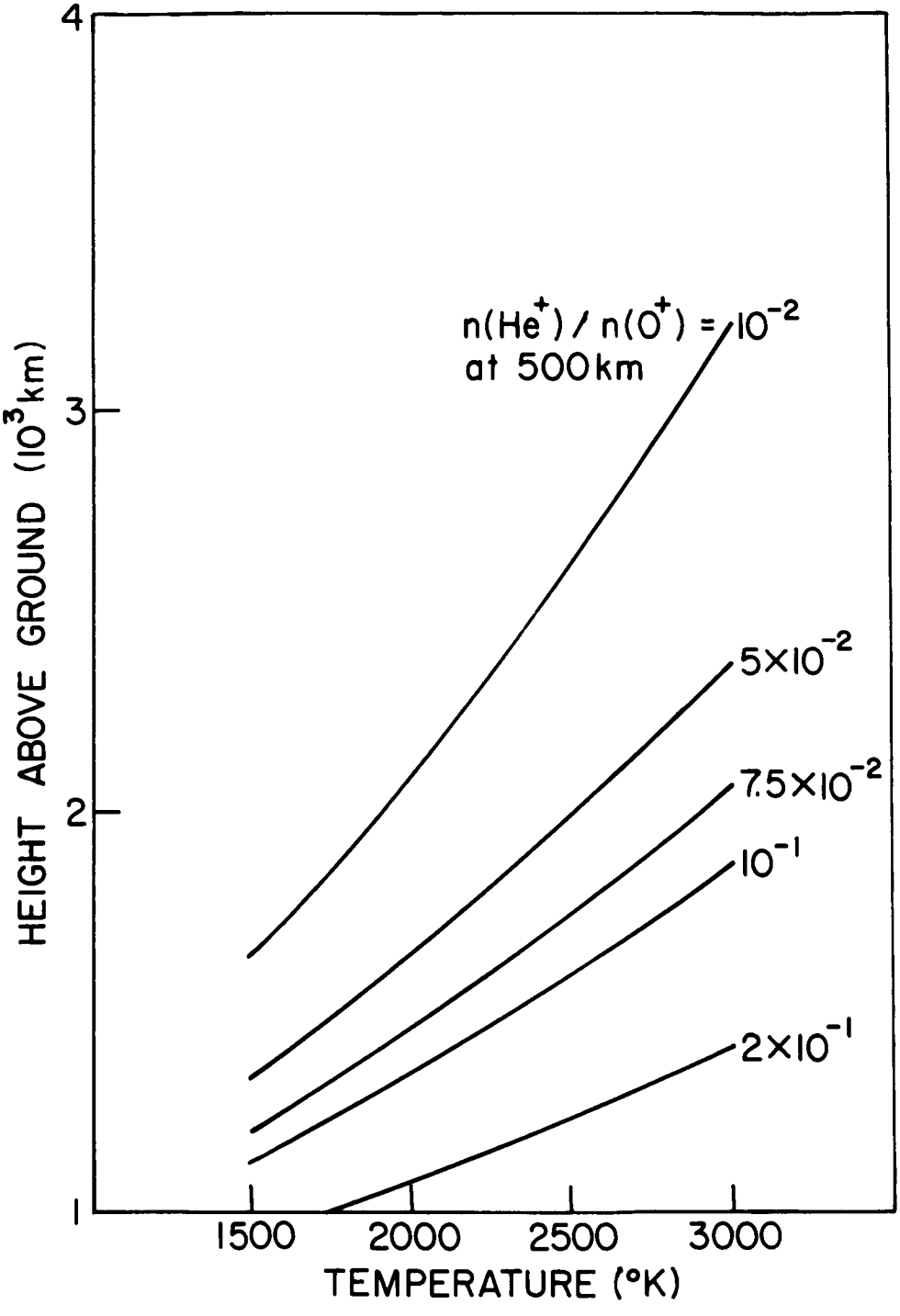

34976

FIG. 30. TRANSITION LEVELS BETWEEN He^+ AND O^+ FOR DIFFERENT COMPOSITIONS AT THE BASE LEVEL (500 KM).

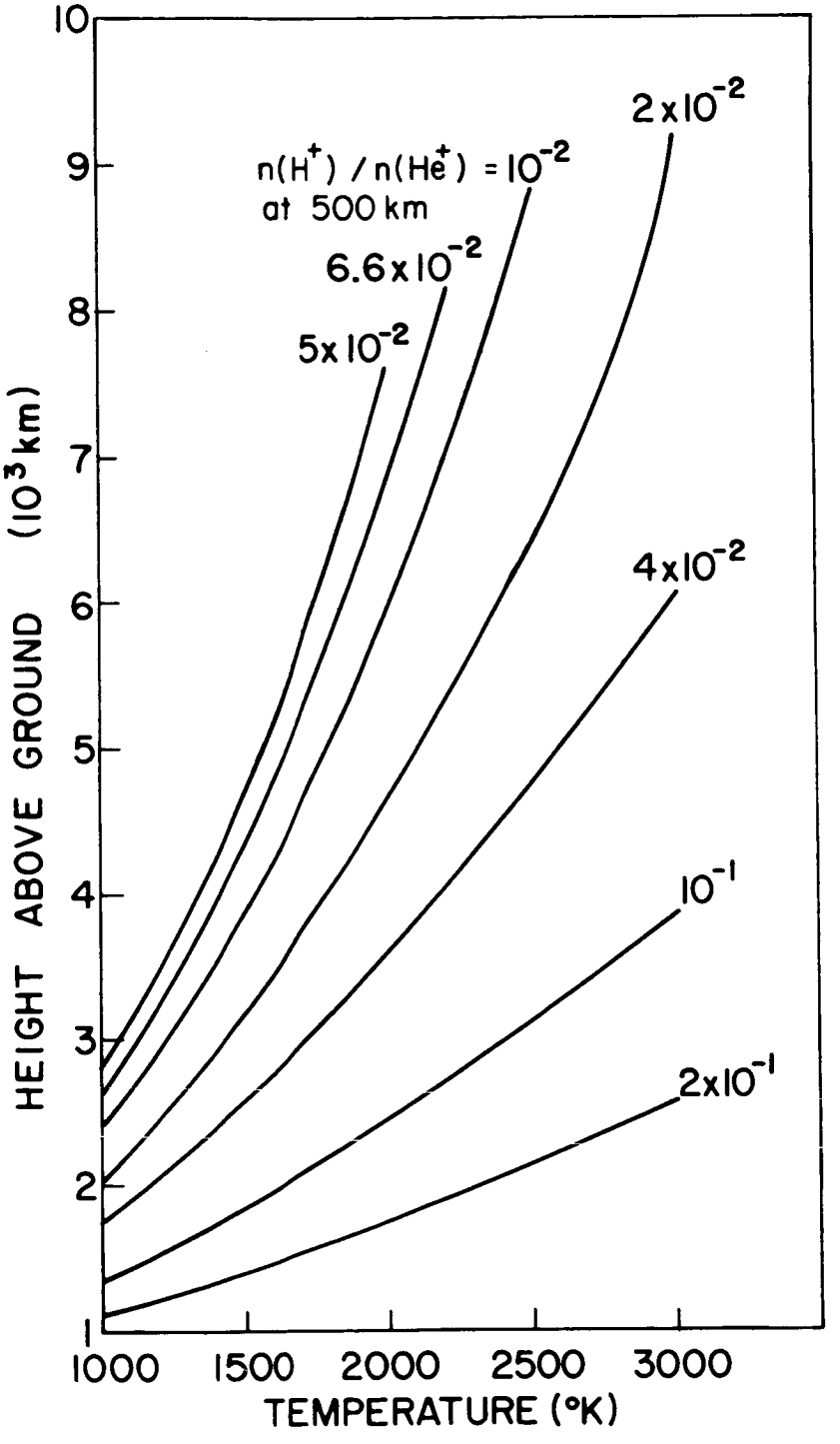

34977

FIG. 31. TRANSITION LEVELS BETWEEN H^+ AND He^+ FOR DIFFERENT COMPOSITIONS AT BASE LEVEL (500 KM).

If the transition levels and the temperature are known, then one can find the ionic composition at the base level. Hence the electron-density profile can be calculated from Eq. (6.1). Evans [Ref. 35] has measured a large change of electron temperature above the peak of electron density in the F2 layer during the daytime. The electron temperature at the height of about 700 km reaches as high as 3000 °K near noon and less than 2000 °K near sunrise and sunset. The ion temperature approaches the electron temperature at high altitude, which has been measured by Evans and Loewenthal [Ref. 34] and predicted by theories of Hanson [Ref. 45] and Dalgarno et al [Ref. 46]. Hence the assumption that the ion temperature and the electron temperature are the same is a reasonable one. The results of the Ariel satellite measurements [Ref. 33] on the transition levels show that, during daytime hours, the transition between He^+ and O^+ is above 1000 km and can be as high as 1400 km at midlatitude. The transition level between He^+ and H^+ cannot be detected by the satellite because of its low orbit.

A sample calculation of integrated normalized electron content is given below.

Height Range (km)	Integrated Electron Content Normalized at Base Level	
	2500 °K	1500 °K
500 - 1,000	3×10^5	2.4×10^5
1,000 - 4,000	3.5×10^5	2.1×10^5
4,000 - 10,000	2.5×10^5	1.3×10^5

The ionic compositions at 500 km are chosen in such a way that the transition level between He^+ and O^+ remains fairly constant above 1000 km and that between He^+ and H^+ is about 3000 km over a temperature range of 2000 - 3000 °K, as suggested by Bowen et al [Ref. 33]. Thus,

$$\eta_{12} = 0.1 \qquad \text{and} \qquad \eta_{23} = 0.04 \ .$$

An illustration of the shape of electron-density distribution with different temperatures is shown in Fig. 32. It is clear that the changes of temperature affect the percentage the most at high altitude.

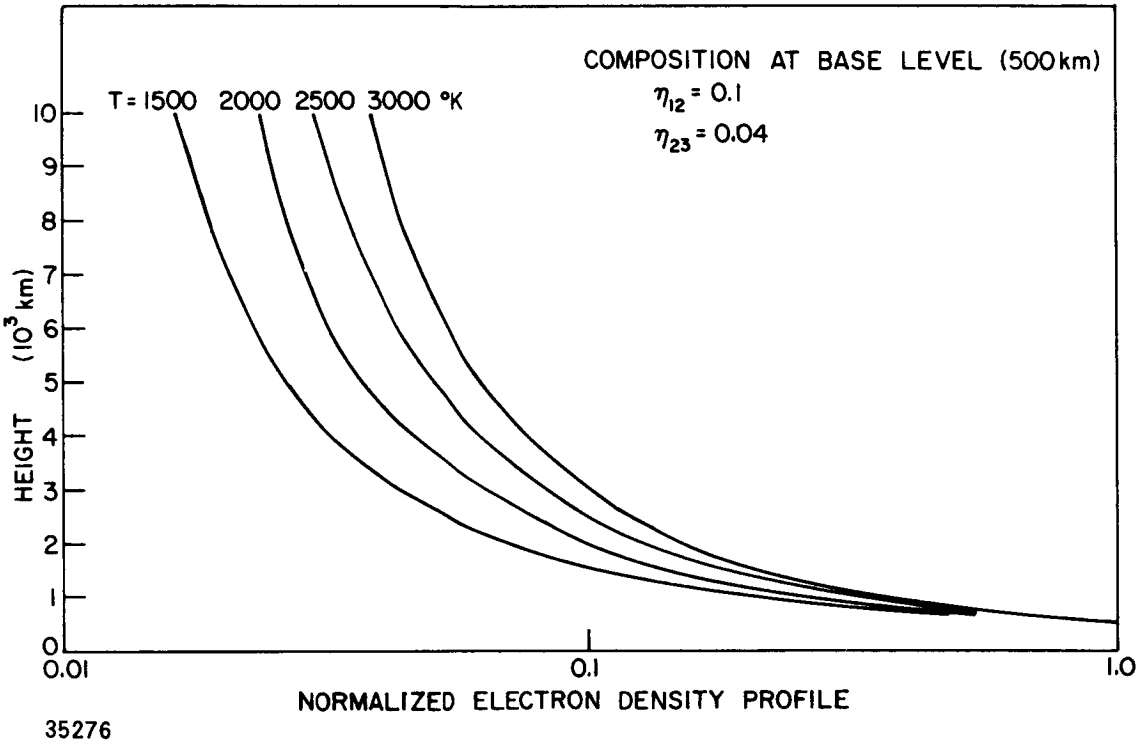

FIG. 32. NORMALIZED ELECTRON-DENSITY PROFILE ABOVE BASE LEVEL FOR DIFFERENT TEMPERATURES.

Now it is desirable to estimate the value of N_{eo} at 500 km for noon and sunset or sunrise. During the entire period of the lunar-radar experiment, the bottomside ionogram was operated every 15 min at Stanford (Chapter V); the averaged diurnal variation of the maximum electron density was thus obtained. Figure 33 shows the results of N_{max}, which increases rapidly after sunrise, reaches its maximum value near noon, and starts to decay in the afternoon until after sunset. The nighttime value of N_{max} remains fairly constant. If the density at 500 km is assumed to vary in the same fashion as N_{max}, a large change of electron density at 500 km between noon and sunset or sunrise would be expected. If it is assumed that the density at 500 km is about one

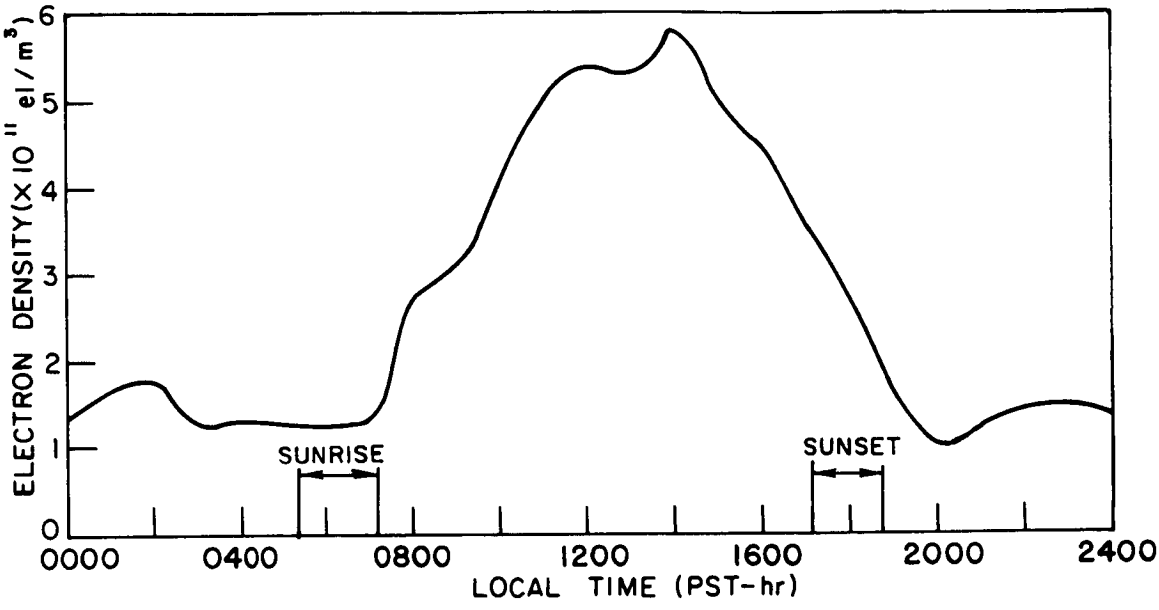

34978

FIG. 33. AVERAGED MAXIMUM ELECTRON DENSITY, N_{max}, MEASURED AT STANFORD DURING THE LUNAR-RADAR-ECHO EXPERIMENT.

tenth of N_{max}, then the density at 500 km would vary from 5.5×10^4 cm^{-3} to 2.5×10^4 cm^{-3}. If the high value of density is used for 2500 °K and the low value for 1500 °K, the net change of electron content for the different height ranges are shown below.

Height Range (km)	Change of Electron Content (el/m^2)
500 - 1,000	10^{16}
1,000 - 4,000	1.4×10^{16}
4,000 - 10,000	10^{16}

It is clear from the above that the calculated electron content in the high altitude region has the same order of magnitude of change as observed by the lunar-radar echoes.

Finally, it is shown that, with a fairly large change of temperature, the change of electron content in the high altitudes calculated from a simple model does give the right order of magnitude of change of electron content.

The Doppler method would measure the net change of electron content, 3.4×10^{16} el/m^2. Now we shall compute the amount of change of electron content that would be deduced from the Faraday method. The result of this calculation shows that the Faraday method would detect a change of about 1.2×10^{16} el/m^2. Therefore, there will be a net difference of change of electron content 2.2×10^{16} el/m^2, which agrees reasonably well with the observed results.

Since the local ionization production is not above 1000 km, the amount of increase and decrease of ionization in the high altitudes or lower magnetosphere will have to be restored or removed from somewhere. It is logical to deduce that the ionosphere serves as the source as well as the sink. Therefore, an electron-flux flow between the ionosphere and lower magnetosphere does exist. In the next section the results of other workers will be discussed to support the idea of electron-flux flow.

D. COMPARISON WITH OTHER RESULTS

Evans [Ref. 47], using radar backscatter at Millstone, detected a large downward drift of the ionization from above 500 km during the 20 July 1963 eclipse. The results of his measurements showed, at the beginning of the eclipse, a large depression of the ionization at heights above 500 km and an increase of ionization near the density peak of the F2 region. The amount of density depression at the high altitudes was about half of the pre-eclipse value. Evans again observed an increase of ionization near the peak during normal afternoon hours [Ref. 35]. This evidence agreed with the lunar-radar measurement of the downward flow of ionization in the afternoon hours.

The results of both Ariel [Ref. 48] and Explorer XVII [Ref. 49] satellite measurements on electron temperatures and ion density in the upper ionosphere and part of the lower magnetosphere indicate an upward

flow of ionized flux. The value of the upward flux is on the order of 10^{12} $m^{-2}sec^{-1}$, which agrees well with the value suggested by the lunar-radar experiment. Hanson [Ref. 45] has predicted theoretically the amount of fast photoelectron drifting upward to be about 10^{12} $m^{-2}sec^{-1}$.

From the above experimental and theoretical results, it is concluded that an electron flux does flow between the ionosphere and the lower magnetosphere.

VII. PLASMA WAKE OF THE EARTH

It should be noted that during the nighttime the moon is in an antisolar direction. It is believed that a large amount of ionization is located beyond the ionosphere, because the Faraday method [Ref. 37, Chapter V] showed no significant changes of ionization throughout the night. The postsunset and predawn increases of ionization in the ionosphere could not be explained by any existing ionospheric theories that have been well developed, and these phenomena contradict the results of all ionospheric experiments. Therefore one must seek an explanation elsewhere. A reasonable approach is to look into the inner-magnetosphere region. Carpenter [Ref. 43] reported that during a typical day, when the magnetic k_p index is between 2 and 4, the spatial position of the knee is marked by a bulge in the electron-density profile which shifts suddenly outward for a distance of about 2 earth radii at 1800 hours (Fig. 34), then remains fairly constant until 2100 hours, when it starts to shift inward again until it reaches the innermost position (3.5 earth radii) at about 0600 hours. The total distance change of the knee is about two earth radii.

Now suppose the observed results of the Doppler-excess method are due to the change in position of the knee. One should be able to determine the electron density at the knee by dividing the change of ionization content by the change in distance of the knee position. The average measured change of electron density is about 4×10^3 cm^{-3}. The upper limit of electron density at $3.5R_\oplus$ is measured as approximately 10^3 cm^{-3} [Ref. 8]. Therefore there is a missing factor of at least 4. In addition, the gradual inward movement of the knee position on the predawn side does not agree with the sharp decrease of electron density measured by the present experiment.

A model of the earth's magnetospheric wake is suggested below to explain the nighttime results. Figure 35 shows a replot of the results shown in Fig. 21, in polar coordinates. It should be noted that, since echoes were obtained only near the time of lunar transit, the azimuthal scale in Fig. 35 may be interpreted either in terms of local time or

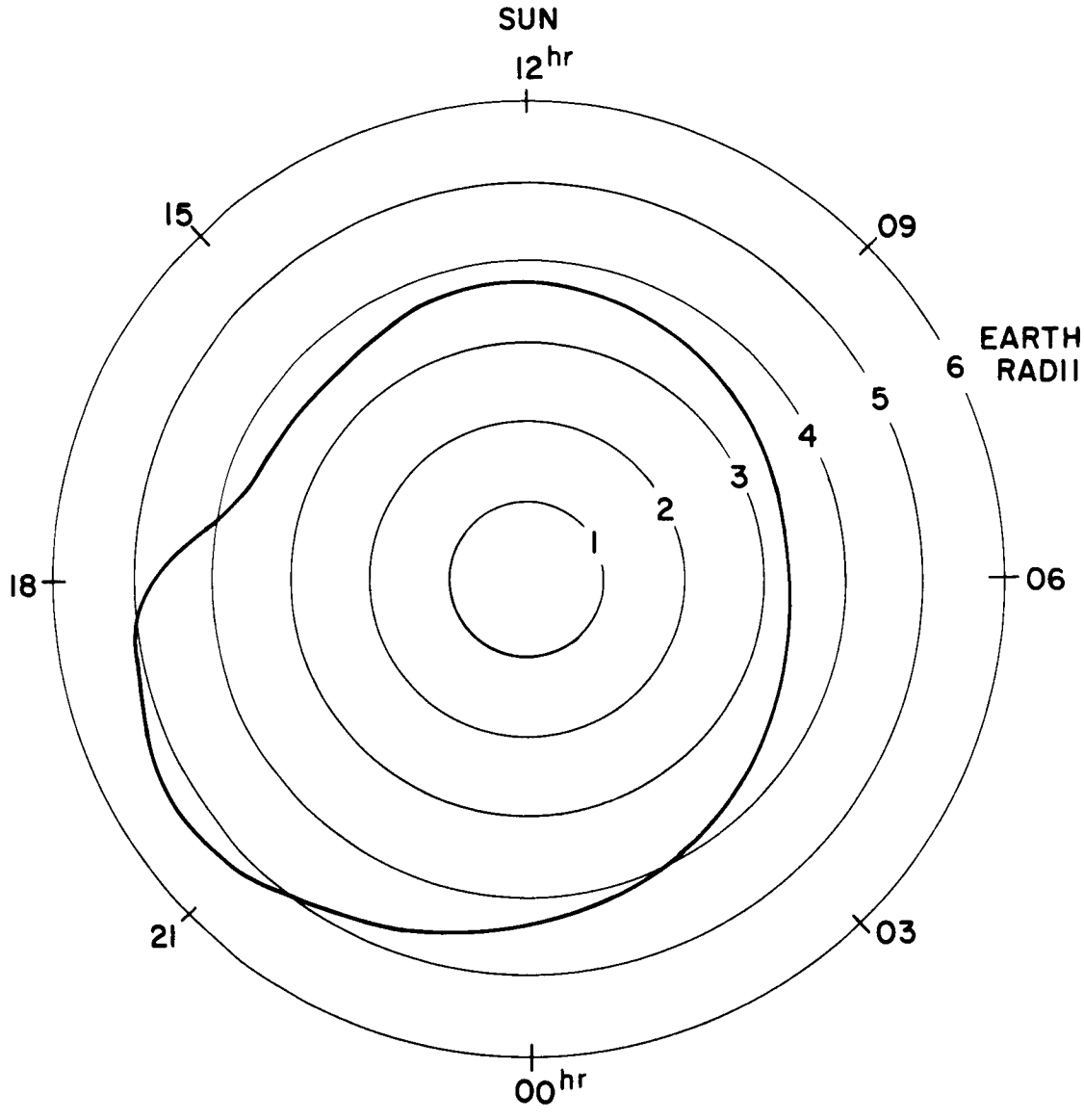

35277

FIG. 34. SPATIAL POSITION OF THE "KNEE" FOR RELATIVE QUIET DAYS (CARPENTER AND JEWELL [REF. 43]).

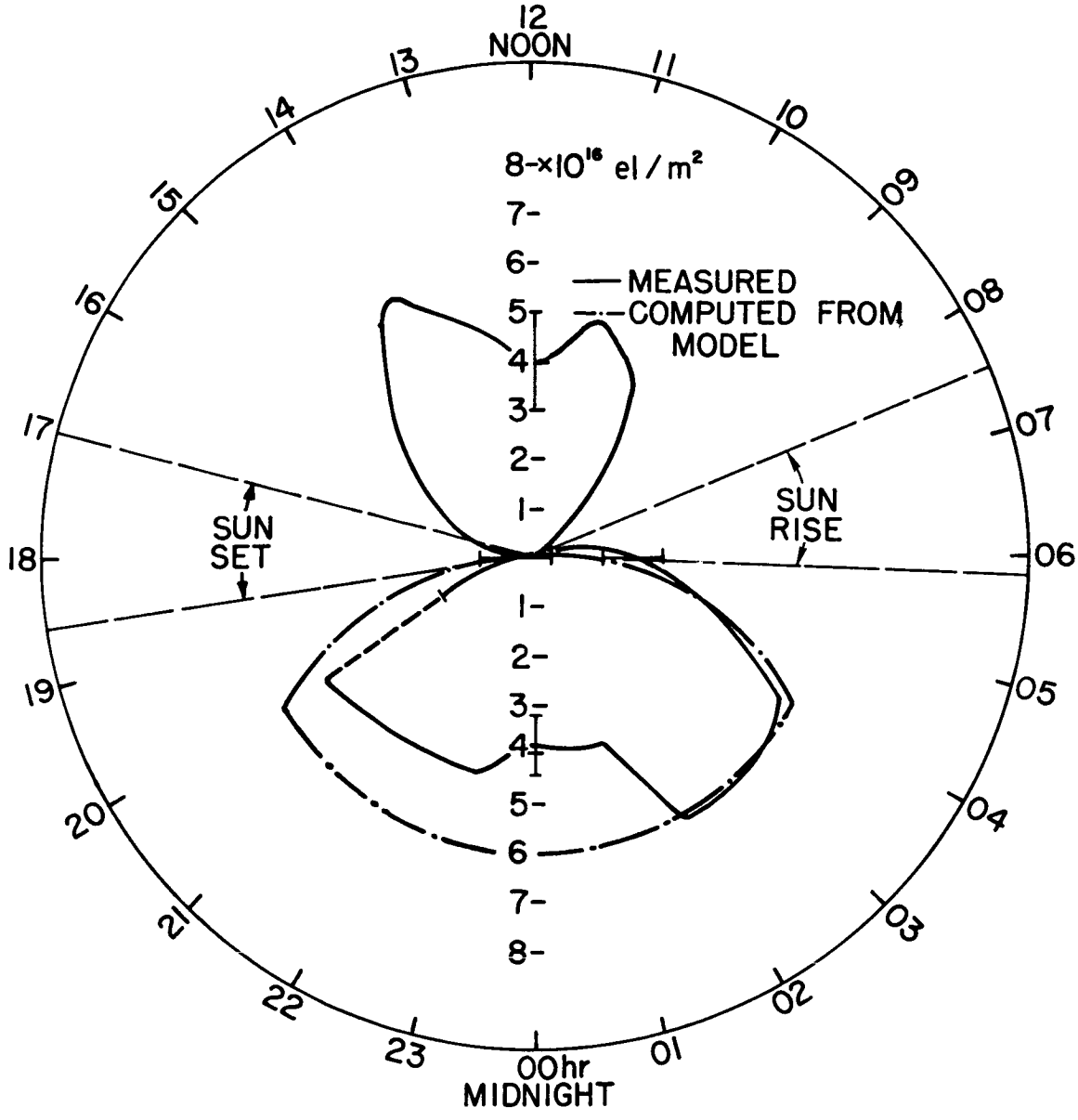

32778-1

FIG. 35. DIURNAL AND DIRECTIONAL CHANGES IN AVERAGE DIFFERENCE BETWEEN COLUMNAR ELECTRON CONTENT DETERMINED FROM DOPPLER AND FARADAY MEASUREMENTS. Measurement results are shown by the solid line, while the broken line represents the results that would be obtained from the model discussed in the text.

in terms of directions from the earth in (or near) the ecliptic plane relative to the earth-sun line. Thus, the 12-hour time represents the solar direction, the 24-hour time the antisolar direction, and 06-hour time the direction of the earth's motion around the sun. The solid line is the result of measurements and the dot-dash line will be explained below. The daytime results have been discussed in the previous chapter. The following remarks are based entirely on the results in the antisolar direction.

It is believed that the main feature of Fig. 35, which shows large changes in integrated density during the postsunset and presunrise hours, is a directional effect related to the distribution of electron densities in the magnetospheric wake. From these characteristics, a model is suggested having the following characteristics:

1. The cislunar electron density beyond the ionosphere in the antisolar quadrant is greater by about 200 cm^{-3} than the solar-wind electron density.
2. The boundary of the discontinuity in density extends at least to the orbit of the moon.
3. This boundary is an extension of the measured magnetospheric shock front, and it intersects the lunar orbit at about 120 deg from the earth-sun line (at 20 hours and 04 hours; see Fig. 35).

It should be pointed out that the boundary of the discontinuities of ionized density is located at the outer boundary of the magnetosheath, which should be distinguished from the shock-front boundary. However, these two boundaries are separated by a small distance, since the thickness of the shock front is on the order of only a few kilometers [Ref. 50]. Therefore the boundary in the following discussion is the magnetosheath boundary.

Figure 36 shows the proposed boundary (solid line). The open circles joined by dotted lines are the shock-wave and magnetopause boundaries measured by IMP-I [Ref. 42].

The radar results are explained as follows: the predawn decrease of integrated electron density beyond the ionosphere is due to the fact that the moon is moving in the solar direction and thus the radar path length in the high-density region is progressively shortened. Hence,

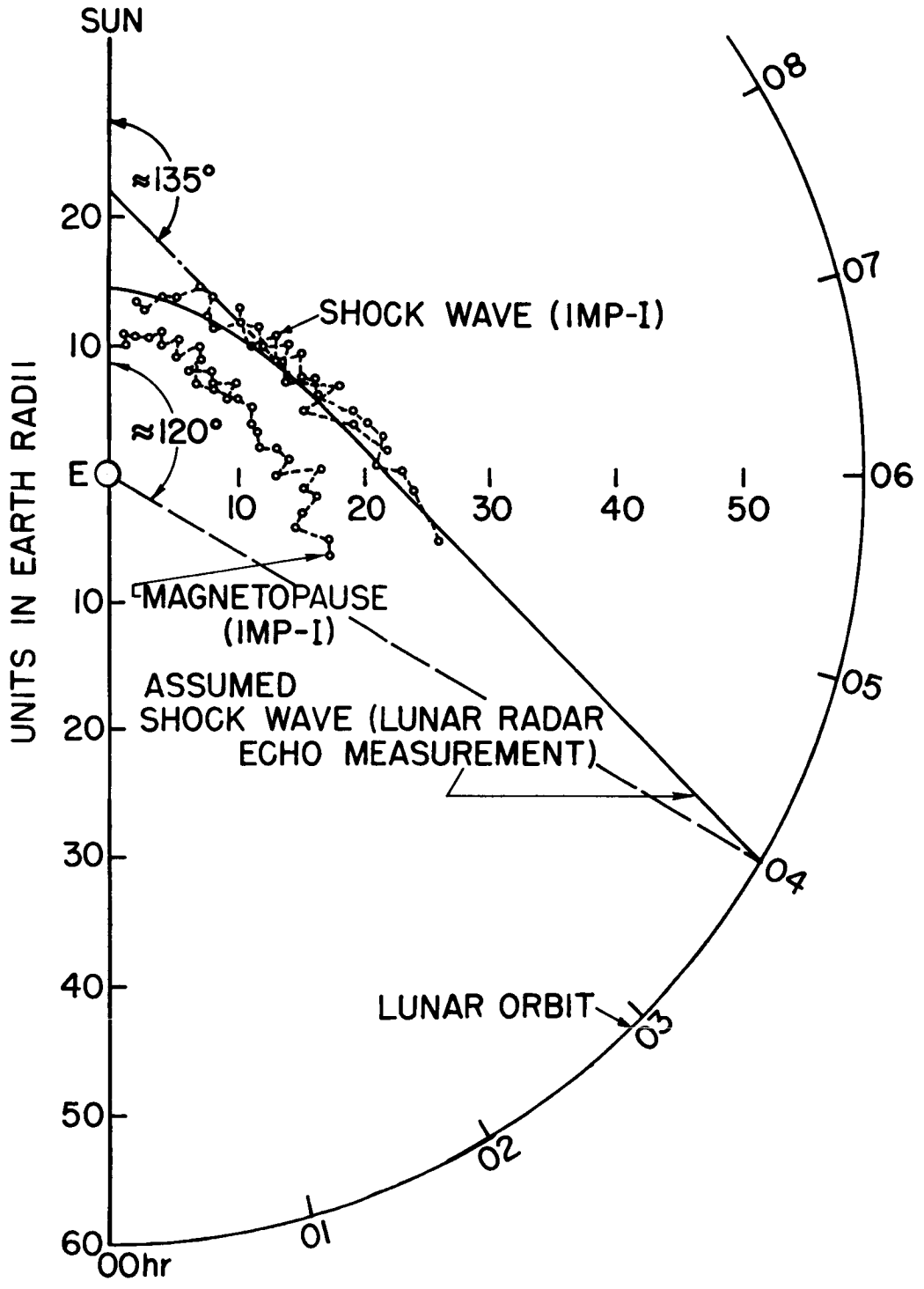

32780-1

FIG. 36. SIMPLIFIED MODEL OF EARTH'S MAGNETOSPHERIC WAKE, USED TO EXPLAIN NIGHTTIME RADAR RESULTS.

a decrease of the cislunar electron content is observed. The postsunset increase is due to the moon's moving in the antisolar direction. The part of the total radar path in the high-density region is lengthened so that the total electron content increases. The boundaries are determined by the sudden cessation of changes of electron content.

A computed relative electron content from the model is plotted in Fig. 35 (dot-dash line) for comparison with the observations. It appears that the principal features of the measurements are explained by this simple model.

Figure 36 shows that the boundary of the proposed model is a simple straight-line extrapolation of the measured shock-wave boundary. At the limits set by the orbit of IMP-I, there is no indication that the shock front is curving back around the earth, as has been proposed in some theoretical models. It should be pointed out that, since the Doppler-excess method is a measure of relative electron content, it is insensitive to the exact shape of the boundary. Even the magnetospheric boundaries measured by IMP-I [Ref. 42] show a large scatter of their positions. The proposed model generally matches the IMP-I results.

Obayashi [Ref. 51] has considered the shape of the shock front from the viewpoint of ordinary shock theory. The distance r to the shock front is expressed by

$$\frac{r}{r_s} = \frac{1 + \sec \beta}{1 + \sec \beta \cos \phi} \tag{7.1}$$

and

$$\sin \beta = \frac{1}{M} , \tag{7.2}$$

where r_s is the distance to the shock on the earth-sun line

β is the mach angle for an unshocked flow

ϕ is the angle (origin at earth) measured from the earth-sun line

M is the mach number of the flux flow in the solar wind.

A set of shock-front curves could be calculated from the above two equations if the mach number M and the distance r_s were known. Figure 37 shows a family of shock fronts (dash lines) for mach numbers between 1.5 and 10. The distance r_s is chosen at 14 earth radii, to agree with the measured distance [Ref. 42]. The solid line is the proposed boundary based on the lunar-radar experiment, appearing to be in good agreement with the shock boundary for mach numbers of 3 to 4, which agrees with the estimated mach number from deep-space-probe magnetic-field and particle measurements [Ref. 51].

The low-energy charged-particle measurements on IMP-I indicate a decrease in density as the satellite crosses the shock front from the postshock regions to the preshock region. The difference in density is from a few to over a hundred particles per cubic centimeter [Refs. 52, 53, 54]. The various instruments, however, are sensitive to different energy levels. It appears that the retarding-potential analyzer can best be used for comparison purposes, since this instrument includes electrons at thermal energies (0 to 5 ev). The Doppler-excess method is sensitive to all nonrelativistic electrons. Preliminary results for the retarding-potential analyzer on the first outbound orbit, as reported by Serbu [Ref. 53], imply an electron density of about 200 cm^{-3} inside the shock front, with no measureable electrons in this low-energy range outside the shock front. Figure 38 shows the electron density calculated from the retarding-potential-analyzer results, assuming an isotropic distribution of directions and a mean energy of 1.75 ev (as measured at 9 earth radii) extending from about 5 to 16 earth radii.

Recent lunar-echo group-delay measurements [Ref. 55] show that the results complement the Doppler-Faraday method. The electron density beyond the ionosphere is about 250 cm^{-3} in the antisolar direction, whereas the density in the solar direction is somewhat less. All the high-density measurements were obtained while the moon was inside the proposed model.

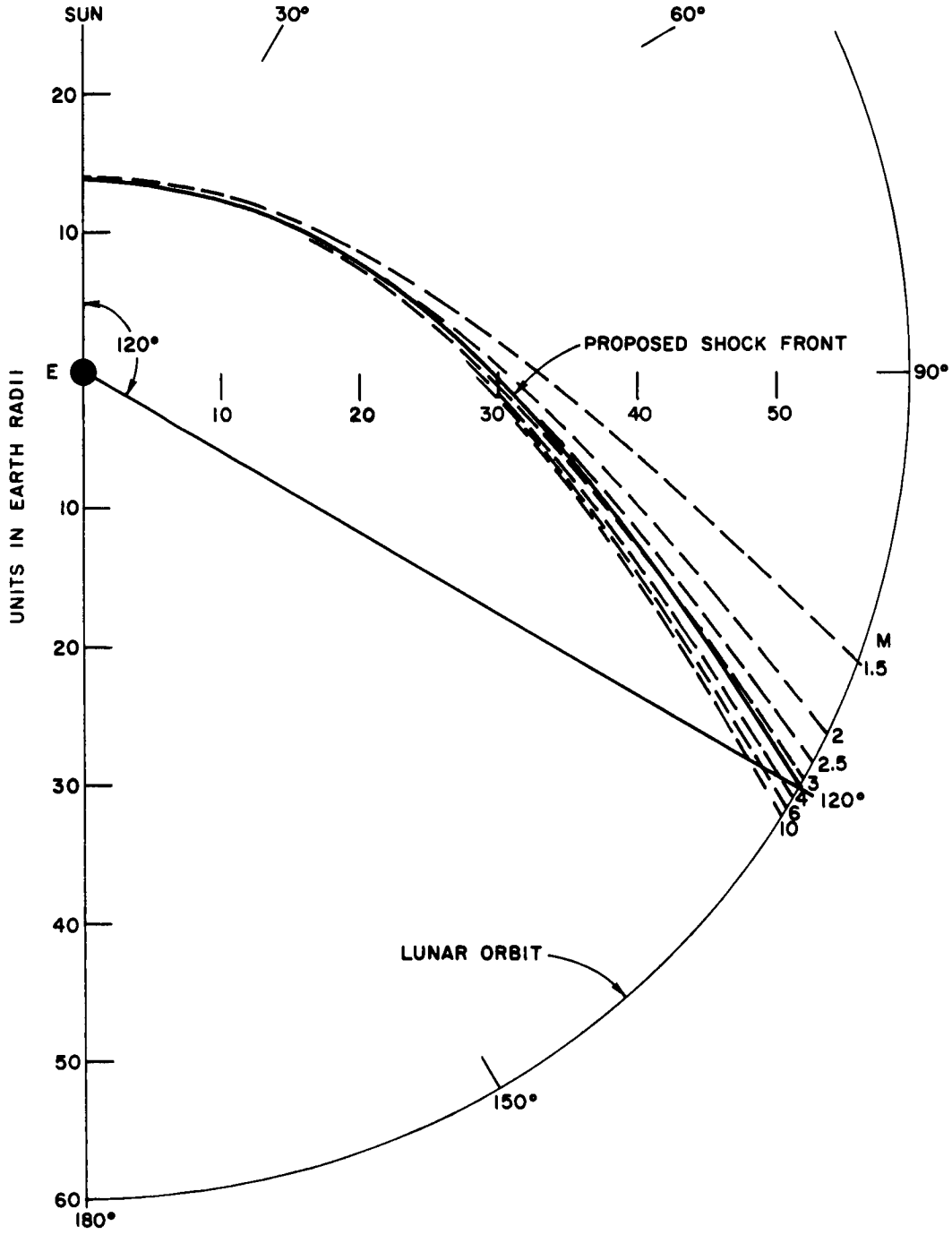

35278

FIG. 37. COMPARISON OF MEASURED AND COMPUTED BOUNDARIES.

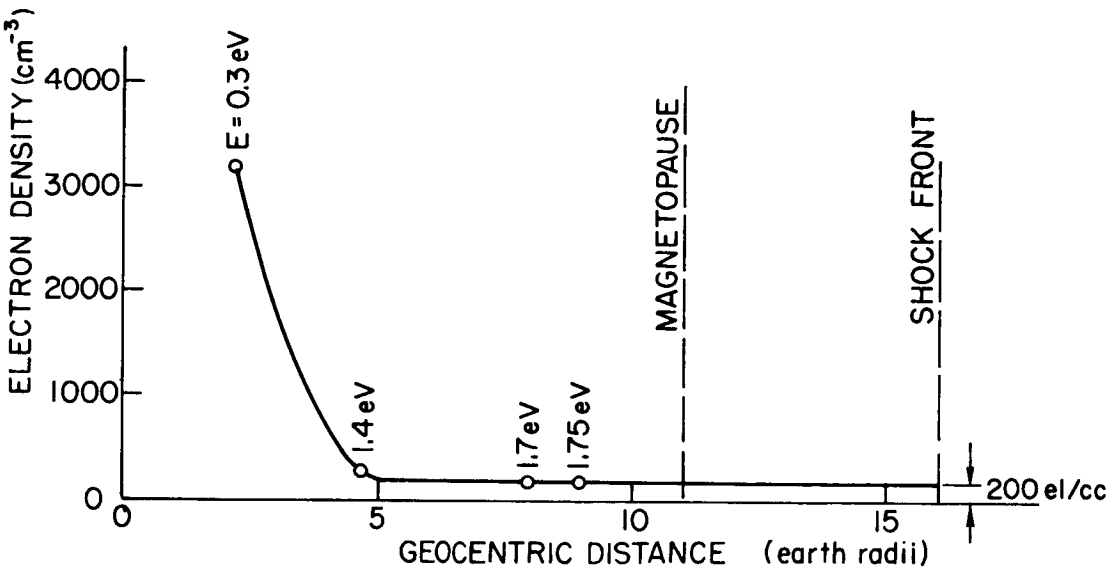

34751

FIG. 38. ELECTRON DENSITY MEASURED BY RETARDING-POTENTIAL ANALYZER ON BOARD IMP-I.

The theoretical ratio of particle densities on the two sides of the shock front is given as [Ref. 56]

$$\frac{n_1}{n_2} = \frac{\gamma - 1}{\gamma + 1} , \qquad (7.3)$$

where n_1 and n_2 are the density of preshock and postshock regions respectively and γ is usually taken as 5/3 or 2 [Refs. 52, 57] depending on the degrees of freedom of particles. If one selects the value of γ as 5/3, the ratio is 4, which is the higher value of the two. If one accepts the solar-wind density in the preshock region as being about 10 cm^{-3} [Ref. 9], then the density in the postshock region should be no more than 40 cm^{-3}. Thus the measured values of the electron density in this region are much too large to agree with the theory. However, the thickness of the shock front is on the order of a few kilometers [Ref. 50], while the thickness of the measured magnetosheath between the shock and the magnetopause is on the order of tens of thousands of kilometers. Whether the density of the solar wind is much larger than the present accepted value, or the 4-to-1 ratio of density applies to only a small region at the shock front, it needs further investigation.

VIII. CONCLUSIONS AND RECOMMENDATIONS

The present experiment on lunar-radar echoes has illustrated a useful method for the detection of large electron-content variations above the ionosphere. It is believed that this is the first time such characteristics of the cislunar medium, both spatial and temporal, have been observed.

The observed electron-content variations during the day are believed to be caused by the exchange of ionization between the ionosphere and the lower magnetosphere. The electron-content variations observed during the night are believed to be related to the spatial distribution of ionization--that is, the electron density inside the earth's magnetospheric wake is greater than the solar-wind electron density.

Extension of the experimental method to a bistatic-radar experiment appears attractive (transmitter and receiver at different locations). The forthcoming Pioneer deepspace probes will have such an experiment to measure the integrated electron content between the earth and the space probe.

Further studies are required to investigate the physical nature of the diurnal exchange of ionization between ionosphere and lower magnetosphere, especially the decay of temperature in the early afternoon. It appears that the forthcoming Alouette II sweep-frequency topside sounder would provide some insight into this mechanism. Since the Alouette II satellite has an apogee of about 3000 km, the orbit of the satellite will sweep through different longitudes and latitudes at different local times. Hence it will be possible to construct a more realistic electron-density profile along a magnetic-field line by combining the Alouette results with the equatorial electron-density profile measured by whistlers. The results of this particular study should be used to check the present lunar-radar experiment. By combining theory with the results of space-probe and radar experiments, progress should be made leading to further understanding of the solar wind and the wake of the earth.

APPENDIX A. DATA PROCESSING

As stated in Chapter III, all data were recorded on a seven-channel magnetic-tape recorder. The signals recorded were Faraday polarization and amplitudes at 25 and 50 Mc, and Doppler. The remaining two channels were used for recording time (voice and WWV) and sync signals that had a period of 5 sec and were synchronized with the transmit-receive cycle.

1. Analog-to-Digital Conversion

The tape-recorded data first went through analog-to-digital conversion. The essential steps of this process are sampling the signals and punching out the sampled data on cards.

The sampling rate was chosen at 100 cps rather than the alternative 10 or 1000 cps because of the limiting factors of both noise and memory size of the IBM-1620.

For each 5-sec period (a complete transmit-receiver cycle, see Fig. 39), an IBM-1620 digital computer was used for the following functions:

1. Search for the starting point of sampling by sampling the sync signal (Fig. 39) until its amplitude changes. The actual sampling is started by delaying 0.2 sec to avoid the noise at the beginning of the receive period.
2. Command to stop sampling at the end of a 2.2-sec period in order to eliminate the noise at the end of the receive period.
3. Store the sample values.
4. Edit the data and make simple calculations.
5. Punch out all the data during the following transmit period.

The events following the commencement of sampling during the 2.5-sec receive period are discussed below.

a. Doppler Excess Frequency

The Doppler channel of the data type that contains a beat note around two cycles is sampled. A two-cycle shift on the beat note was induced so that there would be no confusion about the sign of the beat

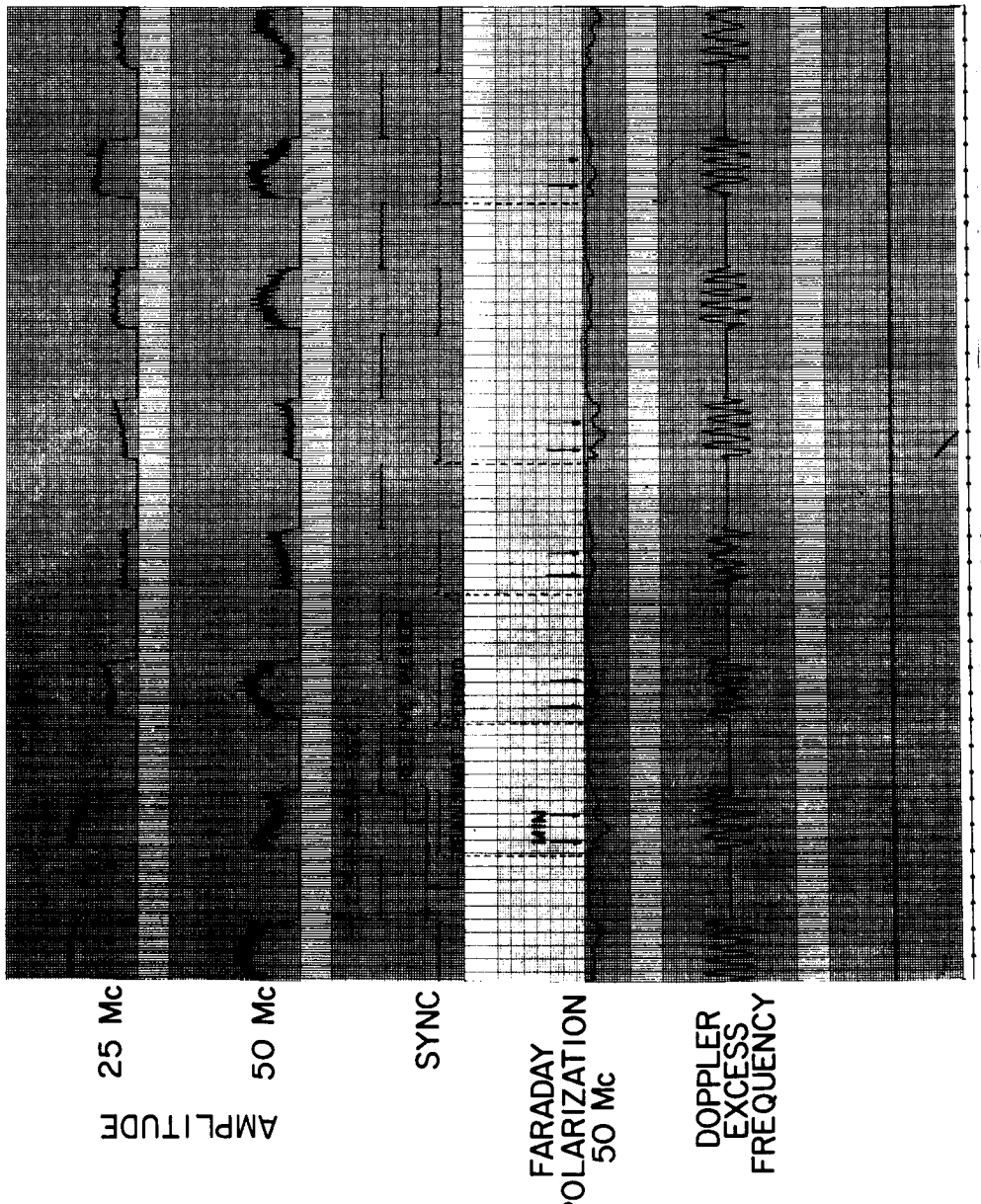

FIG. 39. EXAMPLES OF THE RECEIVED SIGNAL.

frequency. For each 5-sec operating cycle, one averaged value of beat frequency f_b is evaluated.

During sampling period, the computer does the following things:

1. Counts the number of 10-msec intervals
2. Counts the number of zero crossings.

The measured beat note f_b is calculated by

$$f_b = \frac{W/2}{p \times 10^{-2}} , \tag{A.1}$$

where W is the number of zero crossings and p is the total number of 10-msec intervals in the zero crossings.

Since a two-cycle shift was introduced at the receiving end, the true Doppler excess was calculated by

$$\left(\frac{n^2 - 1}{n}\right) f_{DE} = 2 - f_b \tag{A.2}$$

and

$$f_{DE} = \left(\frac{n}{n^2 - 1}\right) (2 - f_b) , \tag{A.3}$$

where n is an integer. Substituting f_b from Eq. (A.1) and $n = 2$ into Eq. (A.3), the final equation for use in the computer is

$$f_{DE} = \frac{4}{3} - \frac{1}{3} \frac{W}{p \times 10^{-2}} . \tag{A.4}$$

To avoid systematic errors, a point was discarded if, in the 2.5-sec interval it covered, the noise on the signal was so great that: (1) any period between two zero crossings was shorter than 150 msec, or (2) there were not at least two periods that were longer than 150 msec.

The output of the Doppler-excess channel consists of Doppler excess frequency f_{DE}, total number of zero crossings W, number of zero crossings with a period shorter than 150 msec, and number of zero crossings with a period greater than 800 msec. Further screening would be executed by the IBM-7090 computer.

b. Faraday Polarization

The Faraday-polarization channels contain the output from the goniometers, which rotate at a rate of 2 sec per rotation. Hence, they are synchronized with the transmit-receive cycle on a 10-sec basis. After the commencement of sampling, 220 points are sampled over a period of 2.2 sec. The samples are digitally filtered by adding each successive group of five points to give 44 averaged data points. Hence each point represents an interval of 50 msec. The 50-msec interval is equivalent to a rotation of 9 deg by a goniometer. Thus, the resolution of the Faraday polarization angle is at least 9 deg. Figure 39 shows clearly that the positions of minima of Faraday polarization can readily be found.

c. Amplitude

The amplitude channels contain the output of the receivers fed by the fixed polarization on the Doppler-excess-frequency antennas. The sampling rate is the same as that of the Faraday polarization. The only difference is that the samples are digitally filtered by adding each successive group of 10 points to give 22 averaged data points.

All the above points are punched on cards, each of which is identified by run number, card type, pulse number, and timing mark.

2. Digital Process

The IBM-7090 computer reads in successive groups of 20 min each and starts to process in the manner described below.

a. Faraday Polarization

The data from both Faraday channels are treated alike. The 44 data points are further smoothed by taking a running mean of successive groups of five points. Then a search of the position of minimum signal

is conducted. Since the goniometer rotates the receiver antenna polarization synchronously in time with the 5-sec transmit-receive period, the position of the minimum signal is a direct measure of the Faraday angle of the received signal. For cases when no echoes or extreme noise occur, a check is made by comparing the maximum signal strength to the minimum signal strength. If the difference between these two signals is less than a certain threshold value, which is predetermined, the point is discarded.

b. Doppler Excess Frequency

The data from the Doppler channel are treated as follows:

1. If more than two zero crossings occur with a period shorter than 150 msec, the point is discarded--this process eliminates the noisy signals. Otherwise the point is taken into account as it is.
2. A smoothing process is applied to the Doppler-excess-frequency data. A successive 1-min run is taken with the condition that each interval must have at least three data points. Otherwise, no value is assigned for the particular point.
3. If there is a break in the running mean, the operation of integration starts over again (see Fig. 5).

The above-processed data for Faraday polarization and Doppler excess frequency are then plotted by the Calcomp plotter (see Fig. 5). All the raw and processed data are then stored on magnetic tape.

REFERENCES

1. I. C. Browne et al, "Radio Echoes from the Moon," Proc. Phys. Soc. (London), B, 69, 1956, pp. 901-920.

2. O. K. Garriott, "The Determination of Ionospheric Electron Content and Distribution from Satellite Observations, I and II," J. Geophys. Res., 65, 1960, pp. 1139-1157.

3. F. de Mendonça, "Ionospheric Electron Content and Variations Measured by Doppler Shifts in Satellite Transmissions," J. Geophys. Res., 67, 1962, pp. 2315-2338.

4. Tor Hagfors, "Density Fluctuations, in a Plasma in a Magnetic Field, with Application to the Ionosphere," J. Geophys. Res., 66, 1961, pp. 1699-1712.

5. J. V. Evans, "The Distribution of Electrons in the Upper Ionosphere from Backscatter Observations," Lincoln Laboratory Report 3G-002 and Supp. 1, Massachusetts Institute of Technology, Cambridge, Mass., Nov 1960.

6. J. E. Jackson and J. A. Kane, "Performance on an RF Impedance Probe in the Ionosphere," J. Geophys. Res., 65, 1960, pp. 2209-2210.

7. J. W. King et al, "Preliminary Investigation of the Structure of the Upper Ionosphere as Observed by the Topside Sounder Satellite, Alouette," Proc. Roy. Soc. (London), 281, 1964, pp. 464-487.

8. R. L. Smith, "Properties of the Outer Ionosphere Deduced from Nose Whistlers," J. Geophys. Res., 66, 1961, pp. 3709-3716.

9. M. Neugebauer and C. W. Snyder, "Solar Plasma Experiment: Preliminary Mariner 2 Observations," Science, 138, 1962, pp. 1095-1096.

10. V. R. Eshleman, P. B. Gallagher, and R. C. Barthle, "Radar Methods of Measuring the Cislunar Electron Density," J. Geophys. Res., 65, 1960, pp. 3079-3086.

11. H. T. Howard, P. Yoh, and V. R. Eshleman, "Radar Doppler Measurements of the Cislunar Medium," J. Geophys. Res., 69, 1964, pp. 535-539.

12. H. T. Howard et al, "Radar Doppler and Faraday Polarization Measurements during the July 20, 1963, Solar Eclipse," J. Geophys. Res., 69, 1964, pp. 540-544.

13. E. J. Opik, "The Lunar Atmosphere," Planet. Space Sci., 9, 1962, pp. 211-244.

14. J. A. Ratcliffe, The Magneto-Ionic Theory and Its Application to the Ionosphere, Cambridge University Press, Cambridge, England, 1959.

15. J. V. Evans, "The Electron Content of the Ionosphere," J. Atmospheric Terrest. Phys., 11, 1957, pp. 259-271.

16. J. V. Evans and G. N. Taylor, "The Electron Content of the Ionosphere in Winter," Proc. Roy. Soc. (London), A, 263, 1961, pp. 189-211.

17. S. J. Bauer and F. B. Daniels, "Measurements of Ionospheric Electron Content by the Lunar Radio Technique," J. Geophys. Res., 64, 1959, pp. 1371-1376.

18. G. N. Taylor, Radio Astonomical and Satellite Studies of the Atmosphere, edited by J. Aarons, North-Holland Publishing Co., Amsterdam, Netherlands, 1963.

19. R. F. Mlodnosky and R. A. Helliwell, "Graphic Data on the Earth's Main Magnetic Field in Space," J. Geophys. Res., 67, 6, 1962, pp. 2207-2214.

20. R. S. Lawrence, C. G. Little, and H. J. A. Chivers, "A Survey of Ionospheric Effects upon Earth-Space Radio Propagation," Proc. IEEE, 52, 1964, pp. 4-27.

21. W. J. Ross, "Second-Order Effects in High-Frequency Transionospheric Propagation," J. Geophys. Res., 70, 3, 1965, pp. 597-612.

22. H. T. Howard, "An Antenna Array for Radar Astronomy Studies in the 20 to 50 Mc Range," Trans. IEEE, PGTAP, AP-13, 3, 1965, pp. 365-368.

23. H. T. Howard, B. B. Lusignan, and V. R. Eshleman, "Radio Astronomy and Propagation Research," Rept. SEL-64-114, (Final Report, Contract AF19(604)-7436), Stanford Electronics Laboratories, Stanford, Calif., Sep 1964.

24. E. Golton, "Calculations and Local Models of the Near Geomagnetic Field," Planet. Space Sci., 11, 1963, pp. 1263-1272.

25. K. C. Yeh and V. H. Gonzalez, "Note on the Geometry of the Earth's Magnetic Field Useful to Faraday Effect Experiments," J. Geophys. Res., 65, 1960, pp. 3209-3214.

26. D. C. Jenson and J. C. Cain, "An Interim Geomagnetic Field," J. Geophys. Res., 67, 1962, pp. 3569-3570.

27. J. W. Wright, "A Model of the F Region above $h_{max}F2$," J. Geophys. Res., 65, 1960, pp. 185-191.

28. J. S. Nisbet, "Electron Density Distribution in the Upper Ionosphere from Rocket Measurement," J. Geophys. Res., 65, 1960, pp. 2597-2599.

29. W. W. Berning, "A Sounding Rocket Measurement of Electron Densities to 1500 Kilometers," J. Geophys. Res., 65, 1960, pp. 2589-2594.

30. S. J. Bauer and J. E. Jackson, "Rocket Measurement of the Electron Density Distribution in the Topside Ionosphere," J. Geophys. Res., 67, 1962, pp. 1675-1677.

31. S. J. Bauer and L. J. Blumle, "Mean Diurnal Variation of the Topside Ionosphere at Mid-Latitude," J. Geophys. Res., 69, 1964, pp. 3613-3618.

32. R. E. Bourdeau, "Ionospheric Research from Space Vehicles," Space Sci. Rev., 1, 1963, pp. 683-728.

33. P. J. Bowen et al, "Ion Composition of the Upper F-Region," Proc. Roy. Soc. (London), 281, 1964, pp. 504-514.

34. J. V. Evans and M. Loewenthal, "Ionospheric Backscatter Observations," Planet. Space Sci., 12, 1964, pp. 915-944.

35. J. V. Evans, "Cause of the Mid-Latitude Evening Increase in f_oF_2," J. Geophys. Res., 70, 1965, pp. 1175-1185.

36. S. J. Bauer and R. E. Bourdeau, "Upper Atmosphere Temperature Derived from Charged Particle Observations," J. Atmos. Sci., 19, 1962, pp. 218-225.

37. O. K. Garriott, F. L. Smith III, and P. C. Yuen, "Observation of Ionospheric Electron Content Using a Geostationary Satellite," Planet. Space Sci., 13, 1965, pp. 829-838.

38. R. V. Bhonsle, A. V. da Rosa, and O. K. Garriott, "Measurements of the Total Electron Content and the Equivalent Slab Thickness of the Mid-Latitude Ionosphere," J. of Res., Natl. Bur. Std. (U.S.), 69D, 1965, pp. 929-937.

39. G. H. Millman, "Radar-Lunar Measurements of the Electron Content of the Ionosphere," J. Geophys. Res., 69, 1964, pp. 429-440.

40. J. E. Titheridge, "The Refraction of Satellite Signals--II Experimental Results," J. Atmospheric Terrest. Phys., 26, 1964, pp. 177-191.

41. F. H. Hibberd, "A Study of the Ionosphere at Mid-Latitude Based on Total Electron Content," Scientific Rept 213, Pennsylvania State University, Pa.

42. N. F. Ness, C. S. Scearce, and J. B. Seek, "Initial Results of the IMP-I Magnetic Field Experiment," J. Geophys. Res., 69, 1964, pp. 3531-3570.

43. D. L. Carpenter and T. R. Jewell, "Temporal and Spatial Variations of the "knee" in the Magnetospheric Electron Density Profile," paper presented at Spring 1965 URSI meeting, Washington, D.C.

44. S. J. Bauer, "On the Structure of the Topside Ionosphere," J. Atmos. Sci., 16, 1962, pp. 276-278.

45. H. B. Hanson, "Electron Temperatures in the Upper Atmosphere," Space Research, Vol. III, edited by W. Priester, North-Holland Publishing Co., Amsterdam, Netherlands, 1963, pp. 282-302.

46. A. Dalgarno, M. B. McElroy, and R. J. Moffett, "Electron Temperatures in the Ionosphere," Planet. Space Sci., 11, 1963, pp. 463-484.

47. J. V. Evans, "An F-Region Eclipse," J. Geophys. Res., 70, 1965, pp. 131-142.

48. A. P. Willmore, "Energy Sources for the Ionospheric Electrons," Nature, 202, 1964, pp. 41-42.

49. L. H. Brace, N. W. Spencer, and A. Dalgarno, "Detailed Behavior of the Mid-Latitude Ionosphere from the Explorer XVII Satellite," Planet. Space Sci., 13, 7, Jul 1965, pp. 647-666.

50. E. N. Parker, "Plasma Dynamical Determination of Shock Thickness in an Ionized Gas," Astrophys. J., 129, 1959, p. 217.

51. T. Obayashi, "Interaction of Solar Plasma Streams with the Outer Geomagnetic Field," J. Geophys. Res., 69, 1964, pp. 861-867.

52. S. Olbert, "Symposium on Shock Waves in Collision-Free Plasma," sponsored by Space Science Division, NASA-Ames Research Center, Moffett Field, Calif., and by the Institute of Plasma Research, Stanford University, Stanford, California, Mar 1965.

53. G. P. Serbu, "Results from the IMP-I Retarding Potential Analyzer," Space Research, Vol. V, edited by D. G. King-Hele, P. Muller, and G. Righini, North-Holland Publishing Co., Amsterdam, Netherlands, 1965, pp. 564-576.

54. J. Wolfe, "Symposium on Shock Waves in Collision-Free Plasma," sponsored by Space Science Division, NASA-Ames Research Center, Moffett Field, and by the Institute of Plasma Research, Stanford University, Stanford, California, Mar 1965.

55. H. T. Howard et al, "Radar Doppler Measurements of the Cislunar Electron Content," J. Geophys. Res., 70, Sep 1965, pp. 4357-4364.

56. P. J. Kellogg, "Flow of Plasma around the Earth," J. Geophys. Res., 67, 1962, pp. 3805-3812.